

Toxicity of combustion condensates on human cells

Dissertation
zur
Erlangung des Doktorgrades (Dr. rer. nat.)
der
Mathematisch-Naturwissenschaftlichen Fakultät
der
Rheinischen Friedrich-Wilhelms-Universität Bonn

vorgelegt von

Nevena Stojičić
aus
Belgrad

Bonn 2009

Angefertigt mit Genehmigung der Mathematisch-Naturwissenschaftlichen Fakultät
der Rheinischen Friedrich-Wilhelms-Universität Bonn.

1. Gutachter: Prof. Dr. Waldemar Kolanus

2. Gutachter: PD Dr. Ruth Hemmersbach

Tag der Promotion: 18.02.2010

Erscheinungsjahr: 2010

Table of contents

Table of contents.....	I
List of figures.....	IV
List of tables.....	VI
1 INTRODUCTION	1
1.1 Air pollution and health impacts.....	1
1.1.1 Combustion as a source of air pollution	1
1.1.2 Particulate matter in ambient air: physical and chemical characterisation.....	2
1.1.3 Chemical composition of combustion exhaust	4
1.1.4 Laboratory flames as a model source of combustion generated particles.....	6
1.1.5 Health effects of airborne particles.....	7
1.1.6 Toxicologically relevant properties of the airborne PM	10
1.2 Toxicity.....	11
1.2.1 Genotoxicity.....	12
1.2.2 Cytotoxicity	13
1.2.3 Test-systems for toxicity assessment.....	13
1.3 Cell death: types and mechanisms.....	13
1.4 Activation of NF-κB in response to stress	15
1.5 Aims of the research.....	18
2 MATERIAL AND METHODS	20
2.1 Material	20
2.1.1 Laboratory equipment	20
2.1.2 Consumable material	21
2.1.3 Chemicals.....	21
2.1.4 Media, buffer and sera	22
2.1.5 Test samples	22
2.1.6 Commercial reaction kits.....	23
2.1.7 Bacterial strain.....	23
2.1.8 Human cell lines	23
2.2 Methods.....	24
2.2.1 Generation and analysis of combustion condensates.....	24
2.2.1.1 Generation of combustion condensates	24
2.2.1.2 Total organic carbon content analysis	26
2.2.1.3 High-resolution transmission electron microscopy	27
2.2.1.4 Spectrophotometry.....	27
2.2.1.5 Ultracentrifugation	27
2.2.1.6 Filtration	28
2.2.2 Prokaryotic cell culture and SWITCH test	28
2.2.2.1 Standard cultivation.....	28
2.2.2.2 SWITCH test	28
2.2.3 Eukaryotic cell cultures.....	30
2.2.3.1 Cultivation of A-549 cell line.....	30
2.2.3.2 Cultivation of U-937 cell line	31
2.2.3.3 Long-term storage of cells	31
2.2.3.4 Growth kinetics of the used cell lines	32
2.2.3.5 Stable transfection of U-937 with pNF- κ B-EGFP/Neo plasmid	32
2.2.4 Flow cytometry	34
2.2.5 NF- κ B-activation assay	35
2.2.6 Apoptosis assays.....	35
2.2.6.1 Annexin V-PE / 7-AAD assay.....	35

2.2.6.2	DNA content and cell cycle analysis	36
2.2.6.3	Active caspase-3 assay	37
2.2.6.4	DAPI staining	38
2.2.7	Crystal violet assay.....	39
2.2.8	MTT test	39
2.2.9	Molecular biological methods	40
2.2.9.1	Total RNA isolation	40
2.2.9.2	Quantification and quality analysis of isolated RNA	40
2.2.9.3	Quantitative real-time reverse transcription PCR (qRT-PCR)	40
2.2.10	Statistical analysis	46
3	RESULTS.....	47
3.1	Physical and chemical analysis of combustion condensates	47
3.1.1	Visual inspection of the presence of soot in combustion condensates	47
3.1.2	Morphological analysis of the soot present in combustion condensates	48
3.1.3	TOC content of combustion condensates depends on combustion conditions	50
3.1.4	UV-spectrophotometry of combustion condensates reveals a presence of nanoparticles.....	51
3.2	Combustion condensates are genotoxic and cytotoxic according to the bacterial SWITCH test.....	53
3.2.1	Toxicity of ethylene combustion condensates depends on their TOC content	54
3.2.2	Toxicity of diesel combustion condensates depends on their TOC content	58
3.2.3	Prolonged storage of combustion condensates has no impact on their toxicity	61
3.2.4	Toxicologically relevant constituent of the combustion exhaust is being captured in all three cool traps	62
3.2.5	Soot has no significant contribution to the toxicity of ethylene combustion condensates	62
3.2.5.1	Increased concentration of soot particles in ethylene combustion condensate does not change its toxic potential.....	62
3.2.5.2	Soot particles larger than 20 nm have no significant contribution to the toxicity of ethylene combustion condensate	64
3.2.5.3	Soot particles ($d \geq 10 \text{ nm}$) are not responsible for the toxic potency of ethylene combustion condensate	65
3.3	Effects of combustion condensates on human cell lines	68
3.3.1	Characterisation of tested human cell lines: cell growth kinetics	68
3.3.2	Combustion condensates impair cell growth.....	69
3.3.3	Combustion condensates induce apoptosis in monocyte-like cell line but not in lung epithelial cell line.....	73
3.3.3.1	Cell cycle analysis and detection of apoptosis	73
3.3.3.2	Microscopic verification of apoptosis	76
3.3.3.3	Detection of early apoptotic changes in cell membrane	78
3.3.3.4	Activation of caspase-3 in cells undergoing apoptosis	81
3.3.4	Effect of ethylene combustion condensate on the activation of NF- κ B signalling pathway in U-937	83
3.3.4.1	Selection of TNF- α -inducible stably transfected U-937-pNF- κ B-EGFP/Neo clone	83
3.3.4.2	Dose-dependant activation of the NF- κ B pathway in U-937-pNF- κ B-EGFP/Neo clone 5a treated with ethylene combustion condensate	86
3.3.5	Role of NF- κ B in the ethylene combustion condensate-induced apoptosis in U-937	90
3.3.5.1	Selection of a suitable NF- κ B inhibitor.....	91
3.3.5.2	NF- κ B inhibition enhances the ethylene combustion condensate-induced apoptosis	94
3.3.6	Effect of the ethylene combustion condensate on the expression of NF- κ B-target genes in A-549.....	96
3.3.7	Removal of soot particles has no effect on the toxicity of ethylene combustion condensate on U-937 cells	99

4	DISCUSSION	102
4.1	Characterisation of combustion condensates	102
4.2	SWITCH test as a pre-screening tool for the combustion condensates' toxicity assessment.....	106
4.2.1	TOC content is a proper dose metric for the evaluation of combustion condensates' toxicity	108
4.2.2	Toxicity of combustion condensates is not soot-mediated.....	109
4.3	Effects of combustion condensates on human cells.....	112
4.3.1	Combustion condensates have a cytotoxic effect on A-549 and U-937	112
4.3.2	Combustion condensates activate NF-κB signalling pathway	114
4.3.3	Anti-apoptotic role of NF-κB in the U-937 cell line treated with ethylene combustion condensate	117
4.4	Outlook.....	118
5	SUMMARY.....	119
6	APPENDIX.....	121
7	REFERENCES.....	128
8	ABBREVIATIONS.....	139

List of figures

Figure 1-1: Detection of nanoparticles ($d < 10$ nm) in ethylene flame exhausts	7
Figure 1-2: Distribution of different PM fractions in the respiratory tract	8
Figure 2-1: Production of ethylene- and diesel combustion condensates	24
Figure 2-2: Plasmid pNF- κ B-EGFP/Neo	33
Figure 2-3: Flow cytometric analysis of apoptosis with Annexin V-PE / 7-AAD assay	36
Figure 2-4: Determination of the real-time PCR efficiency	44
Figure 3-1: Morphological analysis of the soot in combustion condensates	49
Figure 3-2: Ethylene combustion condensates display a broad band absorption in the UV range	52
Figure 3-3: Total organic carbon contents of ethylene combustion condensates show good correlation with their Abs_{250} values	53
Figure 3-4: Toxicity of ethylene combustion condensates depends on their TOC content.....	56
Figure 3-5: Different C/O ratios show no significant impact on the toxicity of ethylene combustion condensates at comparable TOC levels	57
Figure 3-6: TOC content determines the toxicity of diesel combustion condensates	60
Figure 3-7: Toxic potential of combustion condensates is stable after 2 years of storage	61
Figure 3-8: Same amount of TOC in combustion condensates exhibits same toxic effect regardless of the cool trap it originates from.....	62
Figure 3-9: Increased concentration of soot particles does not change the toxicity of ethylene combustion condensate	63
Figure 3-10: Soot particles larger than 20 nm have no significant contribution to the toxicity of ethylene combustion condensate, as estimated with bacterial SWITCH test	65
Figure 3-11: Toxic constituent can not be precipitated after 14 h centrifugation of ethylene combustion condensate at 116 000 x g, as estimated with bacterial SWITCH test.....	66
Figure 3-12: Growth curves for A-549 and U-937 cell lines	69
Figure 3-13: Kinetics of the effect of ethylene combustion condensate on the U-937 cell growth	70
Figure 3-14: Ethylene combustion condensate impairs U-937 cell growth	71
Figure 3-15: Combustion condensates impair A-549 cell growth.....	72
Figure 3-16: Ethylene combustion condensate causes cell cycle distortion and induction of apoptosis in U-937 cells	74
Figure 3-17: Ethylene combustion condensate causes no changes in cell cycle and no induction of apoptosis in A-549 cells	75
Figure 3-18: Ethylene combustion condensate induces DNA morphological changes in U-937 but not in A-549 cells.....	77
Figure 3-19: Ethylene combustion condensate induces cell death in U-937 cells	79
Figure 3-20: Diesel combustion condensate induces cell death in U-937 cells	80
Figure 3-21: Cell viability analysis of two cell subpopulations occurring after treatment of U-937 cells with ethylene combustion condensate	81
Figure 3-22: Flow cytometric analysis of apoptosis by using active caspase-3 assay: representative density-plot and histogram plot.....	82
Figure 3-23: Activation of caspase-3 in U-937 cells treated with combustion condensates	83
Figure 3-24: Lethal effect of 1 500 μ g/ml geneticin (G418) on U-937 cells.....	84
Figure 3-25: Screening of stably transfected U-937-pNF- κ B-EGFP/Neo clones	86
Figure 3-26: NF- κ B activation and appearance of two cell subpopulations in	88
Figure 3-27: Ethylene combustion condensate induces dose-dependant NF- κ B activation in U-937-pNF- κ B-EGFP/Neo clone 5a cells	90
Figure 3-28: MG-132 is an unsuitable inhibitor of TNF- α -induced NF- κ B activation in U-937-pNF- κ B-EGFP/Neo clone 5a	92
Figure 3-29: 2 μ M Bay 11-7082 effectively suppresses TNF- α -induced NF- κ B activation in U-937-pNF- κ B-EGFP/Neo clone 5a	93
Figure 3-30: 2 μ M Bay 11-7082 efficiently inhibits ethylene combustion condensate-induced NF- κ B activation in U-937-pNF- κ B-EGFP/Neo clone 5a	94
Figure 3-31: Inhibition of NF- κ B pathway increases the number of apoptotic cells in U-937 cell culture treated with ethylene combustion condensate.....	95
Figure 3-32: Modulation of IL-6 gene expression in A-549 after treatment with different combustion samples.....	97
Figure 3-33: Modulation of NF κ BIA gene expression in A-549 after treatment with different combustion samples.....	98
Figure 3-34: Soot particles larger than 20 nm have no significant contribution to the toxicity of ethylene combustion condensate, as estimated with apoptosis test.....	99

Figure 3-35: Toxic component of ethylene combustion condensate cannot be precipitated after 14 h centrifugation at 116 000 x g, as estimated with mammalian apoptosis test	101
Figure 6-1: Toxicity of ethylene combustion condensate generated at C/O=0.63	121
Figure 6-2: Toxicity of ethylene combustion condensate generated at C/O=0.68	122
Figure 6-3: Toxicity of ethylene combustion condensate generated at C/O=0.73	123
Figure 6-4: Toxicity of ethylene combustion condensate generated at C/O=0.78	124
Figure 6-5: Toxicity of ethylene combustion condensate generated at C/O=0.83	125
Figure 6-6: Toxicity of ethylene combustion condensate generated at C/O=0.88	126
Figure 6-7: Toxicity of ethylene combustion condensate generated at C/O=0.93	127

List of tables

Table 1-1:	Fractions of airborne particles according to their size	3
Table 1-2:	Organic compounds present in diesel exhaust (from Schauer et al. 1999).....	5
Table 1-3:	NF- κ B target genes and their roles.....	17
Table 2-1:	Primer pairs (forward and reverse) of target and reference genes.....	42
Table 2-2:	Candidate reference genes and their functions	46
Table 3-1:	Total organic carbon content of ethylene combustion condensates obtained in one production series.....	50
Table 3-2:	Total organic carbon content of diesel combustion condensates obtained in one production series.....	51
Table 3-3:	Physical and chemical characterisation of the ethylene combustion sample (C/O=0.93) and its fractions obtained via centrifugation or filtration.....	67
Table 3-4:	Relative distribution of U-937 cells according to their cell cycle phases, after treatment with ethylene combustion condensate.....	74
Table 3-5:	Relative distribution of A-549 cells according to their cell cycle phases, after treatment with ethylene combustion condensate.....	76

1 Introduction

1.1 Air pollution and health impacts

Health effects of air pollution are among the largest environmental problems worldwide. Urban air pollution levels are associated with increased mortality and cardio-respiratory morbidity (Peters et al., 1997; von Klot et al., 2002; Lippmann et al., 2003). Although in many countries urban air pollution has been decreasing (due to the substitution of coal as an energy source in households, employment of filters and catalysts in car industry etc.), pollution levels are still quite high. In urban areas, air pollution originates primarily from combustion sources (industry, traffic).

1.1.1 Combustion as a source of air pollution

In general, there are two main sources of combustion generated particulate emissions in the environment: natural and anthropogenic. Wood fires and volcano eruptions represent natural sources, while traffic, industry and household are main anthropogenic sources of particulate matter. Particulate matter from both natural and anthropogenic sources can be further sub-classified into primary and secondary particles. While primary particles are emitted directly from the sources, secondary particles are being formed in the atmosphere by gas-to-particle phase conversions (Borm et al., 2006). Traffic is one of the most significant sources of anthropogenic aerosols in urban areas (Cass et al., 1998; Cyrys et al., 2003). Most of the traffic emissions come from diesel engines (Cass et al., 1998).

Combustion is a complex sequence of exothermic chemical reactions between a fuel (usually hydrocarbon) and an oxidant (usually oxygen). Complete combustion of a hydrocarbon fuel in the presence of oxygen yields carbon dioxide and water as final products. However, combustion processes are almost never complete. Incomplete combustion occurs when there is a lack of oxygen. Besides water and carbon dioxide, different carbonaceous compounds (e.g. carbon monoxide, soot) are found as products of incomplete combustion of hydrocarbon fuels. Additionally, if air is an oxidant, nitrogen can be oxidized to various nitrogen oxides. A more detailed description of the composition of combustion exhausts is given later (section 1.1.3).

1.1.2 Particulate matter in ambient air: physical and chemical characterisation

Physical characterisation of airborne particulate matter

Atmospheric aerosol comprises solid and liquid particulate matter suspended in air. Residence of the airborne particles depends on their size. Smaller particles can remain longer in the air than the larger ones. Based on their size, airborne particles can be categorised in several fractions (Table 1-1). This classification is a generally accepted convention which resulted from the collaboration of three international organisations: ISO (International Organisation for Standardisation), CEN (Comité Européen de Normalisation) and ACGIH (American Conference of Government Industrial Hygienists).

The PM₁₀ (particulate matter smaller than 10 µm) fraction of airborne particles can remain up to several weeks in the atmosphere (Harrison, 2004). This is a biologically relevant fraction of inhalable particles that can penetrate the respiratory system beyond the larynx (Donaldson and Stone, 2003). For these reasons, the PM₁₀ mass concentration in the air is used as an internationally accepted measure for particulate air pollution. Since 2005, EU legislation 1999/30/EC has set daily and annual limits for PM₁₀ mass concentrations in cities. According to this directive, daily average PM₁₀ concentration is limited to 50 µg/m³ and the annual daily average to 40 µg/m³. Also, the daily average limit for PM₁₀ should not be exceeded more than 35 days per year. The USA National Ambient Air Quality Standards have incorporated PM_{2.5} as an additional indicator for particulate air pollution since 1997. PM_{2.5} refers to the inhalable fraction of the PM which penetrates to the alveolar region of the lungs (Donaldson and Stone, 2003). Future EU standards will also include PM_{2.5} ambient concentrations as an additional measure for air quality. An EU directive adopted in 2008 (2008/50/EC) has set a PM_{2.5} annual daily average limit at 25 µg/m³. This value has to be achieved in urban areas of EU member states latest by 2015.

The importance of ultrafine particles (< 100 nm in size) as significant contributors towards general environmental pollution has been recognised only recently. Primary ultrafine ambient particles mainly originate from incomplete fuel combustion. Ultrafine particulate matter accounts for 1% to 20% of the total mass of airborne particles (US Environmental Protection Agency (EPA), 2002). Due to their small size, the number concentration (number of particles per unit volume) of the ultrafine particles in urban air can reach several hundred thousand per cm³ during high-pollution episodes

(Oberdörster 2001). Accordingly, ultrafine particles account for the majority (50-90%) of the total number concentration of airborne particles.

Different definitions for the term “nanoparticles” (NP) can be found in scientific literature. Airborne nanoparticles represent either particles with sizes smaller than 100 nm (Oberdörster et al., 2005) or smaller than 10 nm (D’Allesio et al., 1998; Sgro et al., 2003; Grotheer et al., 2007). In this study, the term ultrafine particles is used for particles smaller than 100 nm (Donaldson and Stone, 2003; Brown et al., 2004; Stoeger et al., 2006) and the term nanoparticles is used for ambient particulate matter smaller than 10 nm.

Table 1-1: Fractions of airborne particles according to their size

Name of the fraction		Size of the particles	Penetration in respiratory tract
PM ₁₀	thoracic fraction	< 10 µm	beyond larynx (thoracic region)
PM _{10-2.5}	coarse fraction	2.5 - 10 µm	beyond larynx (thoracic region)
PM _{2.5}	fine particles	< 2.5 µm	alveolar region
PM _{0.1}	ultrafine particles	< 100 nm	alveolar region
Nanoparticles		< 10 nm	alveolar region

Chemical composition of airborne particulate matter

A growing number of studies have investigated the chemical composition of PM₁₀ and PM_{2.5} in urban areas (Kuhlbusch et al., 1999; Silanpää et al., 2006; Bell et al., 2007). Recent studies focus more on the investigation of sources and chemical composition of PM_{2.5} than of PM₁₀. This is related to recent evidence on a strong correlation between PM_{2.5} and adverse health effects (Lanki et al., 2006; Pope and Dockery, 2006). Chemical composition of the airborne particulate matter exhibits spatial and temporal variation due to different contributions of local combustion sources and seasonal factors such as residential heating with coal and wood (Silanpää et al., 2006). According to a recent study (Silanpää et al., 2006) on the chemical composition of airborne particulate matter, most abundant constituents of PM_{2.5} in 6 urban sites under investigation were: carbonaceous matter (elemental carbon + organic carbon) and inorganic aerosol (sulphates, nitrates, and ammonium). Carbonaceous matter in PM_{2.5} originated mainly from combustion processes. While the proportion of elemental carbon in total PM_{2.5} varied only slightly among all tested

urban sites (6-9% of total PM_{2.5} mass), the organic carbon fraction varied significantly (15-38% of total PM_{2.5} mass). Secondary aerosol (sulphates, nitrates, and ammonium) is formed in the atmosphere from precursor gases (sulphur dioxide, nitrogen oxides and ammonia) via gas-to-particle phase conversions. On average, secondary inorganic aerosol accounted for about 40% of total PM_{2.5} mass in each of the investigated urban sites (Silanpää et al., 2006). However, the composition of a large fraction of the fine particulate matter (up to 20% of total PM_{2.5} mass) remains unknown (Silanpää et al., 2006).

Elemental carbon and organic carbon are two terms commonly used to describe the carbonaceous matter in the atmosphere which is produced during an incomplete combustion process (Merola et al., 2001). Organic carbon refers to a variety of organic compounds such as aliphatic, aromatic compounds etc. Elemental or black carbon is produced in a fuel-rich and incomplete combustion of hydrocarbons and is usually identified as soot (Sgro et al., 2001). Airborne soot is usually found in form of aggregates of hundreds or thousands of primary soot particles, each sized in the range of 10-30 nm (Sgro et al., 2003; Grotheer et al., 2004; Grotheer et al., 2007).

1.1.3 Chemical composition of combustion exhaust

Since diesel engines are one of the most significant pollutants in urban areas (Cass, 1998), chemical composition of diesel exhaust has been widely investigated. Diesel engine emissions consist of a wide range of organic and inorganic compounds in gaseous as well as particulate phases (Bünger et al., 2006). Concentrations of most diesel exhaust constituents depend on the type of engine, engine load, fuel properties and the effectiveness of an exhaust after-treatment.

Schauer et al. (1999) performed an intensive quantitative analysis of the organic compounds emitted by medium duty diesel-powered trucks. Table 1-2 summarizes the main groups of these organic compounds and their most abundant representatives. The organic compounds present in gaseous phase include alkanes, alkenes, aldehydes, monocyclic aromatic compounds, and polycyclic aromatic hydrocarbons (PAHs). Gas-phase species dominate the organic compound emissions from diesel engines (Schauer et al., 1999). Aldehydes, which represent the most significant fraction of the gaseous emissions from diesel engines, are particularly important because of their health effects. Acetaldehyde and formaldehyde are the most significant contributors to the aldehyde emissions from

diesel engines (Schauer et al., 1999). Among other gaseous components of diesel exhaust, benzene, PAHs, and nitro-PAHs are notable for their adverse health effects. So far, researchers have focused mainly on the particulate matter components for estimation of potential health risks associated with human exposure to diesel exhaust. Diesel particulate matter consists mainly of elemental carbon (50-75%), organic carbon (19-43%) and small amounts (1-2%) of sulphates, nitrates and metals (US Environmental Protection Agency, 2002). Large surface area of diesel particulate matter enables adsorption of organics from the diesel combustion process and/or the adsorption of additional compounds during transport in ambient air. Organic substances adsorbed on diesel particulate matter include C₁₄₋₃₅ hydrocarbon compounds, PAHs with more than or equal to 4 rings, and nitro-PAHs (US Environmental Protection Agency, 2002). PAHs and their derivatives (nitro-PAHs) comprise less than 1% of the mass of diesel particulate matter (US Environmental Protection Agency, 2002). PM_{2.5} mass emissions rate (in mg/km) for medium duty diesel-powered vehicles (Schauer et al., 1999) are much higher (20-fold) than for catalyst-equipped gasoline-powered motor vehicles (Schauer et al., 2002). This however does not hold true for the non-catalyst gasoline-powered motor vehicles, whose emissions are twice as high as those from diesel-powered vehicles. Diesel exhaust differs from gasoline-powered vehicle exhaust by its higher elemental carbon content (Schauer et al., 1999).

Table 1-2: Organic compounds present in diesel exhaust (from Schauer et al. 1999)

Group of compounds	Most abundant representatives and their concentrations
alkanes	butane (3 830 µg/km), isopentane (2 740 µg/km)
alkenes	ethene (8 560 µg/km)
aromatic hydrocarbons	toluene (3 980 µg/km), benzene (2 740 µg/km)
aldehydes	acetaldehyde (41 800 µg/km), formaldehyde (22 300 µg/km)
aromatic aldehydes	benzaldehyde (3 800 µg/km)

1.1.4 Laboratory flames as a model source of combustion generated particles

Diesel fuel is a complex mixture of aliphatic (75%) and aromatic hydrocarbons (25%). Aliphatic hydrocarbons of a common diesel fuel are molecules containing 10-25 carbon atoms (Schauer et al., 1999). Accordingly, the combustion of such mixture of diverse hydrocarbons gives rise to a high variety of combustion by-products. On the other hand, employment of defined gases (e.g. ethylene) as a fuel results in less complex combustion reactions and thus less complex mixture of by-products.

Laboratory flames are excellent sources of combustion generated particles since they operate at steady state and the combustion conditions can be easily controlled and varied (Sgro et al., 2003). For combustion research, ethylene is one of the commonly used fuels for laboratory flames and for generation and study of combustion generated particles (e.g. nanoparticles, soot).

In the last decade, there has been an increasing interest for investigation of combustion generated nanoparticles, as they may impose potential health hazards to living beings. Under laboratory conditions, nanoparticles have been detected in premixed ethylene/air flames (Minutolo et al., 1999). They are not only found in flame regions, where they act more or less as soot precursors, but also in the exhausts of flames (Figure 1-1), of diesel and of gasoline engines (Sgro et al., 2003; Grotheer et al., 2007; Merola et al., 2001). Although emissions of nanoparticles are relatively small on mass basis, their number concentrations exceed those of soot by almost two orders of magnitude (Sgro et al., 2003). Nanoparticles are believed to be distinct species that differ from soot particles in their chemical composition and in their UV-visible light absorption pattern. While soot displays a rather graphite-like structure, nanoparticles are thought to be comprised of aromatics with not more than 2–3 rings linked in a polymer-like way by aliphatic bonds (D'Alessio et al., 1998). In contrast to soot which absorbs in the visible range of the electromagnetic spectrum, nanoparticles are transparent to visible light and absorb only in the UV-range (Sgro et al., 2003). Due to their water solubility (Merola et al., 2001; Sgro et al., 2001; Sgro et al., 2003), nanoparticles can be trapped in aqueous suspensions and their concentration can be determined via their absorbance in the UV-range (Minutolo et al., 1999).

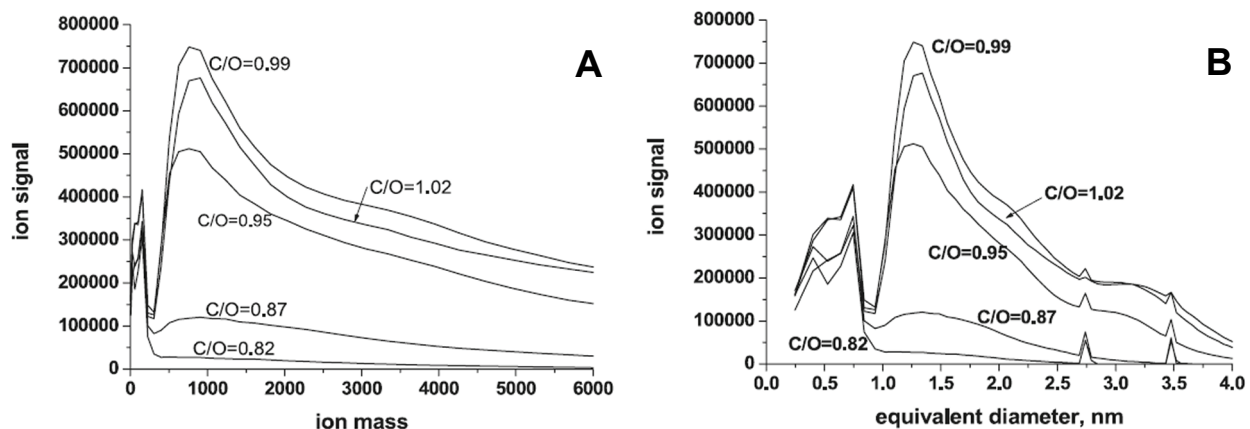


Figure 1-1: Detection of nanoparticles ($d < 10$ nm) in ethylene flame exhausts

Detection of combustion generated nanoparticles in ethylene flame exhausts by photo-ionization mass spectrometry is shown in figures A and B (Grotheer et al., 2004). Nanoparticles were gained during combustion of ethylene in a low pressure burner ($p=123$ mbar) at different combustion C/O ratios. Figure A shows the ion signals plotted as a function of mass, whereas figure B shows the same signals plotted as a function of equivalent diameter. For the calculation of equivalent diameter it was assumed that the particles are in form of spheres and that their density equals 1.2, which is considered as a typical density for "young" soot (Grotheer et al., 2004).

1.1.5 Health effects of airborne particles

Respiratory system as the main route of exposure to particulate matter

Human skin, digestive tract and respiratory tract are always in direct contact with the environment. Respiratory system is the most significant portal of entry for the airborne particulate matter (PM) and the increase in PM concentrations is associated with diverse detrimental respiratory effects. Distribution and deposition of the airborne particles in the respiratory tract mainly depends on particle size (Figure 1-2) and pulmonary clearance mechanisms. In general, the smaller the particle, the deeper it can travel into the airways.

Thoracic (PM_{10}) and coarse ($PM_{10-2.5}$) fractions of particulates pass larynx and penetrate trachea and bronchial regions of the lungs (Cormier et al, 2006). Mucociliary action of the upper respiratory tract is mainly responsible for the clearance of these PM fractions.

Fine ($PM_{2.5}$), ultrafine ($PM_{0.1}$) and nanoparticles reach the unciliated region of the respiratory tract (alveoli). Their clearance from the alveoli is mediated mainly by macrophage phagocytosis.

Due to their small size and their affinity for water (Merola et al., 2001; Sgro et al., 2001; Sgro et al., 2003), nanoparticles can easily overcome the alveolar-capillary barrier and enter the circulation. Then, they can be transported throughout the body to basically any target organ where they can exert hazardous effects.

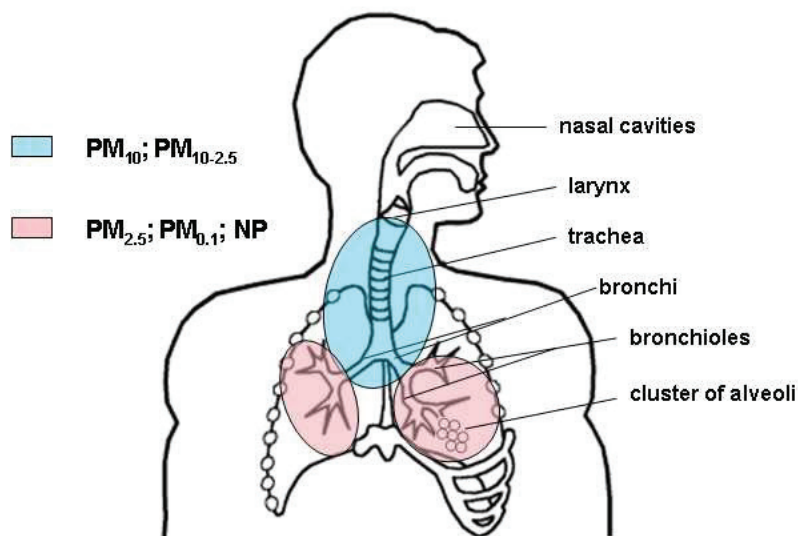


Figure 1-2: Distribution of different PM fractions in the respiratory tract

During respiration, PM_{10} and $\text{PM}_{10-2.5}$ fractions of ambient particles reach the trachea and bronchial region of the lungs. The smaller the particle, the further it can penetrate into the respiratory tract. Fine ($\text{PM}_{2.5}$), ultrafine particles ($\text{PM}_{0.1}$) and nanoparticles (NP) reach the lung alveoli.

Epidemiological studies

Over the last fifteen years, a growing number of epidemiological studies have shown significant associations between the concentration of ambient particulate matter (PM_{10} and $\text{PM}_{2.5}$) and adverse respiratory (asthma, lung cancer) and cardiovascular (atherosclerosis, cardiac arrhythmia, myocardial infarction) effects. Studies on acute health effects of PM show that an increase in daily average PM concentrations strongly correlates with increased daily mortality, use of medications, rate of hospital admissions and clinician visits for cardio-pulmonary diseases (von Klot et al., 2002; Lippmann et al., 2003). Several cohort studies have investigated chronic health effects of PM and have found a statistically relevant correlation between the long-term exposure to $\text{PM}_{2.5}$ and increased mortality rates (Dockery et al., 1993; Pope et al., 1995; Pope et al., 2002). In general, higher PM-associated health risks were observed among susceptible subpopulations including children, elder people and patients with pre-existing cardio-pulmonary diseases such as asthma, chronic obstructive pulmonary disease etc. The number concentrations of ultrafine airborne particles ($\text{PM}_{0.1}$) were shown by Peters et al. (1997) to be more strongly associated with respiratory malfunctions than number and mass concentration of PM_{10} and $\text{PM}_{2.5}$, respectively.

In addition to the adverse health effects shown in epidemiological studies, results on toxic and pro-inflammatory effects of ambient and model ultrafine particles have also

been reported from controlled clinical studies in humans, inhalation/instillation studies in animals, and *in vitro* cell culture systems (Oberdörster et al., 2005).

Uptake of airborne particles and mechanisms of their bioreactivity

Mechanisms underlying adverse respiratory and cardiovascular effects of airborne particles are still not fully understood. One hypothesis is that inhaled particles induce acute local pulmonary inflammation resulting in a systemic release of pro-inflammatory cytokines and chemokines, which may influence cardiovascular endpoints. In this model, induction of oxidative stress in cells is suggested to be a major mechanism for the pro-inflammatory effect of airborne ultrafine particles (Casillas et al., 1999; Xia et al., 2006). Increased oxidative stress is known to activate signalling pathways which lead to the expression of pro-inflammatory genes. The release of pro-inflammatory mediators into the systemic circulation causes a systemic inflammatory response in different extrapulmonary organs (heart, blood vessels etc.). This may give rise to atherosclerotic changes in blood vessels, to thrombogenesis, and to myocardial infarction. An alternative hypothesis considers that inhaled ultrafine particles can translocate from the lung alveoli into the circulation. Via the systemic circulation, they can then be transported throughout the body and thereby directly affect target organs (heart, liver, brain etc). Experiments with model ultrafine particles (elemental carbon, iridium, titanium dioxide etc.) have shown their lung-blood translocation and deposition in different organs such as liver, spleen and brain (Kreyling et al., 2002.; Nemmar et al., 2002; Oberdörster et al., 2002). According to some studies (Nemmar et al., 2001; Nemmar et al., 2002), transportation of ultrafine particles through the lung-blood barrier seems to be rapid (within several minutes). The reported lung-blood translocation efficiency was 25-30% of an applied inhalation dose (Nemmar et al., 2001). The deposition rates in the target organs (e.g. liver, spleen, brain) were up to 1-2% of an applied inhalation dose (Kreyling et al., 2002; Nemmar et al., 2001). There are also reports that inhaled ultrafine particles may be translocated via the olfactory nerve into the brain at 20% translocation efficiency (Oberdörster et al., 2004).

To date, the mechanisms by which ultrafine particles penetrate the cell membrane are not completely clear. Some researches suggest that the uptake of ultrafine particles by a cell does not involve any active type of transport (Nemmar et al., 2001; Nemmar et al., 2002). More likely, ultrafine particles penetrate a cell membrane by a passive transport mechanism such as diffusion (Nemmar et al., 2001; Geiser et al.,

2005). Transportation via diffusion implies that the particles are not being coated by cell membrane and have direct access to intracellular proteins, organelles, and DNA. Besides reports on passive cellular uptake, there are also studies describing active transport of ultrafine particles via phagocytosis (Saxena et al., 2008) or via other types of endocytosis (pinocytosis, clathrin-mediated cytosis). These data are from the studies that have investigated different types of model ultrafine particles (titanium dioxide particles, $d=22$ nm; albumin particles labelled with radioactive technetium, $d\leq 80$ nm; carbon black particles, $d=12$ nm; etc.). Accordingly, this indicates that the mechanism of cellular uptake of particles may depend on the specific particle properties such as size, shape and chemical composition.

1.1.6 Toxicologically relevant properties of the airborne PM

Despite intensive investigation, uncertainty remains concerning the constituents and characteristics of airborne particulate matter responsible for the observed detrimental health effects (Bell et al., 2007). It is still under question which dose metric (mass, size, number, or surface area) is the most relevant for the toxic effects of PM. Determination of the parameter which can serve as a relevant measure for the applied dose can be very useful in understanding the mechanisms of the PM bioreactivity.

As already mentioned, mass concentrations of thoracic (PM_{10}) and fine ($PM_{2.5}$) fractions of the airborne particulate matter are used as metrics for the air quality regulations. Some epidemiological studies (Peters et al., 1997) as well as *in vitro* toxicological studies (Li et al., 2003) attribute the hazardous health effects predominantly to the ultrafine fraction ($PM_{0.1}$) of the airborne particulate matter. Considering the health impact of such small-sized particles, their high number concentrations in the air and their large surface area, the use of weight metric as the only relevant dose metric of exposure to airborne particulates raises doubts. Size seems to play an important role, since it was found that for the same mass concentration, inflammatory response increases with decreasing particle size (Peters et al., 1997; Oberdörster, 2000). Metrics such as particle number concentration (Peters et al., 1997; Wittmaack, 2007) and particle surface area (Oberdörster, 2000; Oberdörster, 2005; Stoeger et al., 2006) have been recently suggested as more suitable metrics for the estimation of the toxicological potency of airborne particles. Since the number concentration of ultrafine particles is generally several orders of

magnitude higher than that of larger particles, ultrafine particulate matter offers a much bigger total surface area per mass unit. Large surface area implicates that larger number of exposed chemically reactive groups may interact with diverse cellular structures. Accordingly, increased surface reactivity may lead to protein denaturation, membrane damage and DNA cleavage (Xia et al., 2006). In addition, due to their vast surface area these particles can serve as carrier for diverse, potentially toxic adsorbed compounds.

In their attempts to determine the toxicologically most relevant dose metric for the ultrafine airborne particles, researchers have often used different model particles of known size and chemistry, such as carbon black particles (Stoeger et al., 2006) and titanium dioxide (Oberdörster, 2000; Oberdörster, 2005). Thereby, very complex and heterogeneous chemical composition of the airborne particles was neglected. Combustion generated particles (e.g. diesel exhaust particles) consist of a large amount of elemental carbon (50-75%), located in the core of the particles (US Environmental Protection Agency, 2002). Usually, the core of the particles is coated with different organic (aliphatic hydrocarbons, PAHs, etc.) and inorganic compounds (sulphates, nitrates, metals). Rising number of studies suggest that the pro-inflammatory and cytotoxic effect of the airborne particulate matter is most likely due to its organic component (Li et al., 2000; Li et al., 2003; Vogel et al., 2005). These findings implicate that organic content may be a proper metric for toxicity assessment of airborne particles. Organic component of PM either contains, or can be metabolised to species such as quinones which can take part in redox cycling reactions in cells to produce reactive oxygen species (Li et al., 2003; Xia et al., 2006). Redox active quinones can be produced via biotransformation of PAHs (Li et al., 2003). There are also reports that transition metals which are adsorbed to the outer surface of the airborne particles may contribute to their reactivity and oxidative potency (Donaldson and Stone, 2003; Pagan et al., 2003).

1.2 Toxicity

Toxicity is the ability of a certain agent to cause injuries to a living cell or organism. One of the primary goals in toxicology is to study the relationship between exposure and harmful effects of a certain agent. Toxic agents can be classified as physical (radiation, heat), chemical (diverse inorganic and organic substances) or biological (viruses, bacteria). Regardless of the type of a toxin, toxic effects are always dose-

dependant. Paracelsus' (1493-1541) quote "the dose makes the poison" implicates that any agent can exhibit toxic effects when it is applied in excessive doses. Many factors can affect the toxicity of a certain substance such as the physical form of the toxin (solid, liquid, or gas), the pathway of administration (inhalation, ingestion, injection etc.), the time of exposure (short-term or long-term), the number of exposures (a single dose or multiple doses over time) and many others. Acute toxicity is a result of a single exposure (acute exposure) to high doses of a toxic substance. Chronic toxicity implies an effect of a repeated exposure to relatively low concentrations of a toxin over an extended period of time (chronic exposure). Chronic exposure may last for months or years. For the assessment of acute toxicity of a given agent, lethality is usually the main effect of interest. LD₅₀ (lethal dose) or LC₅₀ (lethal concentration) are measures of acute toxicity that are used for the assessment of the toxic effects on the population of cells or organisms. Lethal dose (LD₅₀) is an estimated single dose of a given agent that kills 50% of test organisms. Similarly, lethal concentration (LC₅₀) is a concentration of a certain agent that in a given time of exposure causes lethality in 50% of tested cells or organisms. LD₅₀ is usually used as a measure of toxicity in the *in vivo* experiments that involve direct administration (oral, intravenous, dermal) of a tested substance in test animals. However, in *in vivo* inhalation experiments, the concentration of a substance in the air (LC₅₀) is typically used for the lethality assessment (Leeuwen and Vermeire, 2007). In *in vitro* experiments, it is more justified to use LC₅₀ than LD₅₀ as a measure, since cells are exposed to a certain concentration of a substance which is diluted in cell culture medium.

1.2.1 Genotoxicity

Physical or chemical toxins that damage genetic material of an exposed cell are considered genotoxic. DNA damages can either be repaired with no further consequences for the cell or they may remain unrepaired. Unrepaired DNA lesions can lead to cell death or can induce error-prone repair pathways (e.g. SOS response in bacteria) which lead to mutagenesis. In multicellular organisms, mutations which occur in somatic cells can cause cell death or cancer, whereas DNA changes in germ-line cells can be transferred to the next generation and can contribute to various hereditary diseases.

1.2.2 Cytotoxicity

Cytotoxicity is the ability of a certain agent to damage or kill a cell by impairing its metabolism and preventing its growth and proliferation. The most common endpoints considered in the cytotoxicity assessment are those related to cell viability, cell proliferation, cell membrane integrity and ATP content. One example of the cytotoxic effect is the impairment of the cell metabolism due to deleterious effects on mitochondria. The consequential ATP depletion causes inhibition of all energy-dependant processes in cells, which consequently triggers cell death.

1.2.3 Test-systems for toxicity assessment

For toxicity assessment, bacterial tests are useful pre-screening methods due to their simplicity, rapidity and low costs. Commonly used bacterial tests for the assessment of genotoxicity are: the Ames test (Ames et al., 1973), the umu test (Oda et al., 1985), and the SOS chromotest (Quillardet et al., 1982). Results from such bioassays are used to predict the mutagenic and carcinogenic hazards posed to living organisms. The SWITCH test is a rather novel bacterial assay for the concomitant assessment of genotoxic- and cytotoxic potency of a given agent. It was developed by the Cellular Biagnostics research group of the Radiation Biology Division at the German Aerospace Centre (DLR) in Cologne. This test has been successfully applied for the toxicity assessment of diverse physical and chemical agents (Stojicic et al., 2005; Baumstark-Khan et al., 2005).

For *in vitro* cytotoxicity testing on mammalian cells, various bioassays are being employed. Some of those assays use dyes which can only enter dead cells with damaged membranes (e.g. Trypan blue assay). Other tests detect metabolically active cells by assessing the mitochondrial dehydrogenase activity (e.g. MTT test).

1.3 Cell death: types and mechanisms

Apoptosis and necrosis are two morphologically and biochemically different modes of cell death.

Apoptosis, also known as programmed death, has an important role in the development of embryonic and adult tissues, in the resolution of tissue injuries and in the homeostasis of the immune system (negative selection of self-reactive immune cells). Apoptosis is an evolutionary conserved physiological process by which the

organism eliminates cells which are no longer needed during tissue development as well as senescent, abnormal and potentially harmful cells. In addition, in many stress conditions (e.g. exposure to a toxic agent), cells can also undergo apoptosis. The term “apoptosis” (apoptosis gr.- falling of leaves) was first used by Kerr et al. in 1972 when he described a morphologically distinct form of cell death characterised by cell shrinkage, chromatin condensation and fragmentation, blebbing of the plasma membrane and finally fragmentation of a cell into “apoptotic bodies”. Since the apoptotic bodies have an intact membrane, leakage of the intracellular content into the surrounding tissue and subsequent inflammation are prevented. Apoptotic cells are usually recognised and phagocytosed by macrophages. Apoptosis can be induced by various stimuli such as hormones, cytokines, growth factors, viruses and toxins (Zhang et al., 2004). Once the cell receives an apoptosis-inducing signal, a cascade of events occurs that eventually leads to cell death. Key effector components of the apoptosis are caspases. Caspases (cystein-dependant aspartate-specific proteases) comprise a family of proteases which cleave their substrates after aspartate residues (Vaux and Korsmeyer, 1999). To date, 14 members of this protein family have been identified in mammals. In living cells, caspases exist as inactive proteins (zymogens). Caspase zymogens, also known as procaspases, share a similar structure composed of an N-terminal prodomain followed by a large (~20 kDa) and a small (~10 kDa) subunit. During the conversion of a procaspase into its active form, two cleavages occur: one separates the prodomain from the large subunit and another separates the large from the small subunit. The activated form of a caspase is a heterotetramer consisting of two big and two small subunits. According to their role in apoptosis, caspases can be classified as initiator- and effector caspases. Upon activation via autocatalytic cleavage, initiator caspases (e.g. caspase-8, 9) activate the effector caspases. Once activated, effector caspases (e.g. caspase-3, 7) catalyse proteolytic cleavage of their target proteins. The substrates of effector caspases are diverse proteins which have crucial roles in cell survival, or which are involved in the organisation and maintenance of cell structures (DNA, cytoskeleton). The cleavage of fodrin for example, leads to the breakage of the link between the actin skeleton and the plasma membrane which contributes to cell blebbing during apoptosis (Martin et al., 1995). Currently, two main signalling pathways are recognised that lead to apoptosis: the extrinsic or receptor mediated pathway and the intrinsic or mitochondrial pathway. The extrinsic pathway involves activation of cell membrane-located “death receptors” which belong to the TNF- α (tumour necrosis

factor alpha) receptor family. Subsequent signalling events include the activation of the initiator caspase (caspase-8), which is further responsible for the activation of the effector caspase-3 and caspase-7. Cell stress can trigger the intrinsic apoptotic pathway which involves the release of apoptogenic factors from the mitochondria into the cytoplasm. Cytochrome c is one of the apoptogenic factors which are responsible for the activation of pro-caspase-9. Active caspase-9 can consequently trigger the caspase cascade by activating downstream effector caspases such as caspase-3 and caspase-7.

Necrosis is a pathological form of cell death, which occurs after injuries or after excessive contact with cytotoxic agents. Unlike apoptosis, necrosis is characterised by the induction of an inflammatory response due to cellular swelling followed by a burst of the plasma membrane and the release of the cellular content into the surrounding tissue. In contrast to apoptosis, necrosis does not follow a designated molecular pathway.

Although apoptosis and necrosis were originally described as two alternative forms of cell death with well-defined morphological and biochemical differences, rising experimental evidence suggests that they should be rather considered as two extreme ends of a wide spectrum of possible death programmes (Nicotera et al., 1998; Tang et al., 2008). Other types of cell death include apoptosis-like programmed cell death and necrosis-like programmed cell death (Leist and Jäättelä, 2001). The separation between apoptosis and necrosis death programmes is not always clear. It has been also demonstrated that apoptotic cells that fail to be recognised and phagocytosed by macrophages may undergo secondary necrosis (Sanders and Wride, 1995).

1.4 Activation of NF-κB in response to stress

Nuclear factor κB (NF-κB) is a transcription factor involved in many cellular processes such as cell proliferation, cell differentiation, inflammation and immune response. NF-κB proteins are homo- or heterodimers composed of the members of the “Rel protein family”, which includes p50 (NF-κB1), p52 (NF-κB2), Rel (c-Rel), p65 (RelA) and RelB. All of these proteins possess a “Rel homology domain” which is responsible for dimerisation, binding to DNA and interaction with NF-κB inhibitory proteins IκBs (Ali and Mann, 2004). In an inactive state, NF-κB resides in the

cytoplasm, sequestered in the NF-κB/IκB complex. IκB (IκB-α, IκB-β, IκB-ε, IκB-γ, Bcl3, p100 or p105) masks the nuclear localisation sequence on NF-κB and consequently prevents the NF-κB from translocation to the nucleus. An essential step in the activation of NF-κB signalling pathway is the phosphorylation of IκB proteins by IKKs (IκB-kinases). Phosphorylation of the IκB leads to the polyubiquitination of the IκB and its subsequent degradation by the 26S proteasome (Karin and Ben-Neriah, 2000). Liberated NF-κB molecules translocate to the nucleus where they bind to the NF-κB responsive elements (“κB sites”) in the promoter or enhancer regions of the target genes. The “κB sites” have been characterised in the promoters and enhancers of over 150 genes (Pahl, 1999) and some of them are listed in Table 1-3.

NF-κB pathway can be induced by a variety of external or internal stimuli including: physical stress (e.g. radiation), chemical stress, pro-inflammatory cytokines and viral/bacterial infection (Ali and Mann, 2004). NF-κB has one of the key roles in the regulation of cell stress responses, particularly oxidative stress response (Wang et al., 2002). Reactive oxygen species (ROS) are produced in any metabolically active cell as a result of the incomplete reduction of oxygen during respiration. During oxidative stress, the level of the ROS (superoxide anion, hydroxyl radical and hydrogen peroxide) in the cell exceeds the cellular anti-oxidative defence capacity. As a consequence, the ROS may cause damage to diverse cellular molecules. Besides that, ROS act as signalling modulators at concentrations well below those that cause the oxidative damage (Unfried et al., 2007). Induction of oxidative stress is suggested to be a mechanism for the cellular toxicity of airborne ultrafine particles (Li et al., 2003; Xia et al., 2006) and of combustion generated particles in particular (Casillas et al., 1999; Li et al., 2000). Airborne particles in the nano-size range are considered very potent inducers of oxidative stress, especially due to their large surface area. It is believed that the reactivity of the surface area itself, or the species (transition metals, organics) which are adsorbed to the outer surface of the particles may contribute to the reactivity and oxidative potency of airborne particles (Donaldson and Stone, 2003; Borm et al., 2006). Either the generation of ROS and/or the direct particle interaction stimulate a release of calcium ions from the endoplasmatic reticulum stores into the cytoplasm (Stone et al., 2000). Intracellular calcium and ROS activate redox-sensitive transcription factors such as NF-κB. Activation of NF-κB and its translocation to the nucleus upon treatment of human monocytes with ultrafine carbon black particles was shown by Brown et al. (2004).

Dose-dependant activation of NF-κB signalling pathway was also reported in U-937 cells treated with cigarette smoke condensate (Anto et al., 2002). Induction of the NF-κB signalling pathway leads to the expression of many genes involved in the inflammatory processes (Table 1-3). Activation of NF-κB causes also the up-regulation of IκB transcription, which is important for the termination of the signal. However, continuing presence of a certain NF-κB inducing agent can lead to an auto-activating loop as the NF-κB-induced up-regulation of pro-inflammatory cytokines acts itself as a positive feedback on NF-κB activation (Ali and Mann, 2004). By this way, a disease may ensue as a consequence of a prolonged activation of NF-κB signalling pathway. Pathological conditions including cancer (Tai et al., 2000), systemic inflammatory respiratory syndrome, asthma (Barnes and Adcock, 1998), cystic fibrosis (Christman et al., 2000), arthritis (Foxwell et al., 1998), and heart diseases have been linked to the inappropriate regulation of NF-κB. Increased activation of NF-κB has also been observed in *in vitro* or *in vivo* exposures to asbestos (Simeonova et al., 1997), residual oil fly ash (Quay et al., 1998), and diesel exhaust particles (Baeza-Squiban et al., 1999), which suggests that NF-κB-related events contribute to the pathogenesis of occupational and environmental diseases.

Table 1-3: NF-κB target genes and their roles

Genes coding for		Role in
cytokines:	IL-1β, IL-6, TNF-α	immune response, inflammatory response
chemokines:	IL-8, MCP-1	
acute phase proteins:	C-reactive protein	
adhesion molecules:	ICAM-1, VCAM-1	
pro-inflammatory enzymes:	iNOS, COX-2	
regulators of apoptosis:	XIAP, Bcl-2	cell survival
NF-κB-inhibitory proteins:	IκBα (NF-κBIA)	termination of NF-κB activation

As it can be seen in Table 1-3, besides the expression of genes involved in the inflammatory and stress response, NF-κB also regulates the expression of genes involved in apoptosis. Both, an anti-apoptotic (Wang et al., 1996; Liu et al., 1996) and a pro-apoptotic role of NF-κB (Ryan et al., 2000) have been reported so far. One possible explanation for this apparent dual role of NF-κB could be that certain stimuli

may alter the pattern of post-translational modifications of the NF-κB subunits and subsequently modulate their transcriptional potential (Janssens and Tschopp, 2006). The anti-apoptotic activity of NF-κB is based on up-regulation of the anti-apoptotic target genes (e.g. Bcl-2, XIAP). A reduced or completely suppressed transcriptional potential of the NF-κB subunits leads to a repression of anti-apoptotic target genes' expression which could be an explanation for the pro-apoptotic role of NF-κB (Janssens and Tschopp, 2006).

1.5 Aims of the research

Combustion exhausts emitted from traffic and industry sources represent one of the main contributors to the air pollution in urban areas. Urban air pollution has been associated with increased mortality and cardiorespiratory morbidity (von Klot et al., 2002; Lippmann et al., 2003). Investigation on the toxic effects of combustion by-products is very important considering their elevated ambient concentrations in highly populated urban sites.

It was the aim of the current study to contribute to the knowledge concerning the toxicity of the combustion exhausts and especially of the combustion generated soot particles. The exhausts that were studied in this thesis originated from a model combustion system (ethylene/oxygen flame) and from a practical combustion system (diesel combustion). Combustion exhausts were collected in cool traps in the form of condensates. Such combustion condensates were mixed with a medium and applied to different cell models (bacterial cells, human cell lines). Within the toxicity assessment, one of the objectives was to determine the effects of the combustion condensates on cell viability. In order to elucidate the toxic effects of the combustion condensates, the following steps were performed:

- Characterisation of the combustion condensates originating from either model flame exhaust or from diesel exhaust.
- Determination of the biologically relevant concentration range of the combustion condensates with a bacterial pre-screening assay (the SWITCH test).

- Assessment of the toxicity of combustion condensates on the human lung epithelial cell line (A-549) as a model for lung epithelial cells.
- Assessment of the toxic effects of combustion condensates on the human monocyte-like cell line (U-937) as a representative of the extrapulmonary targets.

Mechanisms of the combustion condensates' toxic effects were studied on the human cell lines. One of the hypothesised mechanisms is that combustion by-products exhibit their deleterious effects by activating NF-κB signalling pathway. NF-κB is a transcription factor which regulates the expression of various genes involved in the inflammatory responses, in cell proliferation and in apoptosis (Ali and Mann, 2004). Activation of the NF-κB signalling pathway may have an anti-apoptotic (Wang et al., 1996; Liu et al., 1996) or a pro-apoptotic effect (Ryan et al., 2000), depending on a type of a cell and on an external stimulus that the cells are exposed to.

Investigation of the mechanisms of the combustion condensates' toxic effects included the following steps:

- Determination of the effects of combustion condensates on cell cycle and on the induction of apoptosis.
- Analysis of the activation of NF-κB pathway in the presence of combustion condensates by developing a recombinant cell line carrying an EGFP reporter protein under control of NF-κB-responsive elements.
- Analysis of the NF-κB activation by the combustion condensates via examining the changes in the NF-κB target genes' expression patterns.
- Analysis of the correlation between the NF-κB pathway activation and apoptosis induction by using NF-κB inhibitors. Thereby it was the aim to elucidate whether the activation of the NF-κB signalling pathway in the cells treated with combustion condensates has a pro- or anti-apoptotic effect.

2 Material and Methods

2.1 Material

2.1.1 Laboratory equipment

Analytical scale	AG 285, Metler, Toledo, Spain
Autoclave	Tecnoclav 50, Tecnomara Deutschland, Fernwald, Germany
CCD-camera	CellCam Color, Phase, Lübeck, Germany
Centrifuges	- Megafuge 1.0 R, Heraeus, Munich, Germany - Ultracentrifuge, Optima LE-80K, Beckman Coulter, Munich, Germany
Cryogenic freezer (-195°C)	GT 140, L'air liquide, Paris, France
Flow cytometer	FACScan, Becton Dickinson, San Jose, USA
Freezer (-80°C)	HFC386PLUS-V12, Heraeus, Munich, Germany
Incubator	Function Line, Heraeus, Munich, Germany
Laminar airflow clean bench	Herasafe, Kendro, Berlin, Germany
Microscopes	- light microscope: Axiovert 25, Zeiss, Cologne, Germany - fluorescence microscope: Axiovert 135, Zeiss, Cologne, Germany - el. microscopes: 3000F FEG, JEOL, Tokyo, Japan; TECNAI F30, FEI, Hillsboro, USA - Multilabel Counter 1420 Victor ² , EG&G Wallac, Perkin Elmer, USA - Lambda Fluoro 320, MWG Biotech, Ebersberg, Germany
Microtitre plate readers	BioAnalyzer 2100, Agilent Technologies, Palo Alto, USA
RNA/DNA/Protein-analyser	Multitron, Infors AG, Bottmingen, Switzerland
Shaking incubator	KL2, Edmund Buehler, Tübingen, Germany
Shaker	U-3310, Hitachi, Tokyo, Japan
Spectrophotometer	- TRIO-Thermoblock, Biometra, Göttingen, Germany
Thermocyclers	- Opticon2, MJ Research, Bio-Rad, Munich, Germany
Total organic carbon (TOC)-analyser	Dohrmann DC-190, Rosemount Analytical, Irvine, USA
Vortex	Vortex Genie-2, Scientific Industries, New York, USA
Water bath	Koettermann, Uetze-Hänigsen, Germany

2.1.2 Consumable material

Cell culture flasks: 25 cm ² , 75 cm ²	BD Falcon, Franklin Lakes, USA
Centrifuge tubes: 15 ml, 50 ml	Nunc, Wiesbaden, Germany
Cover slips (d=12 mm)	Menzel-Gläser, Braunschweig, Germany
Cryovials	Nunc, Roskilde, Denmark
FACS tubes (5 ml)	BD Falcon, Franklin Lakes, USA
Filters (0.6 µm pore size)	MN 85/70, Macherey-Nagel, Düren, Germany
Filters (100 nm, 20 nm pore size)	Anotop 10 Plus, Whatman, Maidstone, UK
Immersion oil	Immersol 518 F, Zeiss, Cologne, Germany
Injection needles	B. Braun, Melsungen, Germany
Inoculating loops	Nalgene, Rochester, NY, USA
Microscope slides (76 x 26 cm)	Superfrost, Menzel-Gläser, Braunschweig, Germany
Microtiter 96-well plates	Isoplate-96, PerkinElmer, Boston, USA
Microtiter 96-well strip plates	Costar, NY, USA
Parafilm	Nescofilm, Roth, Karlsruhe, Germany
Pasteur glass pipettes	Brand, Wertheim, Germany
Petri dishes (d=3.5 cm)	Nunc, Wiesbaden, Germany
Petri dishes (d=9.4 cm)	Greiner Bio-One, Frickenhausen, Germany
Plates with 6 wells or 24 wells	BD Falcon, Franklin Lakes, USA
Reaction tubes 0.5 – 2 ml	Eppendorf, Hamburg, Germany
Round bottom tubes (14 ml)	BD Falcon, Franklin Lakes, USA
Syringes (2 ml,10 ml)	B. Braun, Melsungen, Germany
Ultracentrifuge tubes	Ultra-clear #344057, Beckman Coulter, Germany

2.1.3 Chemicals

All chemicals were purchased at Sigma-Aldrich (Steinheim, Germany) except for the ones listed below.

Agarose	Serva Electrophoresis, Heidelberg, Germany
Amphotericin B	Biochrom AG, Berlin, Germany
DNA loading dye (6x)	Fermentas, Burlington, Canada
Ethanol	Merck, Darmstadt, Germany
Fluorescent mounting medium	Dako, Carpinteria, USA
Formaldehyde (37% w/w solution)	Scharlab, Barcelona, Spain
FuGene 6	Roche Diagnostics, Mannheim, Germany
Geneticin (G418 sulfate)	Calbiochem, Darmstadt,Germany
Methanol	KMF Laborchemie GmbH, Lohmar, Germany
MG-132	Calbiochem, Darmstadt, Germany
Neomycin/bacitracin	Biochrom AG, Berlin, Germany
Penicillin/streptomycin	Biochrom AG, Berlin, Germany
RNase A	Roche Diagnostics, Mannheim, Germany
TNF-α (human recombinant)	Peprotech, Rocky Hill, USA
Trypsin/ ethylenediaminetetraacetic acid (EDTA) solution (10x)	Biochrom AG, Berlin, Germany
(0.5% / 0.2% (w/v) in 10x phosphate buffered saline (PBS))	

2.1.4 Media, buffer and sera

Foetal bovine serum (FBS)	Biochrom AG, Berlin, Germany
Luria Bertani (LB)-agar	Sigma-Aldrich, Steinheim, Germany
LB-broth	Sigma-Aldrich, Steinheim, Germany
Minimal essential medium (MEM)-	Gibco, Scotland, UK
alpha culture medium	

2x LB-medium: 40 g LB-broth
 1 l deion. H₂O
 (autoclave at 121°C for 20 min)

5x PBS: 80 g NaCl
 2 g KCl
 14.4 g Na₂HPO₄ x 2H₂O
 2 g KH₂PO₄
 ad 2 l deion. H₂O
 (autoclave at 121°C for 20 min)

The 1x PBS solution was prepared by diluting (1:5) the 5x PBS solution in deion. H₂O.

2.1.5 Test samples

Ethylene and diesel combustion samples were produced at the Institute of Combustion Technology (DLR, Stuttgart). The method of production is described in chapter 2.2.1.1. For high resolution transmission electron microscopic (HRTEM)-analysis and spectrophotometry, carbon black was used as a model soot. For this purpose, carbon black (Printex 90, Degussa, Frankfurt, Germany) containing primary particles of 14 nm average size was used. Carbon black was gained via furnace process (burning of oil at 50% air). For the experiments, carbon black was suspended in deionised water.

2.1.6 Commercial reaction kits

Annexin V- phycoerythrin (PE)	BD Biosciences Pharmingen, Heidelberg, Germany
Apoptosis Detection Kit I	Agilent Technologies, Palo Alto, USA
Agilent RNA 6000 Nano Reagents	Bio-Rad, Munich, Germany
iScript cDNA-Synthesis Kit	Invitrogen, Karlsruhe, Germany
Platinum SYBR-Green qPCR SuperMix-UDG	BD Biosciences Pharmingen, Heidelberg, Germany
PE-conjugated monoclonal active caspase-3 antibody apoptosis kit	Qiagen, Hilden, Germany
RNeasy Plus Mini Kit	

2.1.7 Bacterial strain

S. typhimurium TA1535 pSWITCH

S. typhimurium TA1535 pSWITCH strain was established in the Radiation Biology Division of German Aerospace Centre by transforming the *S. typhimurium* TA1535, one of the tester strains in the Ames test battery (Ames et al., 1973), with the pSWITCH plasmid (Baumstark-Khan et al., 2005). This bacterial strain was already used for rapid genotoxicity and cytotoxicity testing in various studies (Baumstark-Khan et al., 2005; Stojicic et al., 2005, Rabbow et al., 2006).

2.1.8 Human cell lines

A-549

A-549 (CCL-185, ATCC, Manassas, VA) is a human lung epithelial cell line originating from 58-year old male Caucasian patient with lung carcinoma. It is an adherent cell line that has properties of type II alveolar epithelial cells (Lieber et al., 1976).

U-937

U-937 (CRL-1593.2, ATCC, Manassas, VA) is a human neoplastic cell line originating from a 37-year old male Caucasian patient with histiocytic lymphoma (Sundström and Nilsson, 1976). It is a suspension cell line that shows the morphology of monocytes.

2.2 Methods

2.2.1 Generation and analysis of combustion condensates

2.2.1.1 Generation of combustion condensates

Ethylene- and diesel combustion condensates were generated at the Institute of Combustion Technology (DLR, Stuttgart). For their production, combustion exhaust gases were conducted through three sequentially positioned cool traps (glass bottles cooled by liquid nitrogen) where the combustion exhausts were retained in frozen state (Figure 2-1). After thawing at room temperature, each cool trap was rinsed with distilled water to obtain a combustion sample of 5 ml volume in total. Afterwards, the samples were filtrated through a glass fibre filter (pore size=0.6 µm) in order to remove big soot agglomerates. Subsequently, the organic carbon content of the samples was measured in the TOC-analyser. Filtrated samples were used as stock solutions for the experiments.

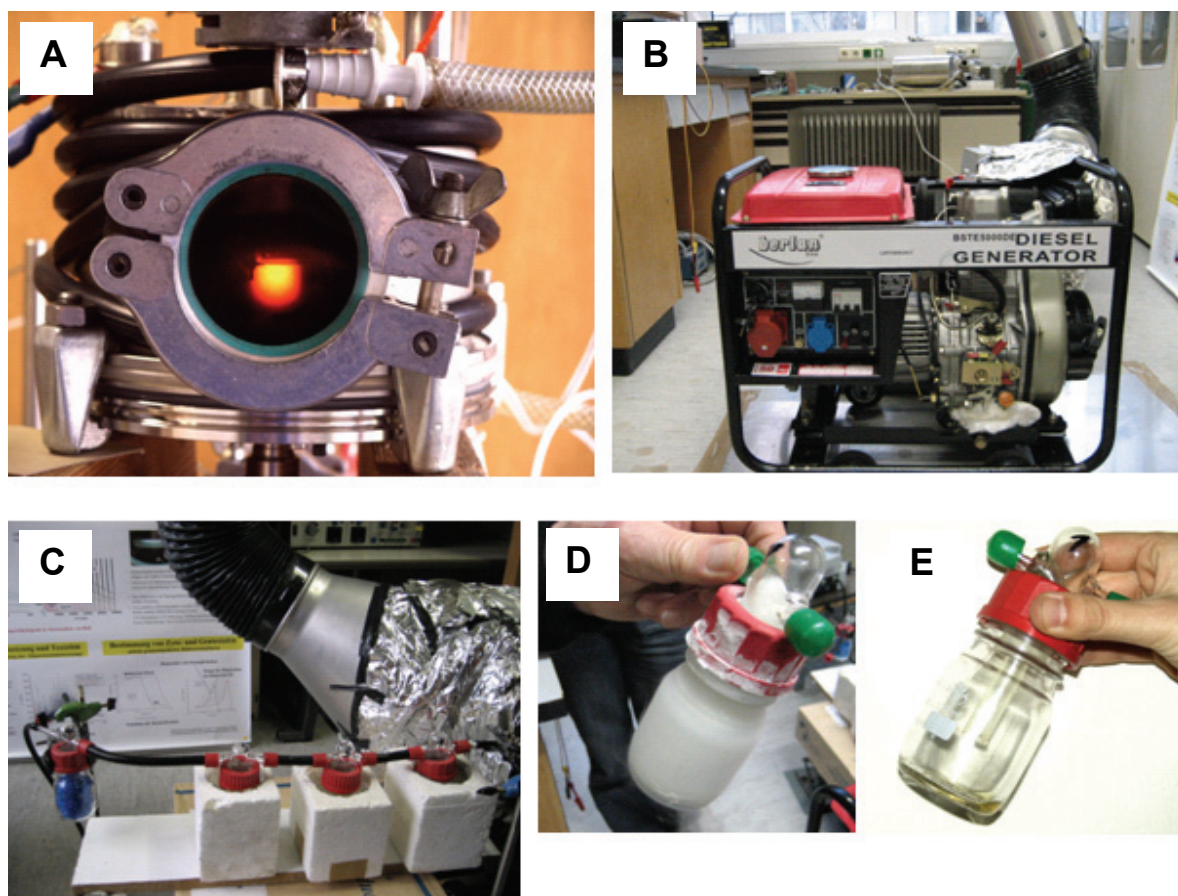


Figure 2-1: Production of ethylene- and diesel combustion condensates

Low pressure burner (A) was utilised for ethylene combustion. Diesel generator (B) was used for the production of diesel combustion condensates. In both cases, exhaust gases were collected in frozen state in three sequentially positioned cool traps (C). Figure also shows the first cool trap with diesel combustion condensate before (D) and after thawing (E) at room temperature.

Ethylene combustion

It is important to explain some of the combustion-specific terminology prior to giving a detailed description of the generation of ethylene combustion samples. The carbon/oxygen ratio (C/O ratio) is a parameter which is used to describe the quality of combustion. The C/O ratio is the relation between the number of carbon and oxygen atoms in a fuel/oxygen mixture. Stoichiometric combustion is the ideal combustion process in which the fuel is burned completely. Stoichiometric combustion for the ethylene/oxygen flames is achieved at C/O=0.33. This value can be calculated from the chemical reaction of ethylene oxidation ($C_2H_4 + 3O_2 \rightarrow 2CO_2 + 2H_2O$), by dividing the number of C atoms in ethylene with the number of oxygen atoms (2/6=0.33). In the case of „fuel-rich“ flames, the actual C/O ratio is larger than the stoichiometric C/O ratio, whereas „fuel-lean“ flames occur at C/O ratios smaller than the stoichiometric ones. Soot is one of the products of the incomplete combustion of hydrocarbon fuels. Sooting threshold is the lowest combustion C/O ratio at which the soot generation occurs. The sooting threshold value is fuel-specific and depends on several parameters such as pressure and temperature. According to Grotheer et al. (2004), the sooting threshold for low-pressure ethylene/oxygen flames is achieved at C/O=0.72. A flame is considered heavily or highly sooting when it operates at C/O ratio values high above the sooting threshold.

For the purpose of this thesis, combustion of ethylene/oxygen mixtures was performed in low pressure burner at 1.6×10^4 Pa (160 mbar). Construction of the burner was thoroughly described elsewhere (Grotheer et al., 2004). Ethylene flame was stabilised on a porous sinter plate (2.5 cm in diameter), which ensured the homogeneity of the flame and required small gas flows so that the burner heat (up to 1000°C) was handled easily. Ethylene was burnt under different C/O ratios, ranging from C/O=0.63 to C/O=0.93. The C/O ratio was varied by keeping the total gas flow constant and varying the individual flows of ethylene and oxygen gases. Exhaust gases were sucked through a sampling nozzle (d=1 mm) which was 37 mm away from the burner. For the sample preparation 10 litres of exhaust gas were drawn under constant flow rate (0.4 l/min). Highly sooting flame (C/O=0.93) caused clogging of the sampling nozzle and only 8 litres of exhaust gas were drawn in this case.

One **production series** included generation of samples under following burning conditions: C/O=0.63, C/O=0.68, C/O=0.73, C/O=0.78, C/O=0.83, C/O=0.88 and C/O=0.93. For each production series, each C/O ratio resulted in three combustion

samples originating from three cool traps. Unless otherwise stated, it was always the sample from the first cool trap that was used in the experiments due to its higher total organic carbon content.

Diesel combustion

Diesel generator (Berlan BSTE5000DE, Bergland Handels GmbH, Klingenthal, Germany) was applied for the production of diesel combustion condensates. For this purpose, commercially available diesel was burnt under “no-load” and “4kW-load” engine operating modes. No-load operating mode means that the generator was not connected to any current-consuming apparatus. On the other hand, for diesel combustion under load mode, the generator was connected to two household appliances requiring 4 kW power in total. Sampling conditions were the same for both engine operating modes: 10 litres of diesel exhaust gas was drawn under constant flow rate (0.4 l/min). One production series included generation of diesel combustion samples under no-load and load engine operating mode. For each type of engine operating mode, three diesel combustion samples (originating from three cool traps) were produced. For the experiments, diesel combustion samples obtained in the first cool traps were used.

2.2.1.2 Total organic carbon content analysis

Total organic carbon content (TOC) is the amount of carbon bound in organic compounds. For the estimation of total carbon (TC) and inorganic carbon (IC) content, two 50 µl-aliquots of the combustion sample were subsequently injected in the TOC-analyser. Total organic carbon content of the combustion condensates was calculated by subtracting the inorganic carbon from the total carbon content (TOC = TC – IC). TOC-analyser measurements are expressed in ppm (parts per million) units.

Determination of the TC-content is based on an oxidation process at high temperatures (680–900°C) in presence of a platinum catalyst. Under these conditions, dissolved and particulate organics are expected to oxidise fully to carbon dioxide, which can be detected by non-dispersive infrared spectrometry. Inorganic carbon content refers to dissolved carbon dioxide, carbonate, and bicarbonate. In the IC-content analysis, acidification of the sample aliquots with the 20% phosphoric acid

converts the inorganic carbon into carbon dioxide which is then quantified via infrared spectrometry.

Total organic carbon content of the combustion samples was determined immediately after their generation. Since the filter which was used for the filtration of the combustion condensates contains organic binding material, measured TOC values of the combustion samples had to be corrected for the contributions of the organics that could be dissolved from the filter. For this purpose, 5 ml of distilled water was filtrated and a filtrate aliquot was consequently measured in the TOC-analyser. Contribution of the organics in the filter (~ 20 ppm) was subtracted from the TOC-measurements of the combustion samples.

2.2.1.3 High-resolution transmission electron microscopy

HRTEM is a valuable technique for studying the crystallographic nanostructures. For the specimen preparation, a drop of a combustion sample was placed directly on the TEM copper grid (covered with a lacey carbon film) and dried under a glow bulb. Specimens were observed under 3000F FEG or TECNAI F30 transmission electron microscope, both operated at 300 kV. Electron microscopes were equipped with a CCD camera for image acquisition.

2.2.1.4 Spectrophotometry

Spectrophotometry is a method applied for the measurement of the fraction of light that is being absorbed by a given solution. The absorbance measurements of the samples (combustion condensates, water suspended carbon black) were performed in 200-700 nm wavelength range.

2.2.1.5 Ultracentrifugation

Ultracentrifugation of the ethylene combustion sample was performed in Optima LE-80K ultracentrifuge, which was pre-cooled down to 4°C. Ultra-clear centrifuge tube was filled with 5 ml of the combustion sample and centrifuged for 14 h at 116 000 x g (35 000 rpm). After centrifugation, tube was removed from the buckets and 2 ml of supernatant was carefully taken with a 2 ml-syringe and placed in a separate FACS-tube. During the suction of the supernatant, needle (19G) of the syringe was kept in

the top part of the supernatant, making sure that the needle does not get in touch with the instable pellet. Afterwards, the pellet was resuspended in the rest (3 ml) of the supernatant.

2.2.1.6 Filtration

Inorganic “Anotop 10 plus” membrane filter with 100 nm pore size was used for the filtration of the ethylene combustion condensate. 2 ml of ethylene combustion condensate was drawn with a 10 ml-syringe. Syringe was connected to the filter and the filtration was performed according to the manufacturer instructions (Whatman, England). The filtrate was collected in a reaction tube. An aliquot of this filtrate was subsequently filtrated through an inorganic “Anotop 10 plus” membrane filter with 20 nm pore size.

2.2.2 Prokaryotic cell culture and SWITCH test

2.2.2.1 Standard cultivation

Stock culture of recombinant *Salmonella typhimurium* TA1535 pSWITCH was cultivated on LB-agar plates supplemented with 50 µg/ml ampicilin. Preparation of agar plates was as follows: 35 g of LB-agar powder was diluted in 1l of deionised water and autoclaved for 20 min at 121°C. After the solution had cooled down to approximately 50°C, 1 ml of sterile filtrated ampicilin (50 mg/ml) was added. The agar was then poured in Petri dishes (d=9.4 cm) and left to solidify at room temperature. The agar plates were inoculated with a single colony of *S. typhimurium* TA 1535 pSWITCH and incubated for 24–48 h at 37°C until visible bacterial colonies appeared. Agar plates with bacterial colonies were kept in the refrigerator (4°C) for up to 8 weeks.

2.2.2.2 SWITCH test

Principles

SWITCH (Salmonella Weighting of Induced Toxicity (Genotoxicity) and Cytotoxicity for Human Health) test is used as a rapid, pre-screening assay for simultaneous testing of both genotoxic and cytotoxic effects of combustion condensates. Construction of the pSWITCH plasmid, which consists of active regions of pPLS-1

(Ptitsyn et al., 1997) and commercially available pGFPuv plasmid was already described (Stojicic et al., 2005). Genotoxicity and cytotoxicity assessment by means of SWITCH test is based on the SOS-Lux (pPLS-1) and LAC-Fluoro (pGFPuv) receptor-reporter system, respectively. Activation of the SOS-inducible promoter (receptor element) in the presence of DNA damage up-regulates the expression of downstream positioned genes for luciferase enzyme (reporter element). The intensity of the emitted light in the reaction of oxidation catalysed by a luciferase is proportional to the concentration of an applied genotoxin (Baumstark-Khan et al., 2001). Under normal conditions, there is a constitutive synthesis of GFPuv reporter protein, since the GFPuv gene expression is under the control of a strong promoter (*P_{lac}*) which is constitutively active in *S. typhimurium* TA1535 strain (Oda et al., 1985). In the presence of a cytotoxic agent, a dose-dependant decrease in the intensity of GFPuv-fluorescence occurs. Besides fluorescence measurements, absorbance measurements of the bacterial suspension were also used for cytotoxicity assessment.

Experimental setup

The SWITCH test was performed according to the procedure that was already described in literature (Baumstark-Khan et al., 2005; Stojicic et al., 2005). Overnight *S. typhimurium* TA1535 pSWITCH culture was diluted (1:200) in fresh 2x LB-medium supplemented with 100 µg/ml ampicillin and further cultivated in shaking incubator at 37°C until absorbance at 600 nm (Abs_{600}) reached 0.2. 75 µl of this culture was added to the wells of a 96-well microtitre plate that already contained either 75 µl of a combustion sample diluted in water or only water (untreated control). Wells, which served as background controls, contained only medium and water diluted samples. Each sample concentration was tested in triplicates. Prepared microtitre plate was immediately placed into the temperature controlled (30°C) microtitre plate reader Multilabel Counter 1420 Victor² for further incubation and measurements. Each measurement cycle started with orbital shaking, followed by luminescence measurement without filter, absorbance measurement at 490 nm and fluorescence measurement (excitation at 405 nm and emission at 510 nm). Each cycle lasted about 10 min, which results in approximately 8 h measurement time (50 cycles in total).

Numerical analysis and dose-effect curves

Numerical analysis was performed as described in Baumstark-Khan et al. (2005). Briefly, relative luminescence (Lux_{rel}) served as a parameter for the assessment of genotoxic potential of the applied agents and it was calculated as the ratio of the background corrected peak luminescence outputs of treated and untreated bacterial samples. For determination of cytotoxicity, relative absorbance (Abs_{rel}) was calculated as the ratio of the background corrected absorbance values measured after 6 h incubation of treated and untreated bacterial samples. Analogous calculation was performed to compute relative fluorescence (Flu_{rel}).

Lux_{rel} , Abs_{rel} , and Flu_{rel} values were plotted as a function of total organic carbon contents of a tested combustion sample. Subsequently, dose-effect curves that best fit the data (regression coefficient $R^2 > 0.9$) were plotted. A sample was considered genotoxic if $\text{Lux}_{\text{rel}} \geq 2$. Luminescence peak values and “peak concentrations” (concentration at which the rel. luminescence is at its maximum) were used for the comparison of the genotoxicity of different samples. Cytotoxicity of different combustion samples was compared according to their LC_{50} values. The LC_{50} value is a concentration of a combustion sample that is lethal for 50% of exposed cell population ($\text{Abs}_{\text{rel}}=0.5$ and $\text{Flu}_{\text{rel}}=0.5$). Lower LC_{50} values indicate higher toxicity.

2.2.3 Eukaryotic cell cultures

2.2.3.1 Cultivation of A-549 cell line

Human lung epithelial cell line A-549 was cultivated in MEM-alpha culture medium supplemented with 10% (v/v) FBS, 100 U/ml penicillin, 100 µg/ml streptomycin, 10 µg/ml neomycin, 0.5 U/ml bacitracin and 2.5 µg/ml amphotericin B. Cells were incubated at 37°C in humidified air with 5% CO₂. Cell culture flasks (75 cm² of growth surface) were used for standard cultivation. Subcultivation was performed at 90–100% cell confluence. For this purpose, medium was aspirated and cells were washed with prewarmed PBS solution. 5 ml of (1x) trypsin/EDTA solution was added in order to detach cells from the flask surface. After 5 min incubation at 37°C, detached cell-aggregates were separated by multiple up-down suction with a pipette. 5 ml of fresh MEM-alpha medium 10% (v/v) FBS was added in order to stop the activity of trypsin, and an aliquot of the cell suspension was taken for counting. Cell density (cells/ml) was determined with a hemocytometer (Fuchs-Rosenthal) and an

appropriate aliquot of cell suspension was diluted in fresh culture medium for further cultivation in a new culture flask.

Standard seeding and treatment procedure for the experiments

If not otherwise stated, A-549 cells were seeded in cell culture dishes at 1×10^4 cells/cm² density for the standard experimental set up. After 2-3 days of incubation (at 50-60% cell confluence), old culture medium was aspirated and fresh medium mixed with a test sample was added to the exponentially growing cells.

2.2.3.2 Cultivation of U-937 cell line

Human promonocytic U-937 cell line was cultivated in MEM-alpha culture medium supplemented with 10% (v/v) FBS, 100 U/ml penicillin, 100 µg/ml streptomycin, 10 µg/ml neomycin, 0.5 U/ml bacitracin and 2.5 µg/ml amphotericin B. Cells were incubated at 37°C in humidified air with 5% CO₂. Cell density was maintained between 1×10^5 cells/ml and 2×10^6 cells/ml, according to the ATCC instructions. Subcultivation was performed by diluting the cell suspension with fresh prewarmed culture medium. For experiments, no passage higher than 45 was used.

Standard seeding and treatment procedure for the experiments

If not otherwise indicated, U-937 cells were seeded at 3×10^5 cells/ml density for the standard experimental set up. On the next day, exponentially growing cells were treated with combustion condensates.

2.2.3.3 Long-term storage of cells

For long-term storage, cells were kept in liquid nitrogen at -196°C. In order to prevent cells from the damaging effect of ice crystals, cryopreservation medium containing complete MEM-alpha medium supplemented with DMSO (dimethyl sulfoxide) was used.

Cells were harvested, counted and centrifuged at 400 x g for 5 min. The pellet was resuspended in cryopreservation medium supplemented with 10% (v/v) DMSO (for A-549) or 5% (v/v) DMSO (for U-937) at a concentration of 1×10^6 cells/ml (1 ml per cryovial). Cryovials with cells were placed in a freezing container (5100 Cryo 1°C,

Nalgene, Schwerte, Germany) and stored at -80°C. On the next day, cryovials were transferred in the cryogenic freezer (-196°C) for further storage.

For recultivation of frozen cells, the content of the cryovial was thawed in water bath at 37°C and cells were transferred in 15 ml prewarmed culture medium. After 24h of incubation, the culture medium was renewed.

2.2.3.4 Growth kinetics of the used cell lines

U-937 and A-549 cells were seeded in 24-well plate at cell densities of 1×10^5 cells/ml and 1×10^4 cells/cm², respectively. Cells were counted twice a day (in the morning and in the evening) for the following 8 days. Medium change was performed every 2-3 days.

Growth kinetics of the cell lines was characterised with a “doubling time” (time required for the number of cells in the population to double). Doubling time (DT) was calculated from the slope ($b(1)$) of linear regression curve plotted in the exponential growth phase of the semi-log “cell density vs. incubation time” plot, according to equation 2-1:

$$DT = \frac{\ln 2}{b(1)} \quad (2-1)$$

2.2.3.5 Stable transfection of U-937 with pNF-κB-EGFP/Neo plasmid

Plasmid

U-937 cells were stably transfected with pNF-κB-EGFP/Neo plasmid for monitoring activation of the NF-κB signalling pathway via EGFP (enhanced green fluorescence protein) reporter protein. This plasmid was kindly provided by Dr. C. E. Hellweg and its construction is described elsewhere (Hellweg et al., 2003).

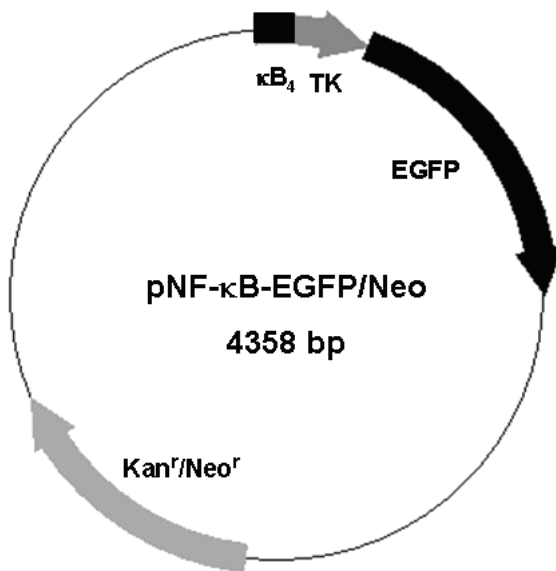


Figure 2-2: Plasmid pNF-κB-EGFP/Neo

The plasmid pNF-κB-EGFP/Neo (Figure 2-2) contains the EGFP gene whose expression is controlled by a synthetic promoter consisting of 4 tandem copies of κB enhancer element (κB_4) and thymidine kinase (TK) minimal promoter. Activation of NF-κB pathway leads to binding of endogenous NF-κB molecules to the κB enhancer element, and thereby transcription of EGFP is being increased (Hellweg et al., 2003). The plasmid also contains Kan^r/Neo^r genes whose product (enzyme aminoglycoside 3'-phosphotransferase) inactivates aminoglycoside antibiotics (neomycin, kanamycin and geneticin G418) and enables the transfected cells to be resistant to these antibiotics.

Stable transfection

During stable transfection an exogenous DNA integrates into host DNA. Unlike transient transfection, where transfected DNA remains extrachromosomal, stable transfection ensures the propagation of the transfected DNA on the next cell generations.

U-937 cells were transfected with the pNF-κB-EGFP/Neo plasmid by lipid mediated DNA transfer (FuGene 6 transfection reagent). FuGene 6-DNA-mixture (3:1) was made in 200 µl serum-free MEM-alpha medium and it was added to U-937 cells (1×10^5 cells /ml). Cells treated only with FuGene 6 served as a mock control. Cells were further incubated in MEM-alpha medium (supplemented with 10% (v/v) FBS) in the presence of FuGene 6 or FuGene 6-DNA mixture. 48 h after transfection, cell

cultures were split (1:6) in cell culture flasks (25 cm^2) and further cultivated in selection medium (complete MEM-alpha medium supplemented with 1.5 mg/ml of geneticin G418). Selection medium was being renewed every 2-3 days. After 2 weeks, when there was 100% death in the mock control, stably transfected cells (G418 resistant cells) were seeded in 96-well plates at concentration of 50 cells per plate and cultivated for 3-4 weeks. This process of obtaining cell clones is known as "limiting dilution method". The pool of stably transfected cells is thereby diluted at such low concentrations, so that statistically there should be not more than one stably transfected cell per well. Appearance of single cell derived cultures (clones) in the 96-well plates was inspected microscopically. TNF- α is a common inducer of the NF- κ B-pathway. Stably transfected U-937-pNF- κ B-EGFP/Neo clones were treated with 10 ng/ml TNF- α or with 0.1 % (v/v) PBS (vehicle control) and subsequently screened for induction of NF- κ B-dependant EGFP expression (chapter 2.2.5).

2.2.4 Flow cytometry

Flow cytometry is based on the analysis of a single cell in a moving fluid stream as it passes through a focused laser beam. This method allows simultaneous measurements of several parameters. Morphologic features of a cell are determined according to the changes in the beam of laser light that are caused by a cell passing through this beam. The intensity of the scattered light detected in direction of the laser beam (forward scatter - FSC) is directly proportional to cell size. Side scatter (SSC) of the laser light is detected at 90° angle from the laser beam and it gives the information about internal complexity and granularity of a cell. DNA alterations or changes in the distribution of diverse proteins can be quantified by staining the cells with appropriate fluorochromes and analysing their fluorescence intensities in the flow cytometer.

The flow cytometer FACScan (fluorescence-activated cell scanner) used in this work is equipped with an argon laser (488 nm) for excitation and three detector channels: FL-1 (530/30 nm bandpass filter; green fluorescence), FL-2 (585/42 nm bandpass filter; yellow/orange fluorescence), and FL-3 (630 nm longpass filter; red fluorescence). For multicolour assays (e.g. Annexin V-PE/ 7-AAD assay) the colour compensation method was applied in order to record only a desired signal in a certain detector channel.

FACScan-measurements were further analysed with WinMDI 2.8 software (WinMDI - Windows Multiple Document Interface) from Joe Trotter (Scripps Institute, La Jolla, 34

CA USA). Morphological properties of the cells and fluorescence intensities of the fluorochromes were displayed in FSC vs. SSC density plots and histogram plots, respectively.

2.2.5 NF-κB-activation assay

Monitoring of the activation of NF-κB signalling pathway in stably transfected U-937-pNF-κB-EGFP/Neo cells was done by measuring the yields of green fluorescence of EGFP reporter protein.

After treatment, cells were washed once in PBS and fixed with 3.5 % (v/v) formaldehyde/PBS solution for 30 min at 4°C. Subsequently, the fixative was diluted with PBS (1:3) and cells were stored in fridge. Prior to FACScan-analysis, cells were pelleted and resuspended in 2 ml PBS. EGFP-fluorescence was recorded in FL-1 channel of FACScan. Morphology and EGFP-fluorescence output of the cells was analysed with WinMDI 2.8 software. Markers (M1, M2, and M3) were set in the EGFP-fluorescence histograms as follows: M1 marker was set according to the autofluorescence intensities of non-transfected U-937 cells, while M2 and M3 markers were set according to the EGFP fluorescence intensities of U-937-pNF-κB-EGFP/Neo cells. M2 marker comprised background EGFP fluorescence of the U-937-pNF-κB-EGFP/Neo cells. Cells displaying fluorescence intensities in the zone of M3 marker were considered EGFP-positive cells. Arbitrarily, the M3 marker is set so that it includes 2.5% of U-937-pNF-κB-EGFP/Neo cell population, in non-treated conditions. The frequency of EGFP-positive cells was used as a measure of NF-κB activation.

2.2.6 Apoptosis assays

2.2.6.1 Annexin V-PE / 7-AAD assay

The Annexin V-PE / 7-AAD staining method was used for detection and quantification of apoptotic cells. The principle of this test is based on morphological changes in the cell membrane during early phases of apoptosis. In the early stages of apoptosis, phospholipid phosphatidylserine (PS) is being translocated from the inner to the outer layer of the cell membrane. The conjugated form of protein Annexin V (Annexin V-PE) binds with high affinity to the PS. Detection of early apoptotic cells occurs via

flow cytometric analysis of the membrane bound Annexin V-PE fluorescence intensity. The DNA-intercalating vital dye 7-aminoactinomycin-D (7-AAD) enables the discrimination between early apoptotic and late apoptotic/necrotic cells. Only membranes of late apoptotic and necrotic cells are permeable to 7-AAD.

After treatment, cells were transferred in 5 ml FACS tubes and centrifuged for 5 min at 400 x g. After washing with 1 ml cold PBS, cells were resuspended in 1x Annexin V binding buffer at 2×10^6 cells/ml. A 250 µl aliquot of such cell suspension was mixed with 5 µl Annexin V-PE and 5 µl 7-AAD. After 15 min staining at room temperature, 740 µl of 1x Annexin V binding buffer was added, and cells were immediately analysed. Annexin V-PE fluorescence intensity (recorded in FL-2 channel) was plotted against the 7-AAD fluorescence intensity (recorded in FL-3 channel). An exemplary density plot is given in Figure 2-3.

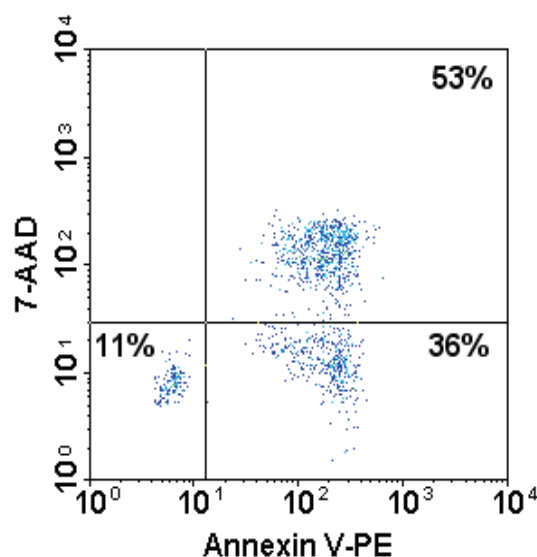


Figure 2-3: Flow cytometric analysis of apoptosis with Annexin V-PE / 7-AAD assay
Annexin V-PE and 7-AAD-stained cells are distributed to different fractions (quadrants) according to their fluorescent signals. Cells appearing in the lower left quadrant are viable since they show negative Annexin V-PE and negative 7-AAD staining (Annexin V-PE⁻ / 7-AAD⁻ cells). The lower right quadrant contains early apoptotic cells (Annexin V-PE⁺ / 7-AAD⁻ cells) and the upper right quadrant shows the fraction of late apoptotic/necrotic cells (Annexin V-PE⁺ / 7-AAD⁺ cells).

2.2.6.2 DNA content and cell cycle analysis

The DNA-intercalating dye propidium iodide (PI) was used for flow cytometric analysis of DNA content. When bound to DNA, PI gives a strong fluorescent signal (emission centred around 600 nm) when excited at 488 nm. The intensity of the PI-

signal is directly proportional to DNA content. Cellular DNA content changes during cell cycle. In G1/G0 phase of the cell cycle, cells possess diploid amount of DNA ($2n$). During S phase amount of DNA duplicates, so that in G2 phase cells contain $4n$ amount of DNA. Cells undergoing apoptosis contain subdiploid ($< 2n$) DNA content due to fragmentation of DNA and subsequent disintegration of cells into apoptotic bodies. This is evident as sub-G1 region in DNA-content frequency diagrams.

After treatment, cells were washed twice in PBS and fixed with ice-cold ethanol (70%, v/v) for minimum 24 h at -20 °C. After fixation, cells were centrifuged and resuspended in staining solution containing 20 µg/ml PI, 200 µg/ml RNase A (ribonuclease) and 0.1% (v/v) Triton X-100 in PBS. Treatment with RNase A is necessary since PI can also bind to double-stranded RNA. Cells were incubated with the staining solution for 1 h at 37°C and subsequently PI-fluorescence was measured in FL-2 channel of FACScan. Doublets and cell debris were excluded from cell cycle analysis. Cell cycle phase distribution of analysed cells was calculated with Cylchred version 1.0.2 software. This programme was developed by Terry Hoy in 1999 (Cardiff University, Cardiff, UK), based on the algorithms described by Ormerod et al. (1987).

2.2.6.3 Active caspase-3 assay

Caspase-3 is one of the key effector caspases. This protease is synthesised as an inactive proenzyme (procaspase) which is activated in cells undergoing apoptosis. Active caspase-3 assay utilises PE-conjugated monoclonal active caspase-3 antibody for detection of active form of caspase-3 (active caspase-3). Intensity of the PE-fluorescence is directly proportional to the amount of active caspase-3.

The active caspase-3 assay was performed according to the manufacturer instructions (BD Biosciences Pharmingen, Germany). After washing with cold PBS, cells were fixed and permeabilised with Cytofix/Cytoperm solution for 20 min on ice. After incubation, cells were washed twice with Perm/Wash Buffer and subsequently incubated (30 min at room temperature) in staining solution which contained 20 µl of PE-conjugated active caspase-3 antibody and 100 µl of Perm/Wash Buffer. After washing with Perm/Wash Buffer, cells were resuspended in 1 ml of the Perm/Wash Buffer for the FACscan-analysis. PE-fluorescence was recorded in the FL-2 channel.

2.2.6.4 DAPI staining

DAPI (4',6'-diamidino-2-phenylindole) is a vital dye which displays enhanced blue fluorescence upon selective binding to double-stranded DNA. DAPI staining enables microscopic analysis of DNA morphological changes (DNA condensation and fragmentation) in cells undergoing apoptosis.

A-549 cells were seeded on round cover slips ($d = 12\text{ mm}$) which were placed in 24-well plates. The cover slips were coated with poly-D-lysine hydrobromide solution (0.1 mg/ml in deion. water) prior to seeding. At 50-60% cell confluence, cells were treated with combustion condensates. After treatment, cells were washed with PBS and fixed with ice-cold methanol for 5 min. Subsequently, cell nuclei were stained with 0.1 $\mu\text{g}/\text{ml}$ DAPI in methanol for 15 min at room temperature (protected from light). After washing twice with PBS, the cover slips were carefully removed from the 24-well plates and placed (cell layer downwards) on glass microscope slides (76 x 26 cm) that carried a drop of fluorescent mounting medium.

U-937 cells were seeded in Petri dishes ($d = 3.5\text{ cm}$) according to the standard seeding protocol (chapter 2.2.3.2) and incubated for 24 h prior to treatment with combustion condensates. After treatment, cells were collected (400 x g, 5 min) and resuspended in 1 ml ice-cold methanol. After 5 min fixation in methanol, cells were stained with 0.1 $\mu\text{g}/\text{ml}$ DAPI solution for 15 min at room temperature. Subsequently, cells were washed twice with PBS, in order to remove the non-bound DAPI. A drop of cells suspended in PBS and a drop of fluorescent mounting medium was placed on the microscope slide (76 x 26 cm) and covered with a cover slip.

Microscope slides carrying A-549 or U-937 cells were left to dry overnight at room temperature. Subsequently, cover slips were sealed with transparent nail polisher and preserved in a dark place prior to the observation under fluorescence microscope. Morphology of the U-937 and A-549 cells' nuclei was observed by using the Axiovert 135 fluorescence microscope with Filter Set 2 ($\lambda_{\text{exc}} = 365\text{ nm}$; $\lambda_{\text{em}} > 420\text{ nm}$). Image analysis was performed with the AxioVision 4.4 software (Zeiss, Germany).

2.2.7 Crystal violet assay

Crystal violet (N-hexamethylpararosaniline) is a cell nuclei stain, which was used to assess the effect of combustion condensates on the cell population growth. Absorbance of the crystal violet dye is proportional to the number of cells (Gillies et al., 1986).

For the crystal violet assay, A-549 cells were seeded in 96-well strip plate at 2×10^4 cells/cm² density. At 40-50% confluence, cells were exposed to different combustion samples or left untreated for up to 72 h. Every 24 h, cells were fixed and stained with 0.1% (w/v) crystal violet in 3.5% (v/v) formaldehyde/PBS solution for 30 min at room temperature. After carefully removing the excess stain by gently submerging the 96-well strip plate in deionised water, the plate was left to air-dry. 0.2% (v/v) Triton X-100 in PBS was added to each well and the plate was left for 30 min on a shaker in order to solubilise the DNA-bound crystal violet dye. Absorbance of the dye was recorded at 562 nm in the Lambda microtiter plate reader. The relative cell growth was calculated as a ratio of absorbance values of treated vs. untreated sample.

2.2.8 MTT test

Cytotoxicity of a certain substance can be measured with a colorimetric assay using the tetrazolium salt MTT (3-(4,5-dimethylthiazole-2-yl)-2,5-diphenyltetrazolium bromide). Mitochondrial dehydrogenases of living, metabolically active cells convert the MTT into a blue-coloured formazan precipitate, which remains in the cell due to its membrane-impermeability. Absorbance of formazan ($\lambda=562$ nm) is proportional to the number of metabolically active cells (Mossmann, 1983).

The MTT-test was used to examine the dose-effect response for the antibiotic G418 on U-937 cell growth. Cells were seeded in 96-well plate at 3×10^5 cells/ml and G418 (100 – 1500 µg/ml) was added the next day. Untreated cells and cells treated with 10% (v/v) DMSO served as a negative and a positive control, respectively. During 7 day incubation, medium was renewed every 2-3 days. After incubation, the 96-well plate was shortly centrifuged to pellet the cells in the wells and then the supernatant (medium) was carefully aspirated. The MTT solution (0.5 mg/ml in serum-free medium) was added to each well. After 1 h incubation with MTT, cells were lysed and formazan crystals were dissolved by adding 100 µl of DMSO-SDS (sodium dodecyl sulphate) solution (10 g SDS in 99.4 ml DMSO and 0.6 ml acetic acid) to each well

and shaking the plate for 20 min. Finally, the absorbance of formazan was measured at $\lambda=562$ nm in Lambda microtitre plate reader. Cell survival was calculated as a ratio of formazan-absorbance of treated vs. untreated samples.

2.2.9 Molecular biological methods

2.2.9.1 Total RNA isolation

Isolation of total RNA was performed with the RNeasy Plus Mini Kit according to the manufacturer's instructions. Briefly, RNA isolation consisted of several steps: lysis of cells and homogenisation of the cell lysates, removal of genomic DNA by using "gDNA eliminator" spin columns, binding of total RNA to RNeasy spin columns, and elution of the RNA from the columns.

2.2.9.2 Quantification and quality analysis of isolated RNA

Quality, integrity and quantity of the isolated RNA were estimated by using the RNA/DNA/Protein-analyser (Agilent BioAnalyzer 2100). The Agilent BioAnalyzer 2100 allows electrophoretic separation and fluorescence detection of labelled RNA on microfabricated chips. Rapidity and automation are some of the advantages of this method over a classic gel-electrophoresis. Specially devised software algorithm extracts information about total RNA sample integrity from entire electrophoretic lane and converts the information into a RIN value (RIN - RNA integrity number) on a scale from 1 to 10 (from completely degraded to highly intact RNA). Only intact RNA samples with $RIN \geq 8$ were taken for further applications.

For the RNA analysis in the BioAnalyzer, the RNA 6000 Nano LabChip (Agilent Technologies, Palo Alto, USA) was filled with a mixture of gel matrix and a fluorescent dye (both supplied in Agilent RNA 6000 Nano Reagents Kit), and consequently 1 μ l of each RNA sample was added to a corresponding well of the chip. One well of the chip was loaded with 1 μ l RNA-ladder (RNA 6000 Nano Ladder, Agilent Technologies, Palo Alto, USA) which was used as a size standard.

2.2.9.3 Quantitative real-time reverse transcription PCR (qRT-PCR)

qRT-PCR (quantitative real-time reverse transcription polymerase chain reaction) method was utilised for gene expression analysis. It was performed in two steps

which included reverse transcription (synthesis of cDNA) followed by quantitative real-time PCR.

2.2.9.3.1 cDNA synthesis

Total RNA was reversely transcribed into cDNA by using the iScript reverse transcriptase from the iScript cDNA-Synthesis Kit. Experimental setup was in compliance with the manufacturer's instructions and the reaction mixture contained following components: 500 ng of total RNA, iScript reaction mix (deoxyribonucleotides, primers), iScript reverse transcriptase and nuclease-free water (Gibco, Scotland, UK). The so called "RT-minus control" did not contain the reverse transcriptase in the reaction mixture. This control was used for detection of genomic DNA contaminations in isolated RNA samples. The reaction mixture was incubated in TRIO-Thermoblock thermocycler as follows: 5 min at 25°C, 30 min at 42°C (optimum activity of the enzyme) and 5 min at 85°C (for the reaction termination). After synthesis, cDNA samples were stored at -20°C.

2.2.9.3.2 Performance of quantitative real-time PCR

Unlike conventional PCR, real-time PCR uses the DNA-intercalating fluorescent dye SYBR-Green I for constant monitoring of DNA amplification by measuring the fluorescence output, as the fluorescence increases when the SYBR-Green dye is bound to double-stranded DNA.

The reaction mixture (total of 25 µl) consisted of cDNA sample (10 ng), Platinum SYBR Green qPCR SuperMix-UDG (containing Taq DNA polymerase, SYBR Green I dye and deoxyribonucleotides), 0.2 µM of each primer (forward, reverse) and nuclease-free water. Primers of the genes of interest (target genes) and housekeeping genes (reference genes) are listed in Table 2-1. All primers were synthesised commercially (Invitrogen, Karlsruhe, Germany). Quantitative real-time analysis was performed in the Opticon2 thermocycler according to the following protocol: after 2 min incubation at 95°C (for the activation of Taq DNA polymerase), there were 44 cycles consisting of: 15 s incubation at 95°C, 30 s incubation at corresponding primer-annealing temperature (59 - 62°C) and 30 s incubation at 72°C for the elongation of the newly synthesised DNA chains.

Table 2-1: Primer pairs (forward and reverse) of target and reference genes			
Genes	Primer sequences	Amplicon length (bp)	Annealing temp. (°C)
HPRT	fwd: TGACACTGGCAAAACAATGCA rev: GGTCCCTTTCACAGCAAGCT	120	62
GAPDH	fwd: CAATGACCCCTTCATTGACC rev: GATCTCGCTCCTGGAAGATG	146	60
PBGD	fwd: CAGCTTGCTCGCATACAGAC rev: GAATCTTGTCCCCGTGGTG	106	60.4
B2M	fwd: GGCTATCCAGCGTACTCCAAA rev: CCAGTCCTGCTGAAAGACAA	184	59.1
IL-6	fwd: CAATCTGGATTCAATGAGGGAGAC rev: CTCTGGCTTGTCCCTCACTACTC	118	59.1
NF-κBIA	fwd: AACCTGCAGCAGACTCCAC rev: TGCTCACAGGCAAGGTGTAG	137	61

* All genes listed are human genes. Abbreviations are: HPRT - hypoxanthine-guanine phosphoribosyltransferase, GAPDH - glyceraldehyde-3-phosphate dehydrogenase, PBGD - porphobilinogen deaminase, B2M - beta-2-microglobulin, IL-6 – interleukin 6, NF-κBIA – inhibitor of NF-κB. fwd - forward; rev – reverse.

2.2.9.3.3 Testing the specificity of DNA amplification

Melting curve analysis

Melting curve analysis was performed in Opticon2 thermocycler directly after the real-time PCR run. This encompassed gradual heating (60–95°C) of generated amplicons and continuous measurement of the SYBR-Green I fluorescence (each $\Delta t=0.2^{\circ}\text{C}$). At specific melting temperature, two strands of an amplicon separate and fluorescence intensity decreases rapidly due to detachment of SYBR-Green I dye from DNA. A single peak in the melting curve analysis indicates the presence of a specific amplicon, while appearance of several peaks indicates primer-dimer formation or presence of unspecific PCR products.

Agarose gel electrophoresis

The specificity of PCR reaction was also verified with agarose gel electrophoresis. PCR products were separated by means of electrophoresis in a 2% (w/v) agarose gel. Mixture of 1 g agarose and 50 ml of 0.5x TBE (tris base/ boric acid /EDTA)-buffer was heated in a microwave until the agarose was completely dissolved. After the agarose solution cooled down to approximately 50°C, the DNA-intercalating dye

ethidium bromide (final conc. 0.5 µg/ml) was added, and the solution was poured into gel chamber and left to harden. Hardened gel was placed in the electrophoresis chamber and covered with 0.5xTBE buffer. DNA-samples were mixed with an adequate volume of 6x DNA loading dye solution and 10 µl of this mixture was loaded into gel pockets. Electrophoresis was performed at 65 V for 1 h. DNA bands were visualised under UV-light ($\lambda = 302$ nm) and photographed with a CCD-camera. A single band on an electropherogram indicates the amplification of only one distinct PCR-product.

2.2.9.3.4 Quantification of qRT-PCR results

Crossing point (CP) determination

Real-time PCR is based on constant monitoring of the fluorescence output of DNA-bound SYBR-Green dye. Fluorescence intensity measured after each PCR cycle is directly proportional to the amount of DNA copies amplified to that point of the PCR reaction.

CP values, which are used for the quantification of PCR results, were determined with the “threshold cycle” method. An arbitrary chosen threshold level was set at a level where the fluorescent signals of all DNA samples begin to increase exponentially. The CP value (also referred to as C_t value; C_t -threshold cycle) is defined as a number of cycles required for the fluorescence intensity of a certain sample to reach (cross) the chosen threshold line (Bustin, 2000). Since the fluorescence intensity reflects the amount of PCR products, samples that initially have more DNA molecules will require less PCR cycles to reach the threshold than samples with fewer DNA molecules (Higuchi et al., 1993). Accordingly, the CP-value is indirectly proportional to the initial number of DNA copies.

Real-time PCR efficiency

In order to estimate the PCR efficiency of each transcript, all available cDNA samples from one experiment were pooled and several dilutions in triplicates of this pool were subjected to PCR (Pfaffl et al., 2002). Logarithmic values of the cDNA pool dilutions (0.008/ 0.04/ 0.2/ 1/ 5/ 25 ng of cDNA) were plotted versus the corresponding CP-values (Figure 2-4). The correlation coefficient (r^2) was calculated with the Opticon Monitor Analysis Software Version 3.0. The efficiency (E) of the PCR was calculated

according to the equation $E=10^{(-1/\text{slope})}$ (Rasmussen, 2001). In optimal case, each DNA molecule is being duplicated in each PCR cycle ($E = 2$).

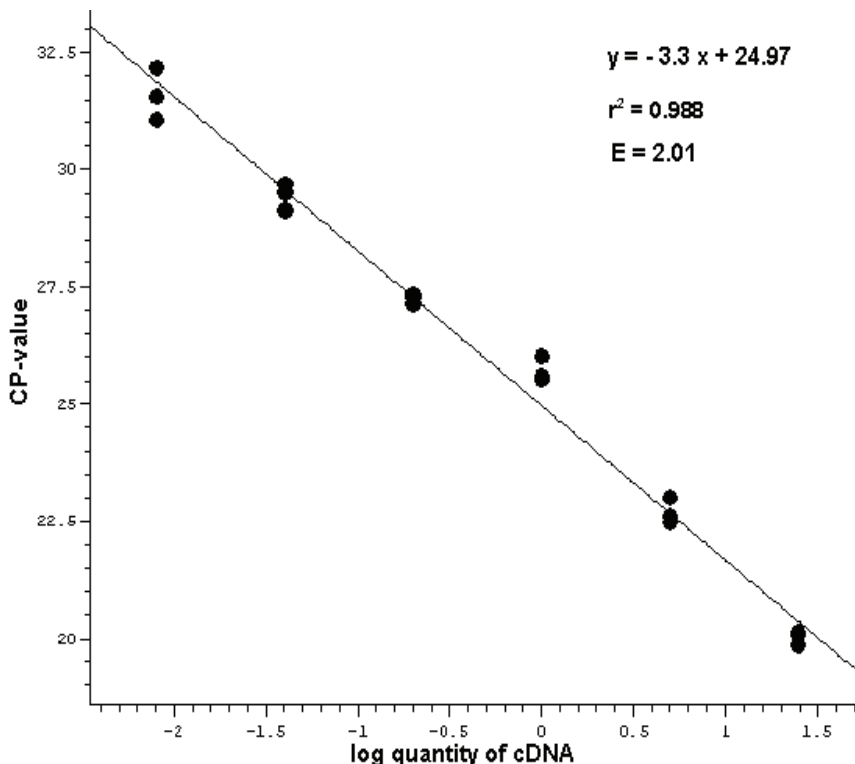


Figure 2-4: Determination of the real-time PCR efficiency

Quantities of cDNA pool dilutions (0.008/ 0.04/ 0.2/ 1/ 5/ 25 ng) are plotted as log values (-2.1/ -1.4/ -0.7/ 0/ 0.7/ 1.4) against the corresponding CP values. The PCR efficiency (E) is calculated according to the equation $E = 10^{(-1/\text{slope})}$.

Relative gene expression analysis

The relative quantification of a target gene expression is based on the relative expression of a target gene versus a reference gene (Pfaffl, 2001). In this thesis, the Microsoft Excel-based REST software (Pfaffl et al., 2002) was used for the calculation of relative gene expressions. Thereby, the relative expression ratio (R) of a target gene is calculated based on the real-time PCR efficiencies of target and reference genes (E_{target} , E_{ref}) and the differences between the mean CP values (ΔCP) of treated (treatment) and untreated (control) experimental groups (equation 2-2).

$$R = \frac{(E_{\text{target}})^{\Delta\text{CP}_{\text{target}} (\text{MEANcontrol} - \text{MEANtreatment})}}{(E_{\text{ref}})^{\Delta\text{CP}_{\text{ref}} (\text{MEANcontrol} - \text{MEANtreatment})}} \quad (2-2)$$

Such normalisation of the target gene expression with the endogenous non-regulated reference gene expression is necessary to compensate the variations between the PCR experiments (inter-assay variations) (Pfaffl, 2001).

REST (Relative Expression Software Tool) utilises the pair wise fixed reallocation randomisation test as a statistical model to estimate differences between target gene expressions in treatment- and control groups. This is being done by repeatedly and randomly reallocating CP values to the treatment and control groups and calculating the expression ratio R according to the formerly mentioned equation 2-2 (Pfaffl et al., 2002). REST determines thereby if the relative target gene expression in treated group is significantly up- or down-regulated in comparison to the relative target gene expression in control group.

Choosing the right reference gene

The so called “housekeeping genes” (hypoxantine phosphoribosyltransferase, glyceraldehyde-3-phosphate dehydrogenase, etc.) are suitable as reference genes since they are present in all nucleated cell types and are necessary for basal metabolism (Thellin et al., 1999). Although these genes are mainly non-regulated and their mRNA synthesis is considered to be stable even under experimental treatments, there are numerous studies which show that the expression of such housekeeping genes may vary under specific experimental conditions (Thellin et al., 1999; Arenz et al., 2007). This is the reason why it is recommended to test the stability of gene expressions of several housekeeping genes under specific experimental conditions before deciding which one/ones should be used as internal standard. For the gene expression analysis in A-549 cells, four housekeeping genes were tested (Table 2-2) for their stability by using the BestKeeper software. BestKeeper is an Excel based macro-sheet software (Pfaffl et al., 2004) which determines the optimal housekeeping genes by calculating the CP variations (standard deviation of CP values) of all tested samples (including controls and treatments) for each candidate housekeeping gene. Furthermore, it calculates the BestKeeper index as a geometric mean of the CP values of the candidate housekeeping genes. The combination of candidate reference genes whose BestKeeper index has the lowest CP variation are then used as reference genes for REST-analysis.

Table 2-2: Candidate reference genes and their functions	
Reference genes	Function
GAPDH	catalyses the oxidation of the glycerinaldehyde-3-phosphate in the glicolysis
HPRT	catalyses the transformation of guanine and hypoxanthine into corresponding 5'-mononucleotides
PBGD	enzyme of the heme biosynthetic pathway
B2M	component of MHC class I molecules

2.2.10 Statistical analysis

If not otherwise stated, data are expressed as mean \pm SEM (standard error of mean). Comparisons between means were drawn by using either two-tailed Student's t-test (two-group comparison) or one-way ANOVA (comparison of more than two groups of data). T-test and one-way ANOVA (analysis of variance) were performed in Microsoft Office Excel 2003. P values smaller than 0.05 were considered significant and were signed with asterisks in the graphs.

3 Results

The results presented in this work include all the steps taken in order to elucidate toxic effects of combustion condensates. The physical and chemical characterisation of ethylene- and diesel combustion condensates was the first step in the study of their toxic effects. In order to determine the biologically relevant dose range, combustion condensates were tested for their genotoxicity and cytotoxicity with the bacterial pre-screening assay (the SWITCH test). This assay was also used to study the role of soot particles in the toxicity of combustion condensates. Toxic effects of the combustion condensates and their mechanisms were studied on the human cell lines A-549 and U-937. This included the study of effects on cellular growth, on cell cycle, on apoptosis induction, and on activation of the NF- κ B signalling pathway.

3.1 Physical and chemical analysis of combustion condensates

3.1.1 Visual inspection of the presence of soot in combustion condensates

The presence of soot particles in ethylene combustion condensates originating from sooting ethylene flames ($C/O \geq 0.78$) was observed already by visual inspection. In ethylene combustion samples, suspended soot particles form black sediment which can be resuspended by vortexing. The degree of turbidity of the greyish combustion samples is directly proportional to the fuel/oxygen ratio during combustion (C/O ratio), indicating higher amount of soot particles at higher C/O ratios. The samples originating from the second cool traps are always less turbid than the samples from the first cool traps, which indicates lower amounts of soot particles. Combustion samples originating from the third cool traps are almost transparent, and no sedimentation can be observed. Samples gained at non-sooting or slightly sooting conditions ($C/O \leq 0.73$) are transparent, regardless of the cool trap they originate from.

Similar observations have been made for the examined diesel combustion condensates. Soot sedimentation was observed in diesel combustion condensates originating from the first cool traps. The suspension is less turbid for the diesel combustion condensates generated at “load” engine operating mode than for the condensates gained at “no-load” operating mode, indicating lower amounts of

suspended soot particles. Samples originating from the second and the third cool traps appear transparent.

3.1.2 Morphological analysis of the soot present in combustion condensates

High-resolution transmission electron microscopy was utilised for the morphological analysis of soot particles in ethylene / diesel combustion condensates and the results were compared with the commonly used soot standard (carbon black). Due to specimen preparation for electron microscopy (chapter 2.2.1.3), aggregation of the soot particles could not be avoided. Accordingly, it is not possible to differentiate with this tool whether single soot particles float freely in suspension or they form agglomerates. Moreover, preparation-induced agglomeration made it quite difficult to distinguish shape and size of single soot particles. HRTEM-images of both ethylene and diesel combustion samples show large soot agglomerates containing spherical and elongated primary particles. The smallest primary particles are around 10 nm in diameter (indicated with arrows in Figure 3-1 A, C). HRTEM-micrographs also show that ethylene and diesel primary soot particles consist of many concentric layers, each consisting of small graphene segments. The term graphitic structure is used here to refer to the similarity of the soot nanostructure to graphitic carbon (Vander Wal and Tomasek, 2004). Single primary soot particles with a higher degree of graphitic structure are found in the ethylene combustion soot compared to the diesel combustion soot. High degree of graphitic structure is characterised by parallel layers of graphene segments. Amorphous soot structures, characterised by less organized and rather randomly oriented graphene segments, are rather present in diesel than in ethylene combustion condensate. Diesel and ethylene soot particles show similarities in morphology of their exterior surfaces. The surface of ethylene and diesel soot is rough and often covered with very small ($d \sim 1$ nm) fullerene-like structures (indicated with an arrow in Figure 3-1 D).

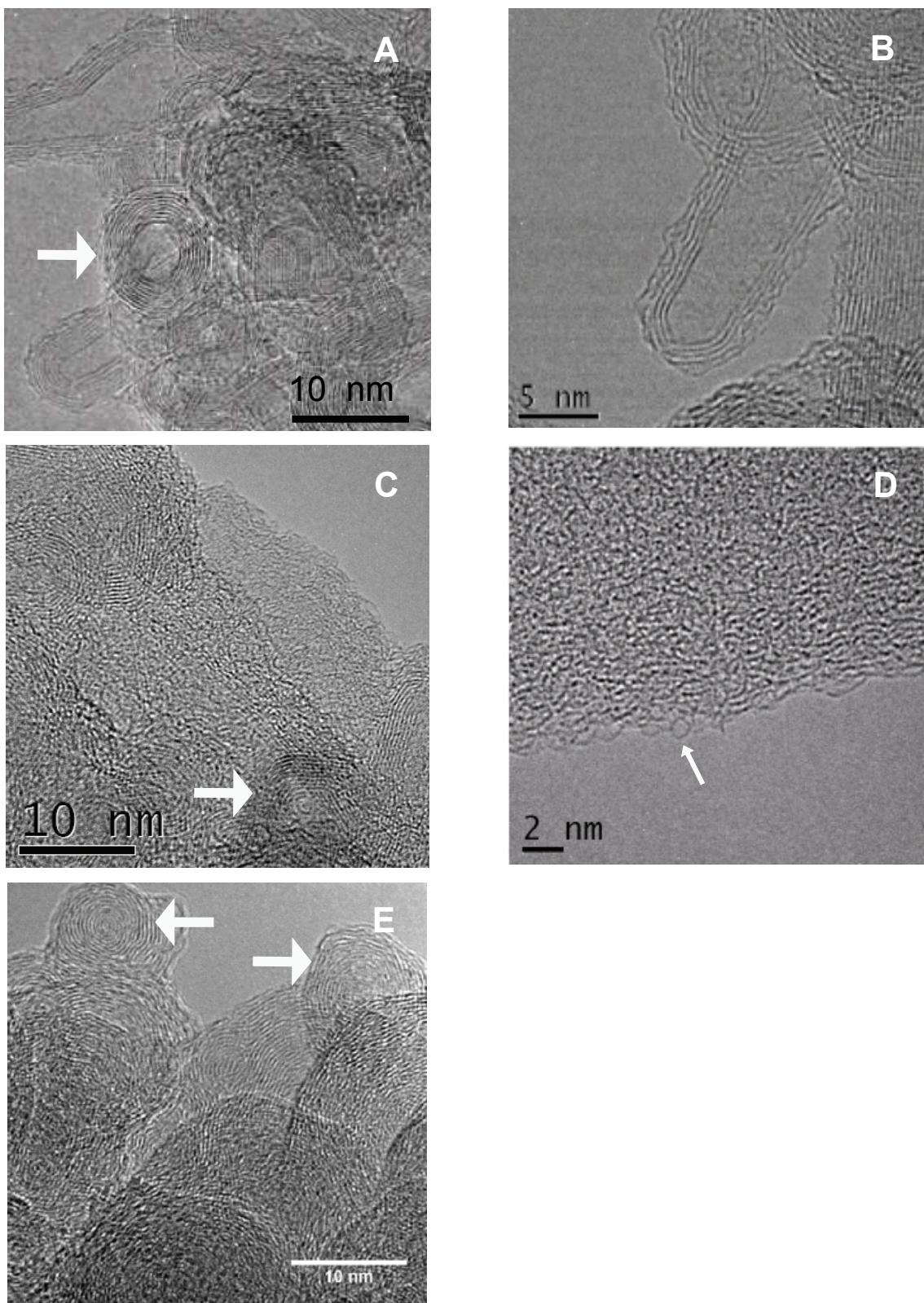


Figure 3-1: Morphological analysis of the soot in combustion condensates

HRTEM-micrographs show nanostructure of soot particles originating from ethylene combustion at C/O=0.88 (A, B) and from diesel combustion under no-load motor operating mode (C, D). As a reference, HRTEM-image of a soot model carbon black (Printex 90) is also shown (E). Primary soot particles (thick white arrows) consist of concentric graphite-like carbon layers and have rough outer surface with fullerene-like structures (thin white arrow).

The HRTEM-images of combustion samples are compared with the HRTEM-images of carbon black (Printex 90, Degussa, Germany) which is commonly used as soot model (Müller et al., 2005). For this purpose, carbon black suspended in water (20 µg/ml) was subjected to the same preparation method for HRTEM analysis. HRTEM-micrograph shows that spherical particles with high degree of graphite-like structures are predominant in the carbon black (Figure 3-1 E). According to the product specifications given by the manufacturer, the average size of the carbon black particles is 14 nm and particles of this size range can be observed in the HRTEM-image (arrows in Figure 3-1 E). Carbon black particles exhibit rather smooth exterior surfaces with few irregularities.

3.1.3 TOC content of combustion condensates depends on combustion conditions

Total organic carbon content is used for the quantification of organic compounds in the combustion condensates. TOC content of the combustion samples was determined according to the method described in section 2.2.1.2. An overview of the TOC content of ethylene and diesel combustion condensates originating from one representative production series is given in Table 3-1 and Table 3-2, respectively.

Table 3-1: Total organic carbon content of ethylene combustion condensates obtained in one production series			
C/O ratio	TOC content (ppm)		
	I cool trap	II cool trap	III cool trap
0.63	134	40	10
0.68	115	25	35
0.73	185	75	11
0.78	243	69	51
0.83	346	92	26
0.88	435	138	41
0.93	769	158	70

For each C/O ratio (fuel/oxygen ratio), the ethylene combustion sample originating from the first cool trap contains a higher amount of TOC than the samples from the

second and third cool traps. TOC content of the samples from the first cool traps is directly proportional to the C/O ratio.

Table 3-2: Total organic carbon content of diesel combustion condensates obtained in one production series			
Engine operating mode	TOC content (ppm)		
	I cool trap	II cool trap	III cool trap
no-load	1146	58	8
4kW-load	422	40	3

During diesel combustion under no-load engine operating mode a higher emission of organic carbon is observed than under 4kW-load operating mode. Samples from the first cool trap contain higher amount of total organic carbon than the samples from the second and third cool traps.

3.1.4 UV-spectrophotometry of combustion condensates reveals a presence of nanoparticles

The characterisation of combustion condensates also included absorption measurements. UV-spectrophotometry of combustion condensates (ethylene-, diesel-) revealed broad band absorption in the UV region (200 - 300 nm). As a representative example, the absorption spectra of ethylene combustion condensates generated at C/O ratios ranging from 0.68 to 0.93 are given in Figure 3-2. The higher the combustion C/O ratio, the stronger is the UV-absorption of the corresponding ethylene combustion condensate (Figure 3-2 A). *In situ* absorption measurements of ethylene flame exhaust (Sgro et al., 2003; Commodo et al., 2007) and absorption measurements of ethylene combustion water samples (Sgro et al., 2001) have shown a large absorption peak of these samples in the UV region (200-300 nm). This wide absorption band in the UV region is mainly attributed to combustion generated nanoparticles (size of 2-4 nm) which are comprised of 2-ring aromatics (Sgro et al., 2001). Considering these findings, the absorbance measured at 250 nm (Abs_{250}) is chosen here as an indicator for the presence of nanoparticles in the examined combustion condensates. As it can be seen in Figure 3-2 A, the absorbance intensity measured at 250 nm increases with higher C/O ratios. This indicates that the

concentration of nanoparticles in the combustion condensates is directly proportional to the applied C/O ratios for the condensates' generation.

The ethylene combustion sample generated at highly sooting conditions (C/O=0.93) exhibits higher absorbance intensities at $\lambda > 300$ nm compared to the other examined samples. Carbon black particles suspended in water, which served as a reference for the suspended soot particles, absorb almost the same intensity of light in the UV and in the visible spectral range (Figure 3-2 B). Taking this information and the fact that the nanoparticles are transparent to visible light (Sgro et al., 2003) into account, it can be concluded that the observed absorbance of the ethylene combustion condensate (C/O=0.93) at $\lambda > 300$ nm is due to the presence of soot particles. Furthermore, the corresponding soot-attributed absorbance in the wavelength range 200 nm < λ < 300 nm of each combustion sample does not significantly contribute to the measured total absorbance intensities in this wavelength range.

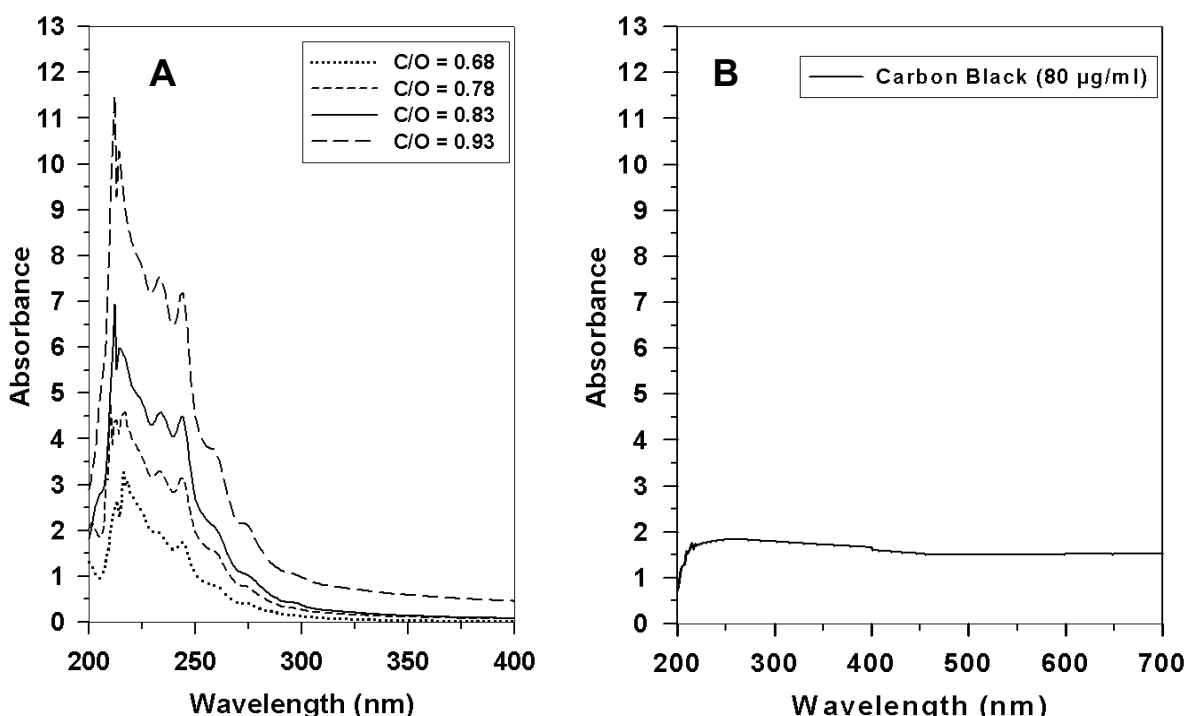


Figure 3-2: Ethylene combustion condensates display a broad band absorption in the UV range

Spectrophotometric analysis of ethylene combustion condensates (A) originating from ethylene/oxygen combustion at different C/O ratios and of carbon black suspended in water (80 µg/ml) (B). A large absorption peak in the UV region (200-300 nm) indicates the presence of combustion generated nanoparticles in each examined ethylene combustion condensate. Carbon black (soot reference) absorbs with more or less same intensity in both UV- and visible region of the spectrum.

The Abs_{250} values of ethylene combustion samples obtained at different combustion ratios (C/O ranging from 0.63 to 0.93) and originating from three cool traps are related to their corresponding TOC contents. Results given in Figure 3-3 demonstrate a linear correlation between the Abs_{250} values and the corresponding TOC contents of ethylene combustion condensates. This means that both Abs_{250} and TOC content can be used as parameters describing the particle concentration in the combustion condensates. Finally, the TOC content was selected in this work as a parameter for describing the combustion condensates.

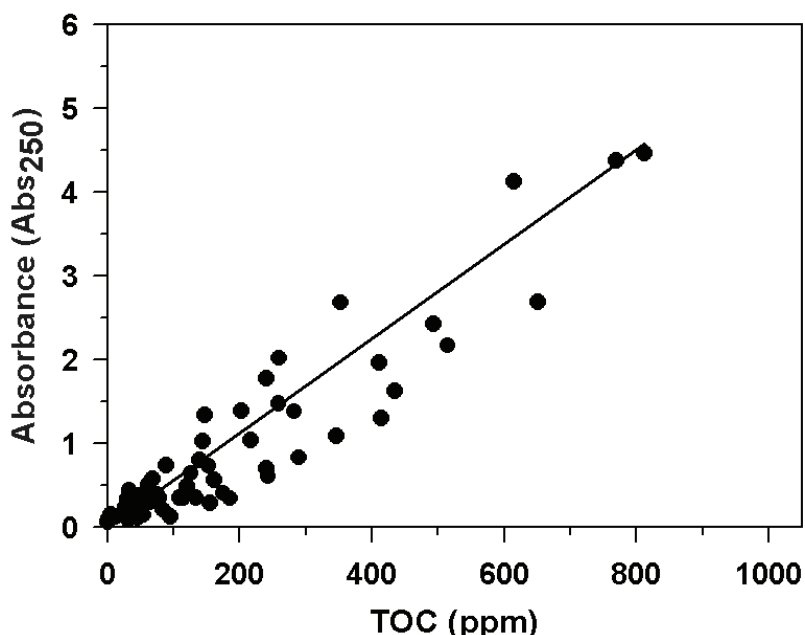


Figure 3-3: Total organic carbon contents of ethylene combustion condensates show good correlation with their Abs_{250} values

The Abs_{250} values of the ethylene combustion condensates obtained at different combustion ratios (C/O ranging from 0.63 to 0.93) and originating from three cool traps are related to their corresponding TOC contents. Abs_{250} parameter is used as an indicator of nanoparticles in the examined combustion condensates.

3.2 Combustion condensates are genotoxic and cytotoxic according to the bacterial SWITCH test

The bacterial SWITCH test was used as a pre-screening method for toxicity assessment of combustion condensates. It is a rapid assay for simultaneous testing of both genotoxic and cytotoxic effects by means of the recombinant *S. typhimurium* TA1535 pSWITCH strain (for detailed description of this assay see chapter 2.2.2.2). Impairment in cell growth and metabolism (cytotoxicity) was monitored via changes in relative intensity of absorbance and GFPuv-fluorescence output of treated cells

compared to untreated cells. DNA damage effects (genotoxicity) were assessed via changes in relative intensity of luminescence output of treated cells compared to the untreated ones (Baumstark-Khan et al., 2005; Stojicic et al., 2005).

3.2.1 Toxicity of ethylene combustion condensates depends on their TOC content

Ethylene combustion condensates, obtained at different C/O ratios (ranging from 0.63 to 0.93), were tested for their toxicity. All tested ethylene combustion condensates originated from the first cool traps.

The SWITCH results of ethylene combustion condensates originating from one production series (ethylene combustion at C/O=0.63, C/O=0.68, C/O=0.73, C/O=0.78, C/O=0.83, C/O=0.88, and C/O=0.93) are given separately in the Appendix. For the sake of clarity, the results of only 4 combustion condensates obtained at representative C/O ratios are shown jointly in Figure 3-4. The cytotoxic potential of the ethylene combustion condensates obtained at different C/O ratios was assessed according to the relative absorbance and relative fluorescence. The corresponding dose-effect curves (best fit regression curves, $R^2>0.90$) for increasing sample concentrations are shown in Figure 3-4 A and Figure 3-4 B, respectively. For low concentrations (< 10 ppm), both relative fluorescence and relative absorbance are close to 1. No difference in the fluorescence/absorbance signals of treated and non-treated bacteria implies that the samples are not cytotoxic in this concentration range. At concentrations > 10 ppm, a rapid dose-dependant decrease in relative fluorescence and relative absorbance occurs. This is due to the impairment in bacterial metabolic activity and growth, caused by a strong cytotoxic effect of the applied agents.

Induction of the SOS-Lux receptor-reporter system, carried on the pSWITCH plasmid of *S. typhimurium* TA1535, was used for genotoxicity assessment. For concentrations lower than ~10 ppm, the bioluminescence of the bacterial culture treated with ethylene combustion condensates is similar to that of the untreated culture (Figure 3-4 C). Consequently, the calculated relative luminescence is close to 1 and genotoxicity is not observed. For concentrations higher than 10 ppm, there is a steep increase in the relative luminescence output. This is due to activation of the SOS repair system in response to deleterious changes in the genetic material of

treated bacteria. After reaching its maximum, relative luminescence decreases dose-dependently. This is probably due to a predominant cytotoxic effect of combustion condensates in this dose range, since the production of bioluminescence requires the presence of ATP and oxygen. A decrease in luminescence output correlates with the pronounced cytotoxic effect of the tested samples, as it can be seen from the decrease in the absorbance and fluorescence signals in the same concentration range (Figure 3-4 A and Figure 3-4 B).

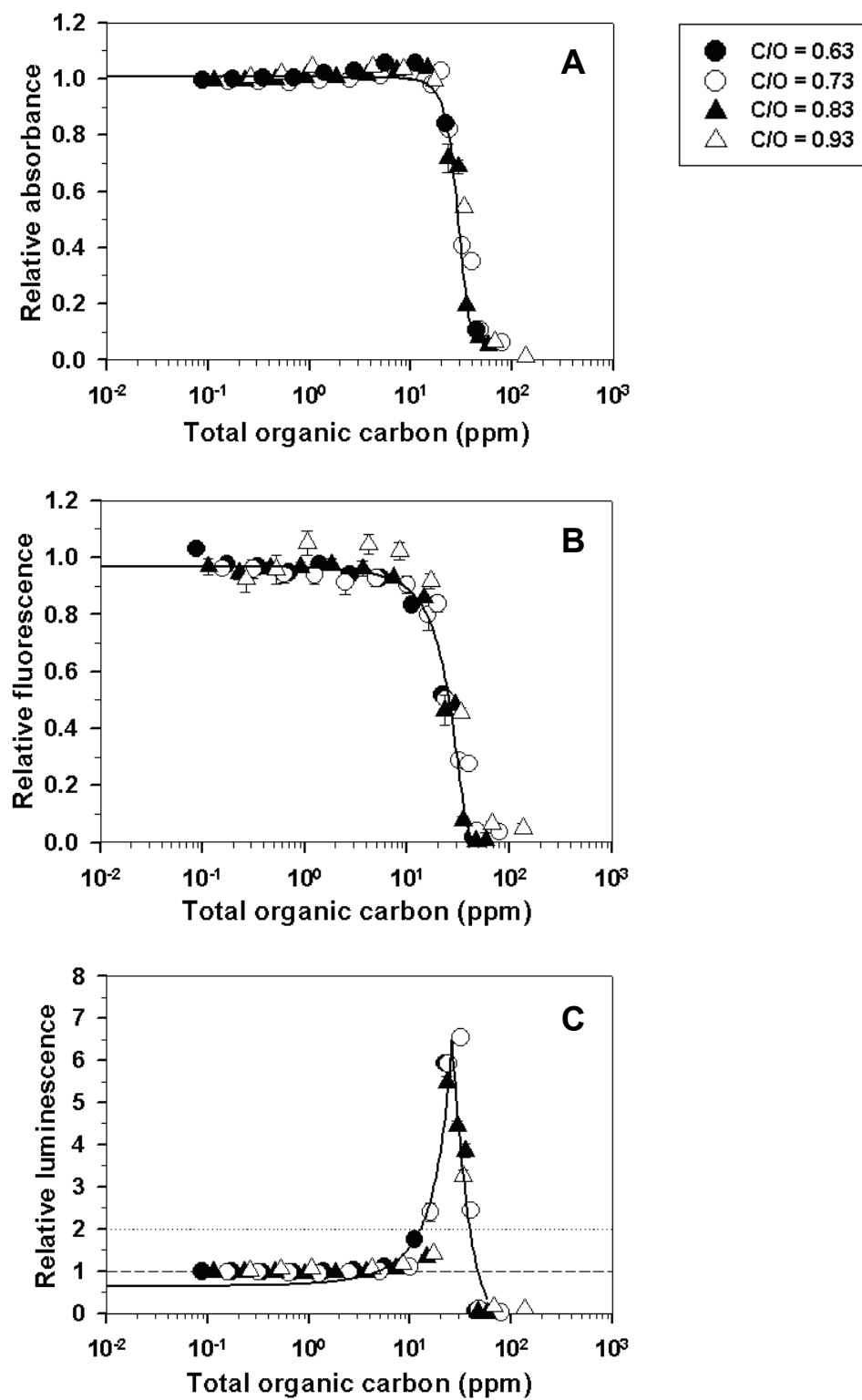


Figure 3-4: Toxicity of ethylene combustion condensates depends on their TOC content

Toxicity of ethylene combustion condensates obtained at C/O ratios ranging from 0.63 to 0.93 as assessed with the SWITCH test. Relative absorbance (A), fluorescence (B) and luminescence (C) profiles of treated bacteria are plotted as a function of TOC content of the combustion samples. Dashed line (relative luminescence = 1) reflects the relative luminescence of the untreated culture. Dotted line (relative luminescence = 2) represents the threshold for defining genotoxicity.

In order to estimate the impact of C/O ratio on the toxicity of ethylene combustion samples, genotoxicity and cytotoxicity of samples gained at different C/O ratios are compared. LC₅₀ values, as determined from relative absorbance and fluorescence plots for each tested combustion sample separately, are used for the comparison of cytotoxicity of different samples. The concentration at which the relative luminescence reaches its maximum (lux peak concentration) and the maximum luminescence value (lux peak value) serve as numeric parameters for genotoxicity. Mean LC₅₀ values, lux peak concentrations and lux peak values shown in Figure 3-5 are averaged from SWITCH results of 3 production series of combustion samples.

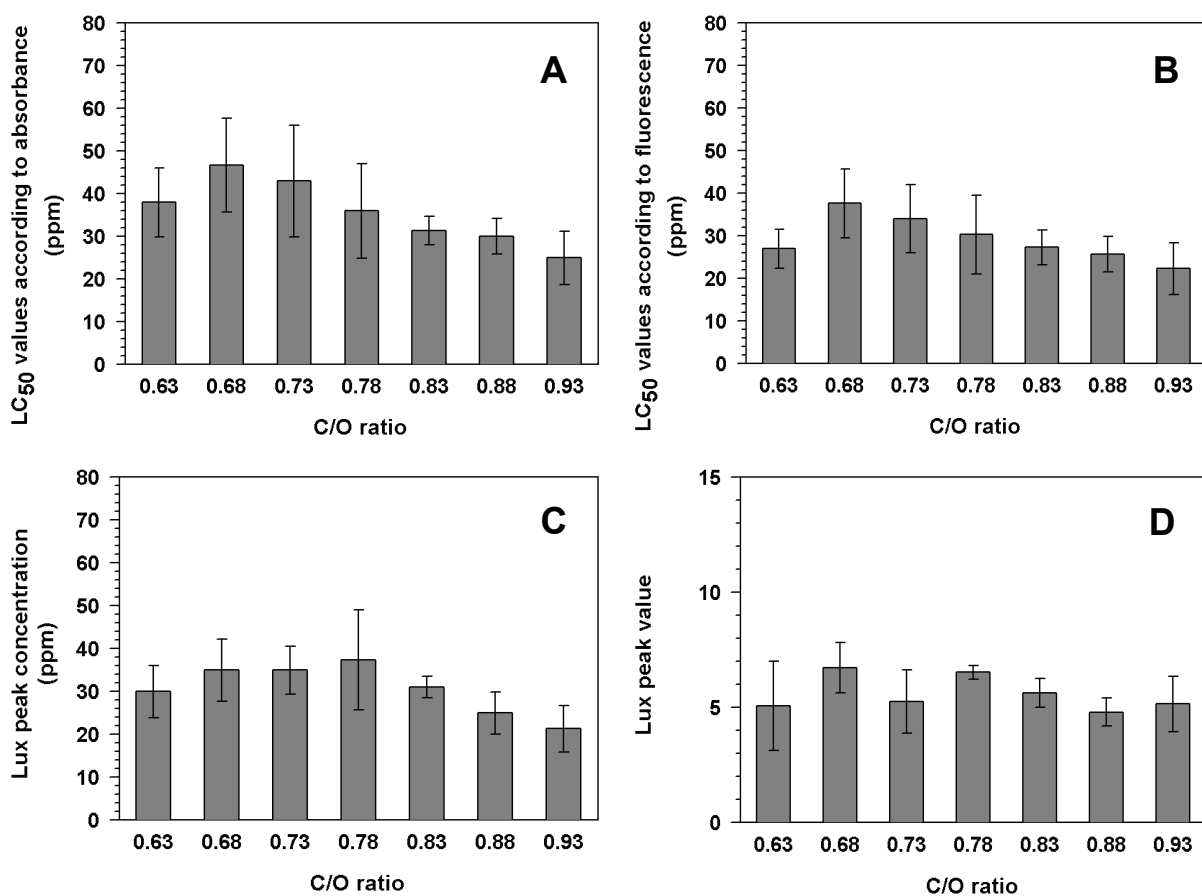


Figure 3-5: Different C/O ratios show no significant impact on the toxicity of ethylene combustion condensates at comparable TOC levels

Cytotoxic potentials of the ethylene combustion condensates generated at different C/O ratios (range of 0.63-0.93) are compared according to LC₅₀ values obtained from the relative absorbance (A) and relative fluorescence (B) profiles in the SWITCH test. Genotoxic potentials of the same samples are compared according to the lux peak concentrations (C) and lux peak values (D) obtained in the same test. Graphs show mean values of the corresponding genotoxic/cytotoxic parameters of three production series of the samples. One-way ANOVA variance analysis was applied for comparison.

According to the absorbance measurements, mean LC₅₀ values of the combustion samples gained at different C/O ratios are in the range between 25 ppm and 46 ppm of total organic carbon (Figure 3-5 A). Similarly, according to the fluorescence

measurements, the range of all mean LC₅₀ values is between 22 ppm and 38 ppm (Figure 3-5 B). All samples exhibit genotoxic potential (lux peak values ≥ 2) and the range of mean lux peak concentrations (21 ppm – 37 ppm) is quite similar to the range of LC₅₀ values (Figure 3-5 C). Genotoxic potential of the samples gained at different C/O ratios was compared with one-way ANOVA variance analysis. Same analysis was undertaken for the comparison of their cytotoxic potential. Results of the variance analysis reveal no significant difference between the genotoxicity/cytotoxicity of the combustion samples in respect to the C/O ratio. This means that the toxic potential of tested samples only depends on their TOC content and not on the condition (C/O ratio) used for the samples' generation. This makes the TOC content a relevant parameter in the assessment of the toxicity of combustion condensates.

3.2.2 Toxicity of diesel combustion condensates depends on their TOC content

Diesel combustion condensates produced during 4kW-load and no-load engine operating mode were assessed for toxicity using the bacterial SWITCH test. Two samples obtained at no-load and two samples gained at 4 kW-load engine operating mode were tested in a wide concentration range (0.1 - 190 ppm of total organic carbon), and the corresponding dose-effect curves are presented in Figure 3-6. All tested samples originated from the first cool traps.

Results obtained with the SWITCH test show the toxic potential of diesel combustion condensates to be correlated to the samples' TOC content. Dose-effect responses for the samples obtained at two different diesel engine operating modes can be fitted by the same regression curve (Figure 3-6). This means that the same amount of total organic carbon in diesel combustion condensates exerts the same toxic effect, regardless of the type of engine operating mode during the sample generation. For concentrations higher than 10 ppm of total organic carbon, relative absorbance and relative fluorescence values decrease dose-dependently due to the cytotoxic effect of the diesel combustion samples (Figure 3-6 A, B). TOC concentration of tested diesel combustion samples which caused 50% death in the cell population (LC₅₀) is 24 ppm and 19 ppm according to the relative absorbance and relative fluorescence dose-effect curves, respectively. For concentrations higher than ~ 5 ppm, diesel

combustion samples exert a dose-dependant increase in the DNA damage-induced bioluminescence (Figure 3-6 C). Maximum genotoxic effect (lux peak value = 4.2) is achieved at 20 ppm of total organic carbon. A further increase in TOC concentrations causes a decrease of the measured bioluminescence output, due to the predominant cytotoxic effect of the diesel combustion condensates.

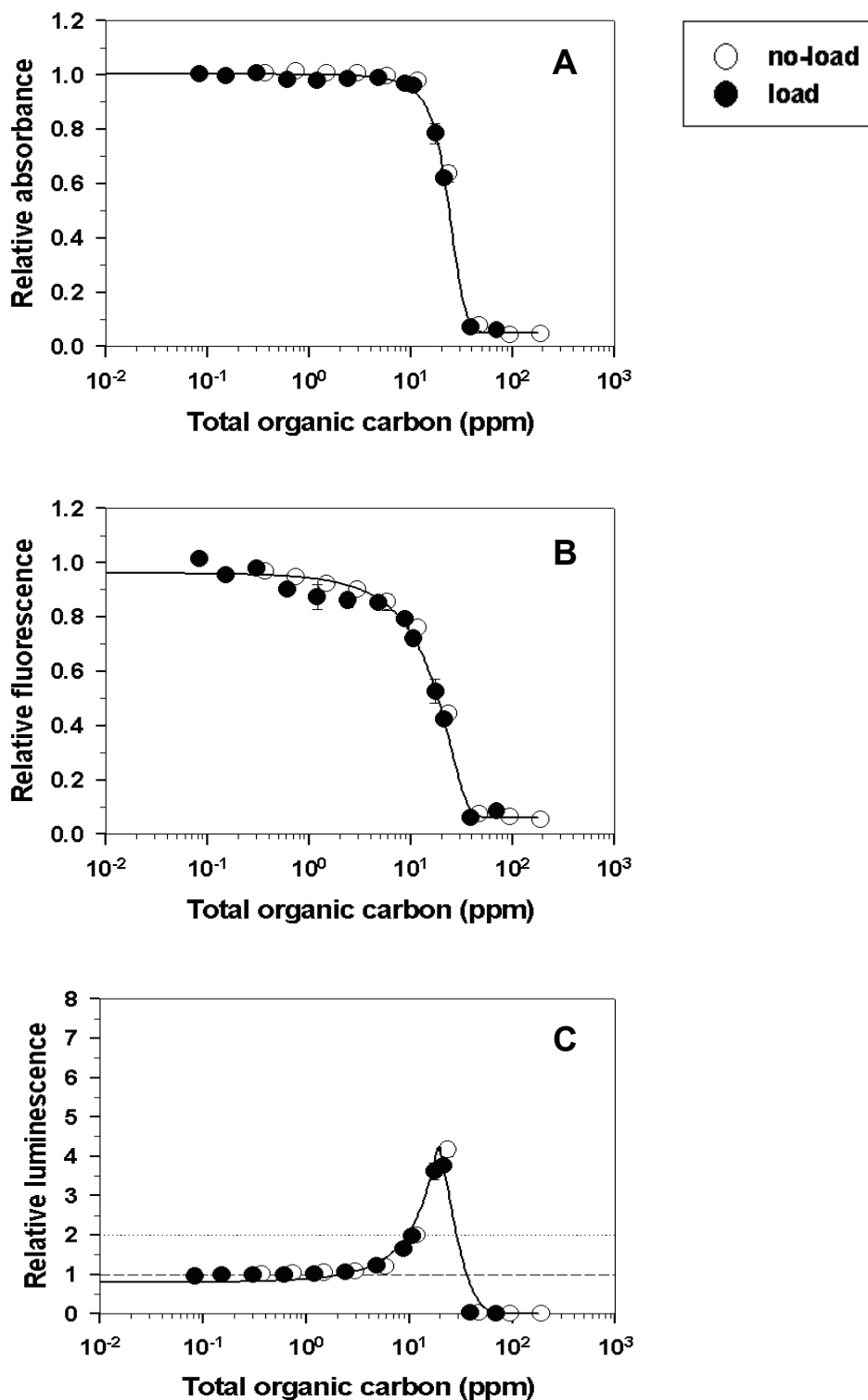


Figure 3-6: TOC content determines the toxicity of diesel combustion condensates

Toxicity of diesel combustion condensates obtained from no-load and 4kW-load operating conditions of the diesel engine was tested with the SWITCH test. Relative absorbance (A), relative fluorescence (B) and relative luminescence (C) profiles of treated bacteria are plotted as a function of TOC content of the condensates. The dashed line (relative luminescence = 1) is the luminescence of the untreated culture. The dotted line (relative luminescence = 2) represents the threshold for genotoxicity.

3.2.3 Prolonged storage of combustion condensates has no impact on their toxicity

Immediately after production, combustion condensates were stored in the refrigerator (+ 4°C). The condensates proved to be stable for a long period of time. Figure 3-7 exemplarily shows SWITCH test results of the ethylene combustion condensate generated at C/O=0.83 (A, B) and of diesel combustion condensate gained at no-load engine operating mode (C, D), after different storage periods. Results show that the toxic potential of tested condensates does not change after 2 years of storage.

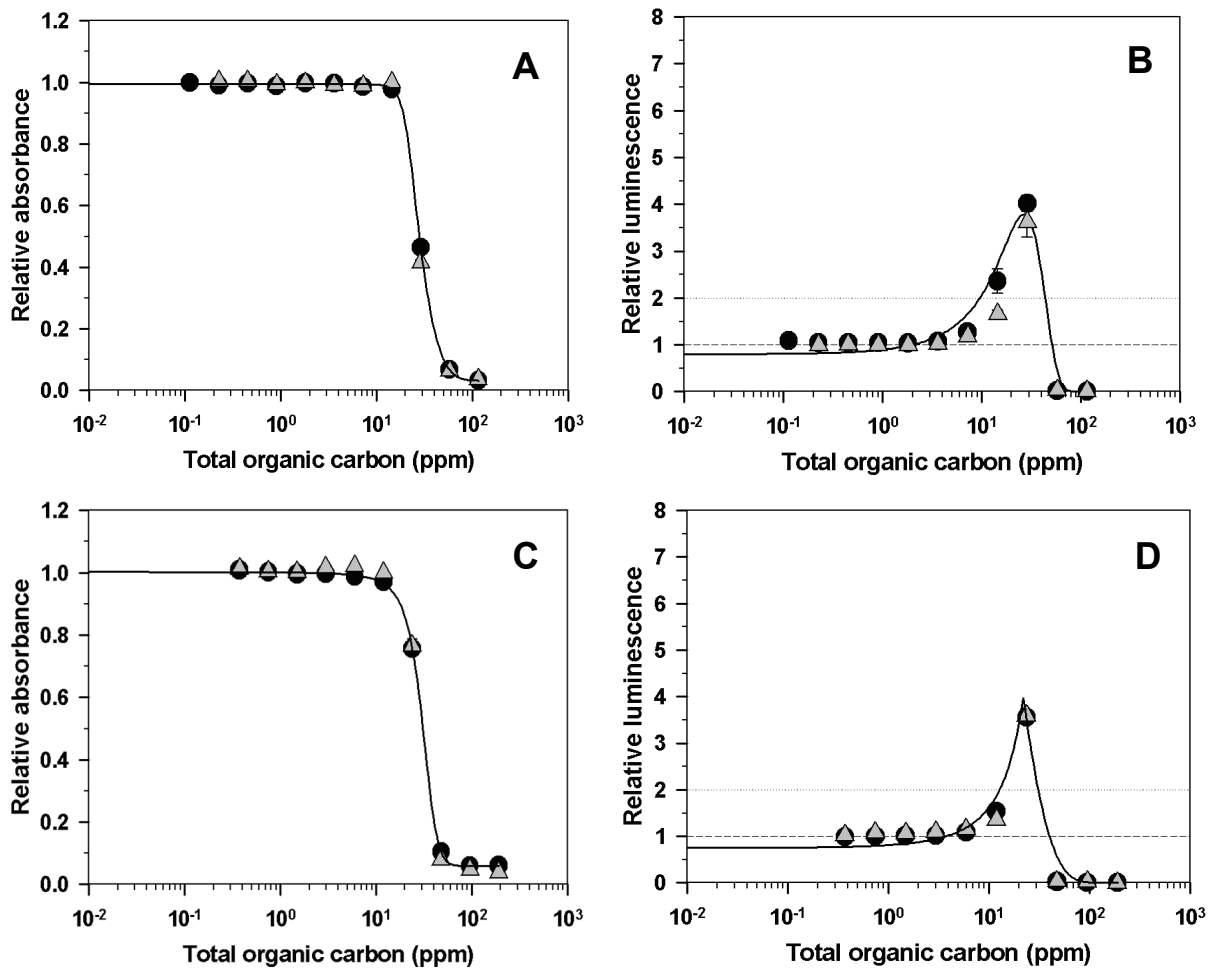


Figure 3-7: Toxic potential of combustion condensates is stable after 2 years of storage

Figures show dose-effect results for the ethylene combustion condensate gained at C/O=0.83 burning conditions (A, B) and diesel combustion condensate (C, D), as assessed with SWITCH test. Each condensate was tested before (black circles) and after (gray triangles) 2 years of storage at 4°C.

3.2.4 Toxicologically relevant constituent of the combustion exhaust is being captured in all three cool traps

Toxicity of the combustion condensates originating from three cool traps was tested separately in bacterial SWITCH test. Representative SWITCH results are shown (Figure 3-8 A, B) for the ethylene combustion condensates ($C/O=0.93$) from all three cool traps. No significant difference was found in the toxicity of the ethylene combustion condensates originating from different cool traps, when related to their total organic carbon content. This means that all three cool traps contain constituent(s) of the combustion exhaust responsible for the observed toxic effects. Moreover, this affirms the former observations that TOC content is a good indicator for the toxicity of combustion condensates.

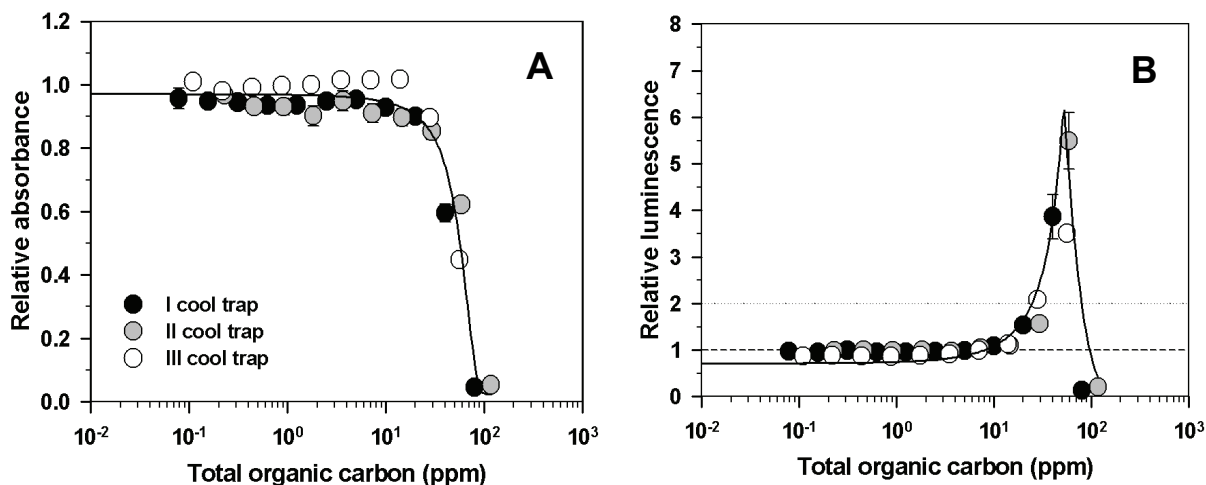


Figure 3-8: Same amount of TOC in combustion condensates exhibits same toxic effect regardless of the cool trap it originates from

Toxicity of the ethylene combustion condensates ($C/O=0.93$) originating from I, II or III cool trap was assessed with SWITCH test. Cytotoxic effect of these condensates is monitored via changes in the relative absorbance of the treated bacterial culture (A). Increase in bioluminescence output over the threshold (relative luminescence=2) indicates genotoxic effect of tested combustion condensates (B).

3.2.5 Soot has no significant contribution to the toxicity of ethylene combustion condensates

3.2.5.1 Increased concentration of soot particles in ethylene combustion condensate does not change its toxic potential

If the toxicity of combustion condensates is due to soot particles, than an increased concentration of soot particles in the condensates should increase their toxicity. In order to test this hypothesis, the following experiment was conducted. Ethylene

combustion condensate (generated under C/O=0.93 combustion conditions) was centrifuged in Eppendorf 5417R centrifuge at 20 817 x g for 90 min and at 4°C. After centrifugation, soot particles formed a visible black pellet on the bottom of the centrifuge tube. Half of the supernatant volume was carefully aspirated, not disturbing the pellet. Then the pellet was resuspended in the remaining supernatant, thereby increasing the concentration of soot particles twofold. The same centrifugation procedure and the aspiration step afterwards were performed with the ethylene combustion condensate containing twofold increased concentration of soot particles. This way, the ethylene combustion condensate containing fourfold increased amount of soot particles was produced. The effect of the increased concentration of soot particles was tested with the bacterial SWITCH test. Same dilutions of the non-centrifuged ethylene combustion condensate and the ethylene combustion condensate with twofold and fourfold increased soot concentration were applied in the SWITCH test. Dose-effect curves of all tested samples show the same result (Figure 3-9). This indicates that a twofold and a fourfold increase in the concentration of soot particles do not change the toxic potential of the ethylene combustion condensate.

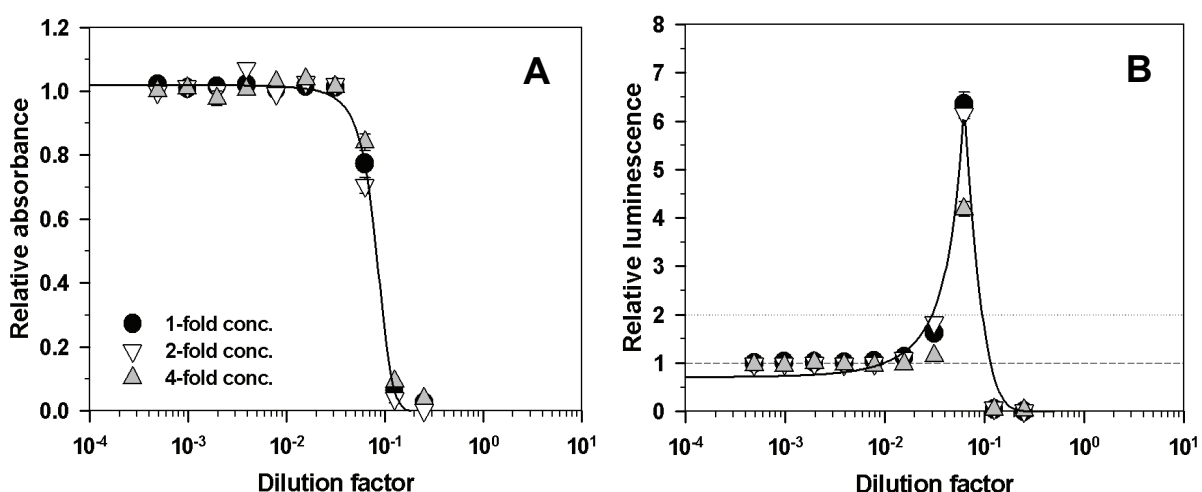


Figure 3-9: Increased concentration of soot particles does not change the toxicity of ethylene combustion condensate

Twofold (white down-triangles) and fourfold (gray up-triangles) increase in the concentration of soot particles in ethylene combustion condensate (C/O=0.93) does not change the toxicity of the original ethylene combustion condensate (black circles).

3.2.5.2 Soot particles larger than 20 nm have no significant contribution to the toxicity of ethylene combustion condensate

In order to test whether soot particles contribute to the toxic effects of ethylene combustion condensates, ethylene combustion condensate (C/O=0.93) was filtrated (detailed description in chapter 2.2.1.6). First filtration step was achieved by using “Anotop 10” inorganic membrane filter with 100 nm pore size, which retained particulate matter larger than 100 nm. Black deposit on the filter membrane indicated efficient retention of soot agglomerates. In further text, the filtrate obtained via filtration through the 100 nm-pored filter will be referred to as “**filtrate 1**”. The second filtration step was performed by filtering the filtrate 1 through the “Anotop 10” inorganic membrane filter with 20 nm pore size. Thereby, the “**filtrate 2**” was obtained. There was no visible black deposit on the membrane of the 20 nm-pored filter. This proves the efficiency of the first filtration step, since all soot agglomerates were successfully retained with the 100 nm-pored filter.

The toxicity of filtrate 1 and filtrate 2 was tested with the SWITCH test and compared to the toxic potential of non-filtrated ethylene combustion condensate. Same dilutions of the non-filtrated ethylene combustion condensate, filtrate 1 and filtrate 2 were applied in this test. Results show no difference in toxic potentials of the non-filtrated sample and of two filtrates (Figure 3-10). Relative absorbance profiles of the bacterial cultures treated with non-filtrated sample or with the filtrates (1 and 2) are almost identical. Same conclusion can be drawn for their relative luminescence profiles. These results imply that soot particles larger than 20 nm have no significant contribution to the toxicity (geno-/cytotoxicity) of ethylene combustion condensate.

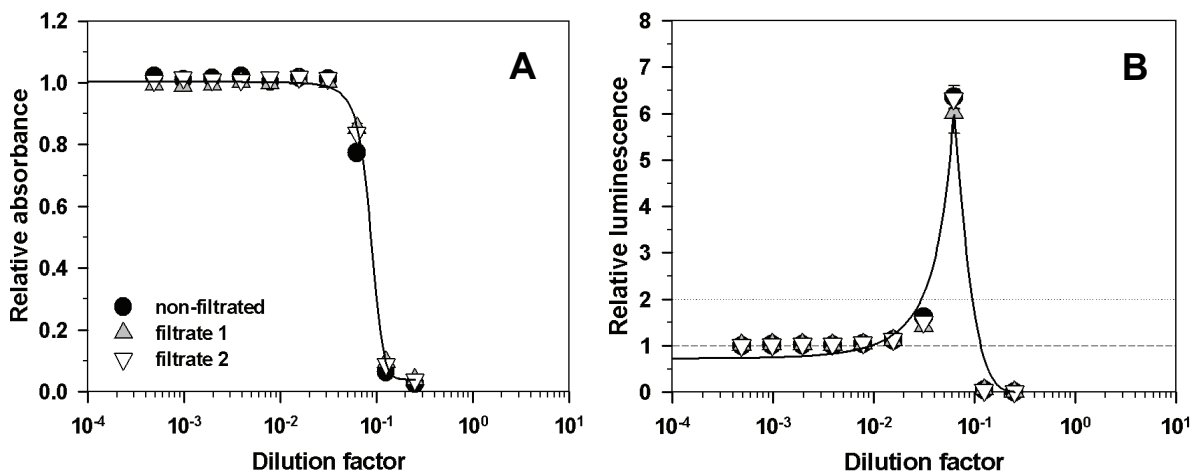


Figure 3-10: Soot particles larger than 20 nm have no significant contribution to the toxicity of ethylene combustion condensate, as estimated with bacterial SWITCH test
Toxicity of the filtrate 1 (gray up-triangle), filtrate 2 (white down-triangle) and non-filtrated ethylene combustion condensate (black circle) was assessed with SWITCH test. Tested samples show no difference in their cytotoxic (A) and their genotoxic potential (B).

3.2.5.3 Soot particles ($d \geq 10 \text{ nm}$) are not responsible for the toxic potency of ethylene combustion condensate

In order to prove that the soot particles ($d \geq 10 \text{ nm}$) do not contribute to the toxicity of the combustion condensates, the ethylene combustion sample ($\text{C/O}=0.93$) was centrifuged in Optima LE-80K ultracentrifuge (with SW55Ti rotor) at severe conditions (14 h at 116 000 $\times g$, at 4°C) in order to precipitate soot particles (method described in chapter 2.2.1.5). According to the manual of the Beckman Coulter rotors, pelleting efficiency of the SW55Ti rotor at 116 000 $\times g$ (35 000 rpm) speed is $k=118$. Considering the fact that the centrifugation lasted 14 h, it is easy to calculate that the particles with a sedimentation coefficient $s \geq 8 \text{ S}$ ($1 \text{ S} = 1 \text{ Svedberg unit}$) will be precipitated at this speed and duration ($s=k/t[\text{h}]$). According to literature data (Grotheer et al., 2004), smallest primary soot particles which can be found in exhaust gases have a mean diameter of 10 nm and their mass is considered to be in order of $\sim 10^5 \text{ u}$ ($\sim 1.66 \times 10^{-22} \text{ kg}$). The enzyme aldolase with the molecular weight of 38 000 u ($6.3 \times 10^{-23} \text{ kg}$) has a sedimentation coefficient of 8 S (according to the manual of Beckman Coulter rotors). Since the mass of primary particles is higher than the molecular weight of the aldolase, it was considered that the applied centrifugation speed was sufficient to pellet all soot particles ($d \geq 10 \text{ nm}$) in the ethylene combustion condensate. After centrifugation, soot particles formed a visible and well

distinguishable black pellet at the bottom of the centrifuge tube. The centrifuged sample (5 ml) was divided in two fractions: 2 ml of supernatant (considered to be soot-free) and 3 ml of resuspended pellet (containing soot particles). Toxicity of these two fractions as well as the toxicity of the non-centrifuged sample was tested in the bacterial SWITCH test. Same dilutions of the samples were applied in this test. As Figure 3-11 shows, there is no difference in the toxicity of the non-centrifuged sample, supernatant and the resuspended pellet. Relative absorbance profiles (Figure 3-11 A) for all three tested samples show good congruence and fit the same regression curve. The same conclusion can be drawn for the relative luminescence profiles (Figure 3-11 B). These results show that the toxic constituent can not be precipitated after 14 h centrifugation of ethylene combustion condensate at 116 000 x g. Furthermore, this means that soot particles ≥ 10 nm have no significant contribution to the toxic potential of ethylene combustion condensates.

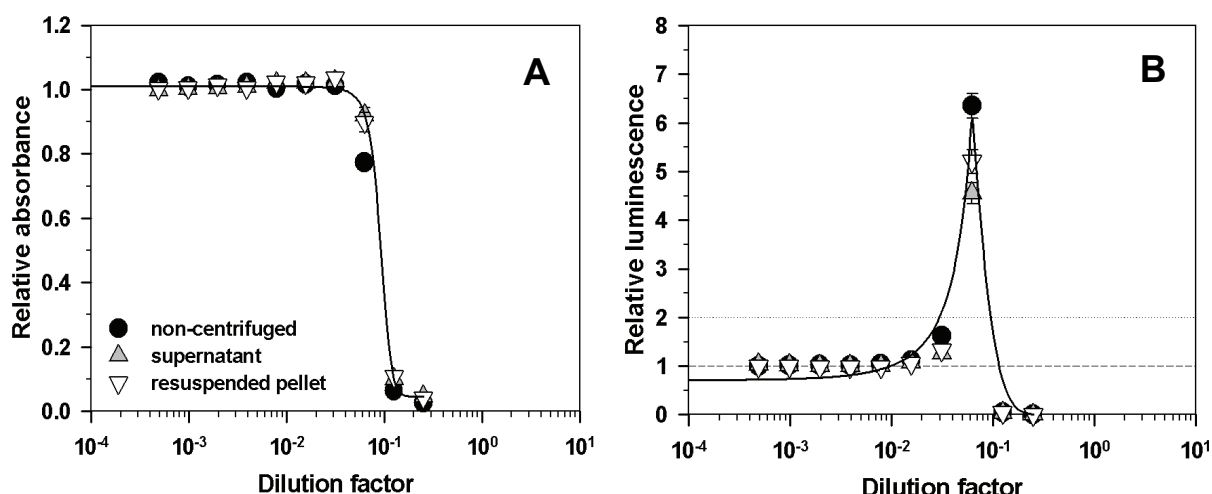


Figure 3-11: Toxic constituent can not be precipitated after 14 h centrifugation of ethylene combustion condensate at 116 000 x g, as estimated with bacterial SWITCH test

After centrifugation at 116 000 x g for 14 h, toxicity of supernatant (gray up-triangle), resuspended pellet (white down-triangle) and the non-centrifuged sample (black circle) was assessed with the bacterial SWITCH test. Tested samples show no difference in their cytotoxic (A) and their genotoxic potential (B).

All aforementioned fractions of the ethylene combustion condensate (chapters 3.2.5.1; 3.2.5.2; and 3.2.5.3), obtained via centrifugation or filtration, were examined for their TOC content and absorbance in the UV- ($\lambda = 250$ nm) and visible light range ($\lambda = 600$ nm). This physical and chemical characterisation of the non-treated ethylene combustion condensate and its fractions is given in Table 3-3. Absorbance measurements at 250 nm (Abs_{250}) and at 600 nm (Abs_{600}) served as indicators for

nanoparticles and soot particles, respectively. No measurable absorbance at 600 nm indicates the absence of soot particles in filtrate 1, in filtrate 2 and in the supernatant obtained after centrifugation for 14 h at 116 000 x g. These samples display measurable absorbance at 250 nm ($\text{Abs}_{250}=1-1.3$), indicating the presence of nanoparticles. Centrifugation and filtration treatments did not significantly affect Abs_{250} or TOC content of all analysed ethylene combustion condensates' fractions. Mean Abs_{250} value and mean TOC value of all analysed fractions are 1.4 ± 0.2 and 169 ± 9 , respectively.

Table 3-3: Physical and chemical characterisation of the ethylene combustion sample (C/O=0.93) and its fractions obtained via centrifugation or filtration

Sample fraction	obtained by	Abs_{250}	Abs_{600}	TOC (ppm)
non-centrifuged/non-filtrated ethylene combustion sample		1.38	0.15	166
filtrate 1	filtration through 100 nm-pored filter	1.10	0	161
filtrate 2	filtration of filtrate 1 through 20 nm-pored filter	1.31	0	164
concentration level 1 (2-fold increased conc. of soot particles)	centrifugation at 20 817 x g for 90 min	1.72	0.30	180
concentration level 2 (4-fold increased conc. of soot particles)	centrifugation at 20 817 x g for 90 min	1.50	0.57	158
supernatant	centrifugation at 116 000 x g for 14 h	1.00	0	171
resuspended pellet	centrifugation at 116 000 x g for 14 h	1.46	0.23	181

3.3 Effects of combustion condensates on human cell lines

Results presented so far have shown that the toxicity of combustion condensates can be verified with the bacterial assay. For human health risk assessment, it is important to investigate the toxic effects of combustion condensates on cell systems of higher evolutionary level. For this purpose, two human cell lines were selected as described below.

The cell line A-549 is a permanent line derived from a human alveolar cell carcinoma. In this work, it was used as a model to study the effects of combustion condensates on human lung alveolar cells. Besides the respiratory system, which is the main portal of entry for the components of the combustion exhaust, the extrapulmonary targets (blood cells, heart, liver etc.) became of large interest ever since the published data showed that some components of the combustion exhaust may overcome the lung-blood barrier and enter the systemic circulation (Oberdörster et al., 2002; Nemmar et al., 2002). Human monocyte-like neoplastic cell line U-937 was used in this thesis as a representative of the extrapulmonary targets.

3.3.1 Characterisation of tested human cell lines: cell growth kinetics

Toxic agents can influence cellular growth and proliferation. Understanding the growth characteristics of test cell models is therefore important for proper experimental set up.

Generation of a growth curve is useful in evaluating growth characteristics of a certain cell line. Monitoring of the cell growth kinetics provides information about duration of certain growth phases and the speed of cell proliferation (the doubling time). For the analysis of growth kinetics of A-549 and U-937 cell line, cells were seeded in 24-well plate and cell number was determined at regular time-points during 8 days cultivation period (chapter 2.2.3.4).

A-549 cell growth curve (Figure 3-12 A) displays typical three phases: lag phase, exponential phase (log-phase) and stationary phase. After seeding, there is a slight decrease in the cell density (lag-phase) due to the fact that the attachment efficiency of the seeded cells is not 100% and the cells also need some time to adjust to the new environment before they start to proliferate. Lag-phase of the A-549 cells lasts approximately 24 h. No apparent lag-phase is recorded in the growth kinetics of the U-937 cell line (Figure 3-12 B), as suspension cells do not need to attach to the

surface of the vessel in order to proliferate. Log-phase is a period of active cell proliferation during which the number of cells increases exponentially. The speed of cell proliferation in the exponential phase can be characterised by the doubling time (chapter 2.2.3.4). The doubling time of the A-549 and U-937 cell line is 18 h and 27 h, respectively. After 6-7 days of cultivation, the proliferation of both cell lines reached the plateau phase (stationary phase) and the number of cells remained constant.

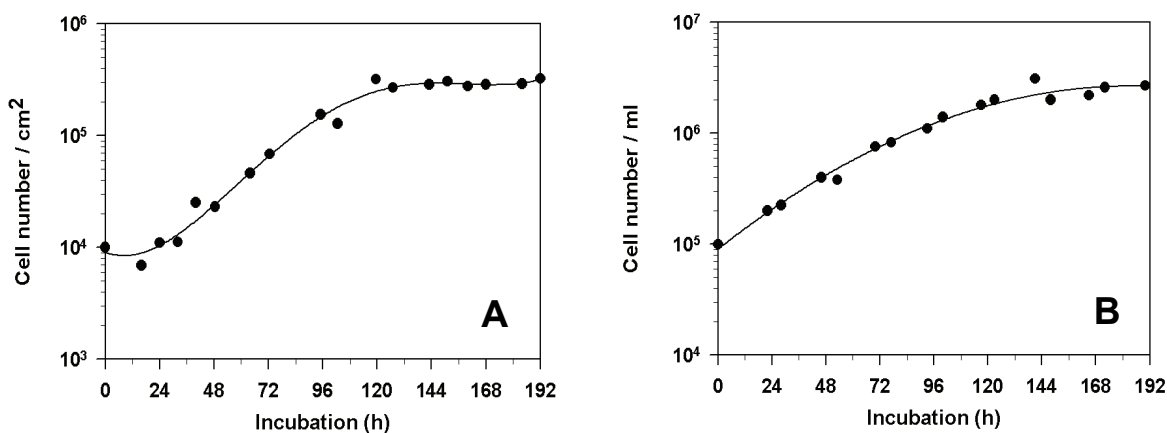


Figure 3-12: Growth curves for A-549 and U-937 cell lines

Cells were seeded in 24-well plate and counted at regular time-points twice per day for the next 8 days. Medium was renewed every 2-3 days. Cell density of the adherent cell line A-549 (A) is expressed as cell number per cm^2 , while the cell density of the suspension cell line U-937 (B) is expressed as cell number per ml.

3.3.2 Combustion condensates impair cell growth

The cytotoxic effect (impairment of cell metabolism and growth) of combustion condensates was studied on both human cell lines: U-937 and A-549.

U-937 cells were treated up to 72 h with different concentrations of ethylene combustion condensate ($\text{C}/\text{O}=0.93$) in order to study the effect of the combustion condensate on cell growth (Figure 3-13). After treatment, cells were centrifuged (400 x g, 5 min) and resuspended in 0.5 ml PBS prior to the FACS-analysis.

FSC vs. SSC density plots revealed that treatment with the ethylene combustion condensate at concentrations above 4.8 ppm of total organic carbon caused splitting of one compact cell population into two subpopulations: R1-gated and R2-gated (Figure 3-26). Since the results of the Annexin V-PE/7-AAD apoptotic assay (Figure 3-21) demonstrated that the R1-gated cell population consists predominantly of viable cells, it was decided to take the number of R1-gated cells as an indicator for

cell viability. An incubation for 7 h with ethylene combustion condensate has no effect on cell growth (Figure 3-13). After 24 h incubation, there is a dose-dependant decrease in the number of viable cells in the treated culture compared to the untreated one. This effect is even more pronounced for longer incubation time (24 - 72 h). At concentration of 2.4 ppm of total organic carbon, ethylene combustion condensate has no impact on cell growth for all tested incubation time-points.

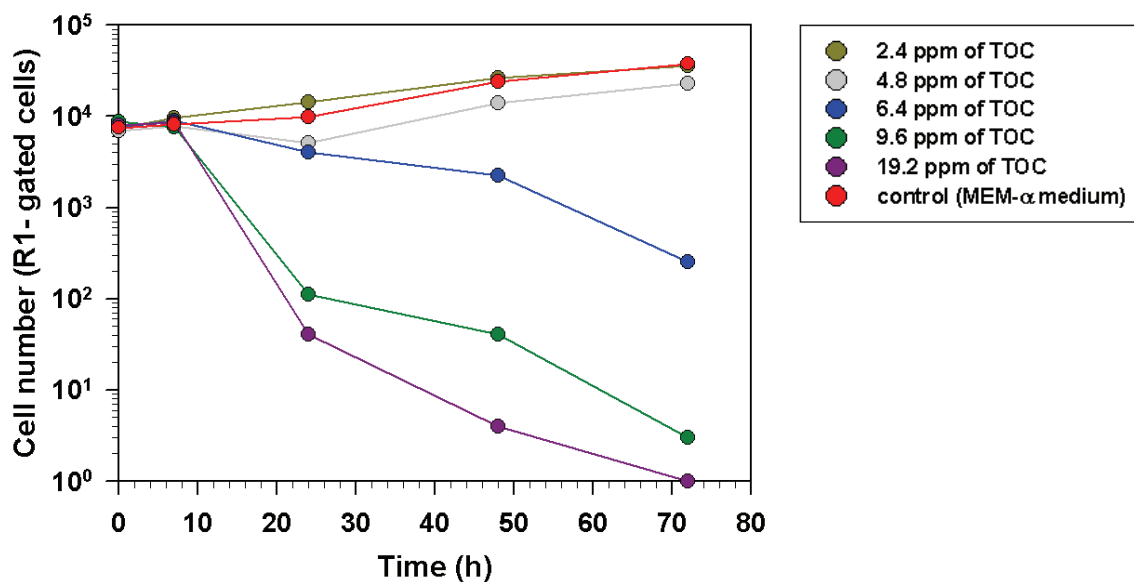


Figure 3-13: Kinetics of the effect of ethylene combustion condensate on the U-937 cell growth

U-937 cells were seeded at 3×10^5 cells/ml and treated on the next day with different concentrations of ethylene combustion condensate ($C/O=0.93$) as indicated in the legend, or left untreated (control). After 7 h/ 24 h/ 48 h and 72 h of incubation, cells were centrifuged and resuspended in PBS for the FACS-analysis. Each sample was measured for 20 s in the FACS. The number of viable cells is assessed as the number of R1-gated cells in FSC vs. SSC density plot. Results of one representative experiment are shown.

According to the results shown in Figure 3-13, 48 h was chosen as a suitable time-point for studying a dose-response in U-937 cells, since for this time-point there was a clear distinction between the effects of different doses of ethylene combustion condensate. For the dose-response analysis (Figure 3-14), relative cell growth (N/N_0) was calculated as number of R1-gated cells of the treated cell population divided by the number of R1-gated cells of the untreated population. Ethylene combustion condensate containing 2.4 ppm of total organic carbon allowed survival of nearly all treated cells after 48 h of treatment (Figure 3-14). Same treatment with ethylene combustion condensate containing approximately 5 ppm of total organic carbon

caused death in 50% of the U-937 cell culture. The 48 h incubation of cells with 9.6 ppm of total organic carbon caused death of almost all (99.9%) treated cells.

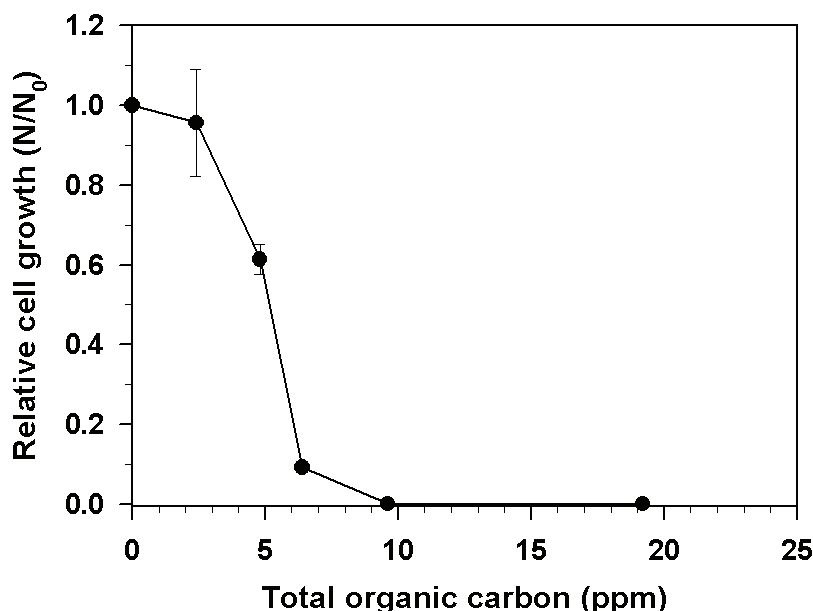


Figure 3-14: Ethylene combustion condensate impairs U-937 cell growth

After 48 h of incubation with the ethylene combustion condensate obtained from the ethylene combustion in the highly sooting conditions ($C/O=0.93$), U-937 cells were centrifuged and resuspended in PBS prior to the FACScan-analysis. Each sample was measured for 20 s in the FACScan. The number of viable cells is assessed as the number of R1-gated cells in FSC vs. SSC density plot. Relative cell growth is determined as a number of viable cells in treated culture divided by the number of viable cells in untreated culture (N/N_0). Data shown are averaged from two experiments.

The cytotoxic effect of combustion condensates was also studied on the human alveolar cell line A-549. Crystal violet proliferation assay (chapter 2.2.7) was utilised to assess the effect of different combustion condensates on A-549 cell growth. With this assay, relative cell number can be assessed by measuring the absorbance ($\lambda = 562$ nm) of crystal violet stain. Relative cell growth is calculated as the absorbance of cells treated with combustion condensates divided by the absorbance of the untreated cells. The crystal violet assay gives a greater data accuracy when the experiments are carried out for at least two cell generations (Gillies et al., 1986). Taking into account that the doubling time for the A-549 is 18 h, the 48 h time-point is chosen to study the dose-effect of combustion condensates on the A-549 cell growth. Furthermore, choosing the same incubation time (48 h) allows better comparison of the effects on A-549 and U-937 cell lines.

A dose-dependant reduction in A-549 cell growth can be observed after 48 h treatment with samples obtained from combustion of ethylene at C/O ratio of 0.63

and 0.93. The same holds true for the treatment with diesel combustion sample obtained during a no-load operating mode of diesel engine (Figure 3-15). Dose-effect curves for the ethylene combustion samples gained at non-sooting ($C/O=0.63$) and highly sooting conditions ($C/O=0.93$) progress similarly. Diesel combustion condensate compared to model flame exhaust displays a higher cytotoxicity in the lower concentration range (< 10 ppm of total organic carbon). Reduction in cell growth by 50% (LC_{50}) is achieved after treatment with ethylene combustion condensate ($C/O=0.63$) at concentration of 10 ppm of TOC. Similarly, 50% reduction in cell growth is achieved with ethylene combustion condensate ($C/O=0.93$) at concentration of 7 ppm or with diesel combustion sample at concentration of 2 ppm of total organic carbon. At concentration of 20 ppm of total organic carbon, all tested samples have the same cytotoxic effect and cause death of 80% of treated cells.

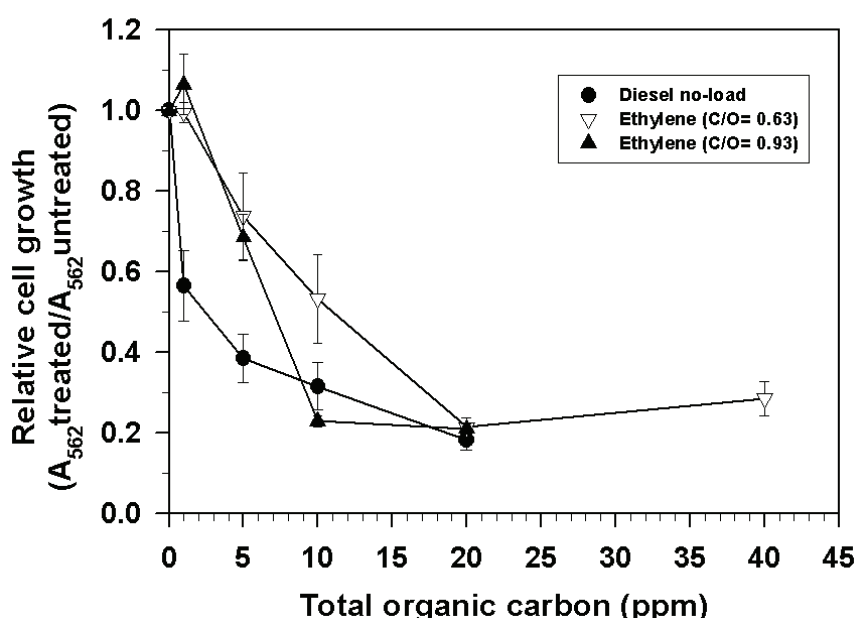


Figure 3-15: Combustion condensates impair A-549 cell growth

A-549 cells were treated for 48 h with ethylene combustion condensates (obtained at $C/O=0.63$ or at $C/O=0.93$ combustion stoichiometry) or with diesel combustion condensate obtained during no-load operating mode of a diesel motor. Cells were fixed with 3.5% formaldehyde/PBS and stained with 0.1% crystal violet solution. Relative cell growth is calculated as relative absorbance ($\lambda=562$ nm) of treated cells divided by the absorbance ($\lambda=562$ nm) of untreated cells.

3.3.3 Combustion condensates induce apoptosis in monocyte-like cell line but not in lung epithelial cell line

3.3.3.1 Cell cycle analysis and detection of apoptosis

Application of the PI-staining method combined with flow cytometry enables the measurement of cellular DNA content and thereby cell cycle analysis (chapter 2.2.6.2). Cells undergoing apoptosis contain sub-diploid DNA content and display PI-fluorescence intensities in the sub-G1 region of histogram plots.

U-937 cells were treated with different concentrations of ethylene combustion condensate and the changes in the cell cycle distribution were observed. Figure 3-16 shows one representative experiment. Overview of the cell cycle distribution after treatment of U-937 cells with ethylene combustion condensate is given in Table 3-4. Relative populations of subG1-, G1/G0-, S-, and G2/M events were calculated with the Cyclched software. “>G2” events symbolise cells with DNA content higher than 4n. In untreated cell culture, a common cell cycle distribution with two major peaks can be observed (Figure 3-16 A). First peak (G1/G0) indicates diploid cells (containing 2n DNA content), whereas second peak shows the cells in G2/M phase with 4n DNA content. Cells in G1 and G0 phase as well as cells in G2 and M phase have an identical DNA content, respectively. Therefore, G2 and M phase cells can not be discriminated with this method. In untreated culture, the proportion of cells in G1/G0 phase is higher than in G2/M phase (Table 3-4).

The lowest tested concentration of ethylene combustion condensate (2.4 ppm of total organic carbon) causes almost no changes in the cell cycle distribution compared to the untreated control (Figure 3-16 B). At concentration of 4.8 ppm of total organic carbon, the proportion of cells in G1 and G2 phase becomes almost equal. After treatment with 6.4 ppm and especially 9.6 ppm of total organic carbon, the cell cycle distribution shows severe distortion: G1/G0 and G2/M peak can not be easily identified and there is a reduction of cells in S and G2/M phase (Figure 3-16 D, E and Table 3-4).

Fragmentation of DNA followed by disintegration of a cell into apoptotic bodies occurs during late stages of apoptosis. The apoptotic bodies may contain part of DNA fractions. This gives rise to sub-diploid DNA content of apoptotic cells which is evident as a sub-G1 region in the histogram plots. An increase in number of recorded events (cell counts) in sub-G1 region can be observed after treatment with ethylene combustion condensate containing 6.4 ppm of total organic carbon (Figure 3-16 D

and Table 3-4). This increase in number of apoptotic cells is even more evident after treatment with ethylene combustion condensate containing 9.6 ppm of total organic carbon (Figure 3-16 E and Table 3-4).

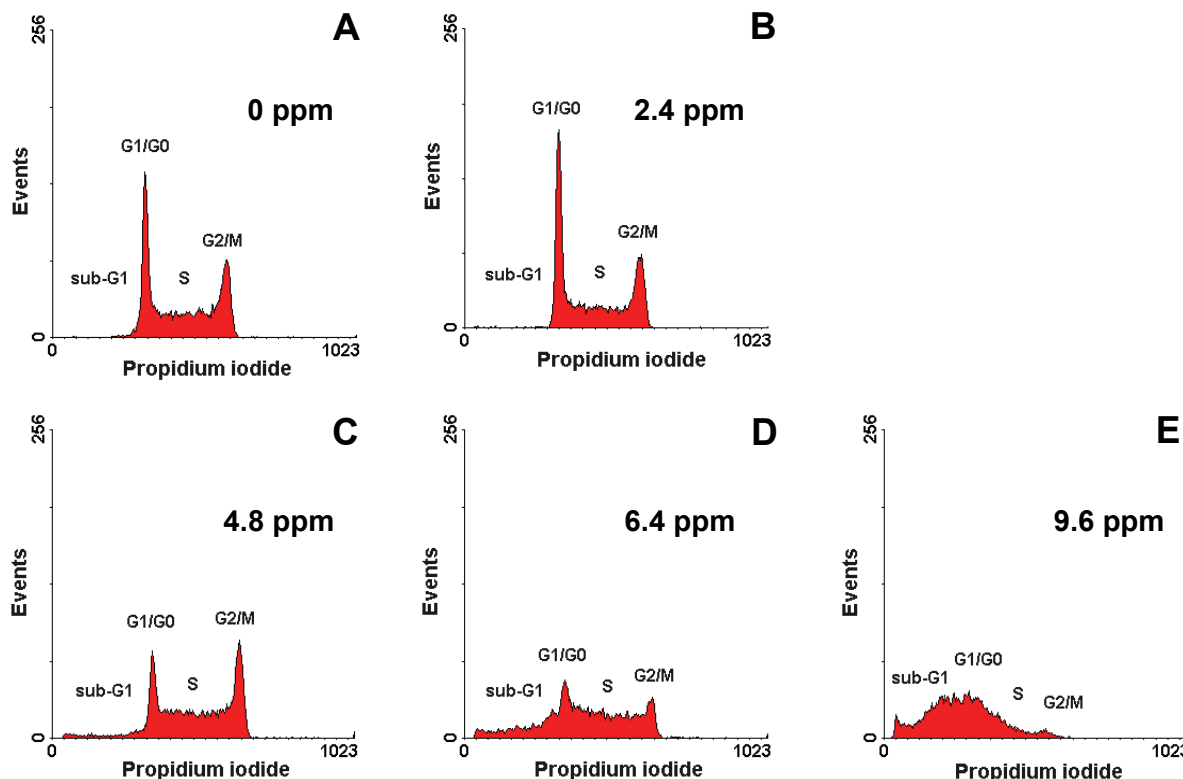


Figure 3-16: Ethylene combustion condensate causes cell cycle distortion and induction of apoptosis in U-937 cells

U937 cells were treated with indicated total organic carbon concentrations of ethylene combustion condensate ($C/O=0.93$) for 24 h. Cells were harvested, fixed with ethanol and stained with propidium iodide prior to flow cytometric analysis. Induction of apoptosis can be observed as an increase in number of recorded events in sub-G1 region.

Table 3-4: Relative distribution of U-937 cells according to their cell cycle phases, after treatment with ethylene combustion condensate

Ethylene combustion condensate (ppm of TOC)	Sub-G1(%)	G1/G0 (%)	S (%)	G2/M (%)	>G2 (%)
0	1	25	60	13	1
2.4	1	31	52	16	0
4.8	5	15	61	18	1
6.4	9	35	49	7	0
9.6	16	40	39	5	0

For A-549 cells the response is quite different from the U-937 cells. There are no changes in cell cycle distribution of A-549 cells after treatment with ethylene combustion condensate (2.4 – 9.6 ppm of total organic carbon) compared to the untreated culture (Figure 3-17 and Table 3-5). It can clearly be seen that there are no events recorded in the sub-G1 region of the DNA-content histogram plot, indicating no induction of apoptosis.

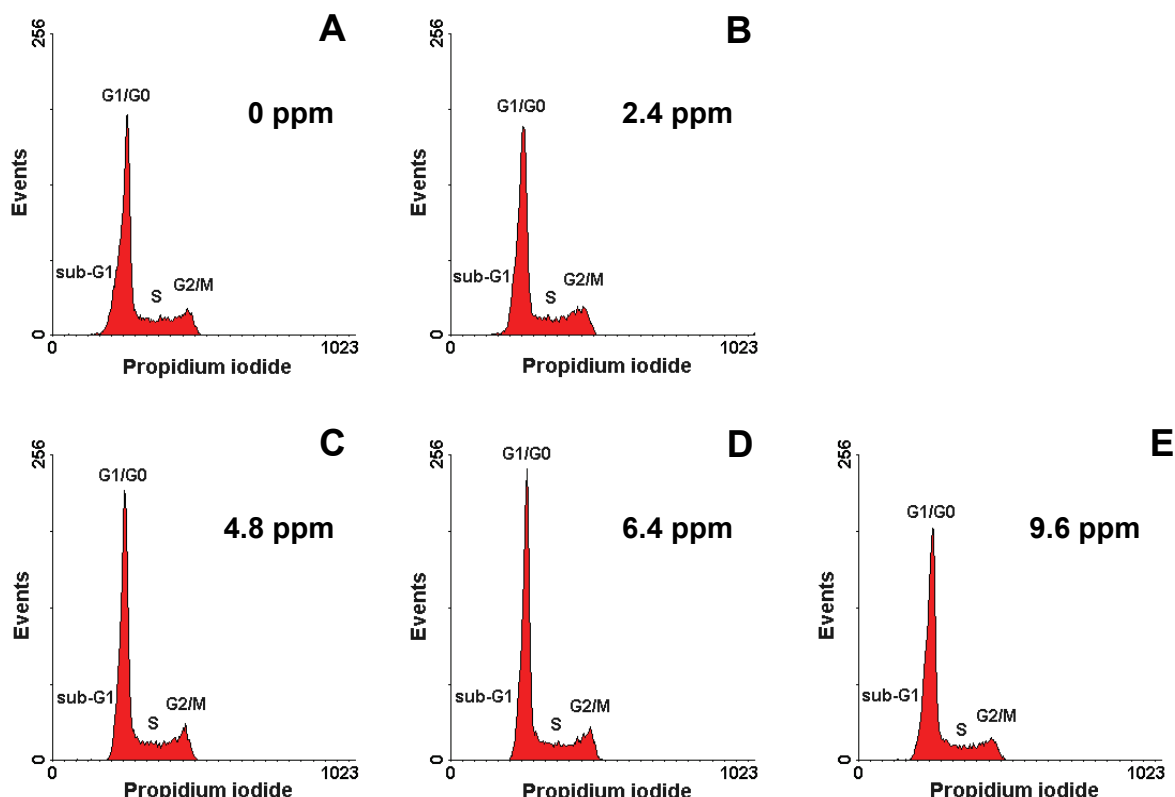


Figure 3-17: Ethylene combustion condensate causes no changes in cell cycle and no induction of apoptosis in A-549 cells

A-549 cells were treated with indicated total organic carbon concentrations of ethylene combustion condensate ($C/O=0.93$) for 24 h. Cells were harvested, fixed with ethanol and stained with propidium iodide prior to flow cytometric analysis. Absence of sub-G1 peak indicates no induction of apoptosis.

Table 3-5: Relative distribution of A-549 cells according to their cell cycle phases, after treatment with ethylene combustion condensate

Ethylene combustion condensate (ppm of TOC)	Sub-G1(%)	G1/G0 (%)	S (%)	G2/M (%)	>G2 (%)
0	1	74	19	6	0
2.4	1	60	32	7	0
4.8	1	64	29	6	0
6.4	0	65	28	7	0
9.6	1	69	25	5	0

3.3.3.2 Microscopic verification of apoptosis

DNA morphological changes in cells undergoing apoptosis (condensation and fragmentation of DNA) can be monitored via DAPI-staining method (chapter 2.2.6.4). DAPI displays enhanced blue fluorescence upon selective binding to double-stranded DNA.

DAPI-staining clearly shows condensation and fragmentation of DNA in U-937 cells treated with ethylene combustion condensates containing 6.4 or 9.6 ppm of total organic carbon (Figure 3-18 B, C). Untreated U-937 cells contain DNA evenly dispersed across the nucleus with no signs of fragmentation (Figure 3-18 A). In contrast to the U-937 cells, there are no morphological changes in A-549 cells' nuclei after treatment with indicated concentrations of ethylene combustion condensates (Figure 3-18 E, F). Nuclei of both untreated (Figure 3-18 D) and treated A-549 cells are compact and homogenously stained with no sign of DNA fragmentation.

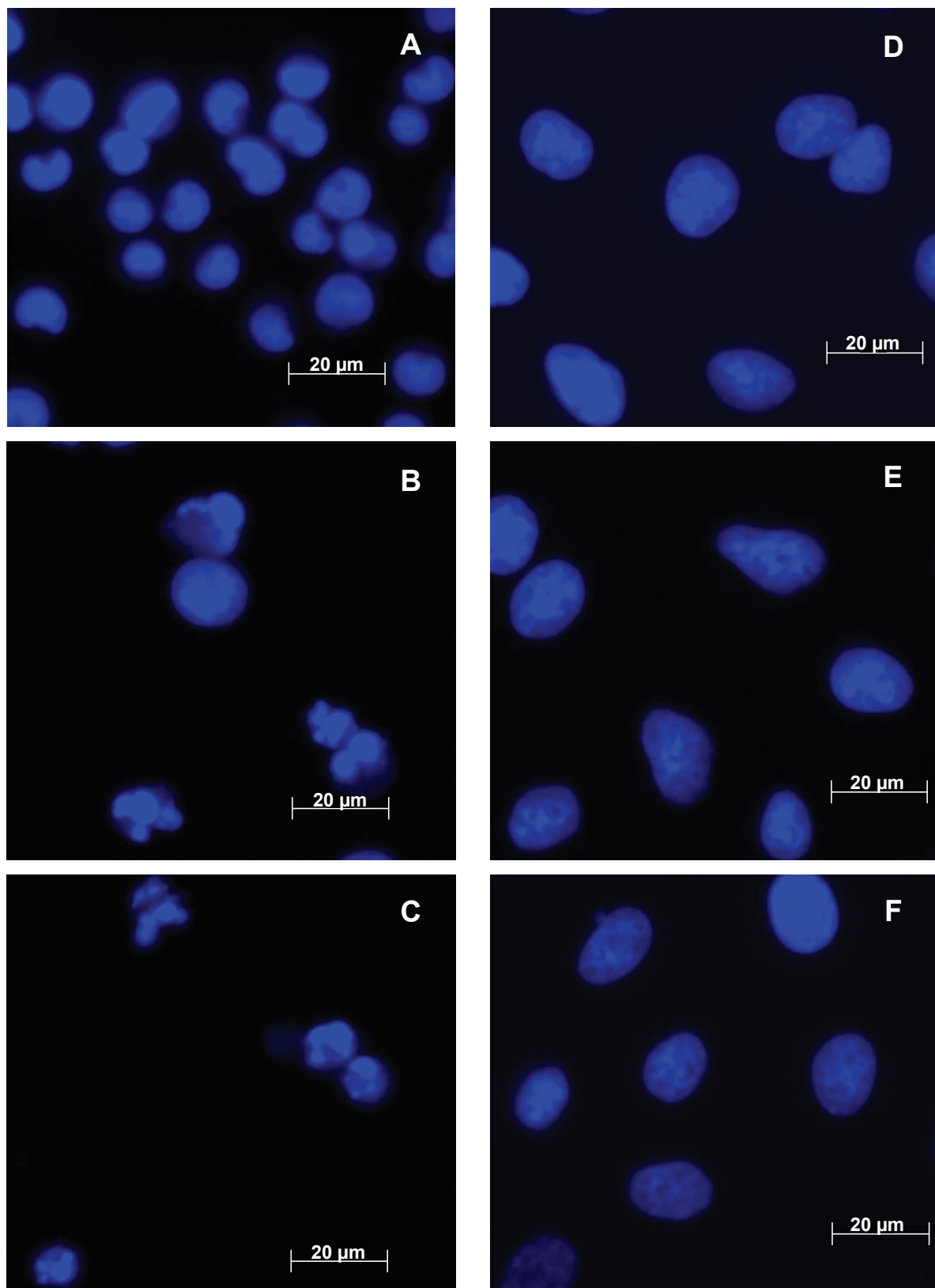


Figure 3-18: Ethylene combustion condensate induces DNA morphological changes in U-937 but not in A-549 cells

U-937 cells were treated 24 h with ethylene combustion condensates of the following concentrations: 0 ppm (A), 6.4 ppm (B) and 9.6 ppm (C) of total organic carbon. Same treatment was performed with A-549 cells: 0 ppm (D), 6.4 ppm (E) and 9.6 ppm (F) of total organic carbon. After incubation, cells were stained with DAPI and observed under fluorescence microscope. Representative images are shown.

3.3.3.3 Detection of early apoptotic changes in cell membrane

Since the previously described results (Figure 3-17; Figure 3-18) showed no induction of apoptosis in A-549 cells treated with ethylene combustion condensate, additional apoptosis tests were performed only with U-937 cells for the verification of the observed apoptotic effects.

The Annexin V-PE / 7-AAD assay is an apoptosis test based on detection of externalisation of the membrane protein phosphatidylserine, which is an early event in apoptosis. Therefore, this assay allows detection of cells at early stages of apoptosis (early apoptotic cells) and can discern them from late apoptotic/necrotic cells (for detailed method description see chapter 2.2.6.1).

For the assessment of apoptosis with this assay, U-937 cells were treated for 24 h with the ethylene combustion condensates containing 4.8 – 9.6 ppm of total organic carbon. After staining with Annexin V-PE and 7-AAD, cells were analysed in flow cytometer. Morphological properties of the cells were observed in the FSC vs. SSC plots; the Annexin-PE and 7-AAD fluorescence intensities of the whole cell population (R3-gated cells in Figure 3-21) were taken for evaluating the percentages of early apoptotic and late apoptotic/necrotic cells, as it is described in the Methods (chapter 2.2.6.1). Results demonstrate that the rate of apoptosis in U-937 cell cultures increases dose-dependently after treatment with ethylene combustion condensate (Figure 3-19 A). Since this assay cannot distinguish between late apoptotic and necrotic cells, the percentage of early apoptotic cells is taken as an indicator for the induction of apoptosis. The spontaneous apoptosis rate in the untreated cell culture is 6%. After treatment with the lowest tested concentration (4.8 ppm of total organic carbon), there is no significant induction of apoptosis. The number of early apoptotic as well as of late apoptotic/necrotic cells significantly increases after treatment with ethylene combustion condensates containing 6.4 ppm or 9.6 ppm of total organic carbon. These data indicate that apoptosis might not be the only cell death mode induced by ethylene combustion condensate. However, no quantification of necrotic cells is possible with this assay. Maximum number of early apoptotic cells (38%) is detected in the cell culture treated with ethylene combustion condensate containing 9.6 ppm of total organic carbon.

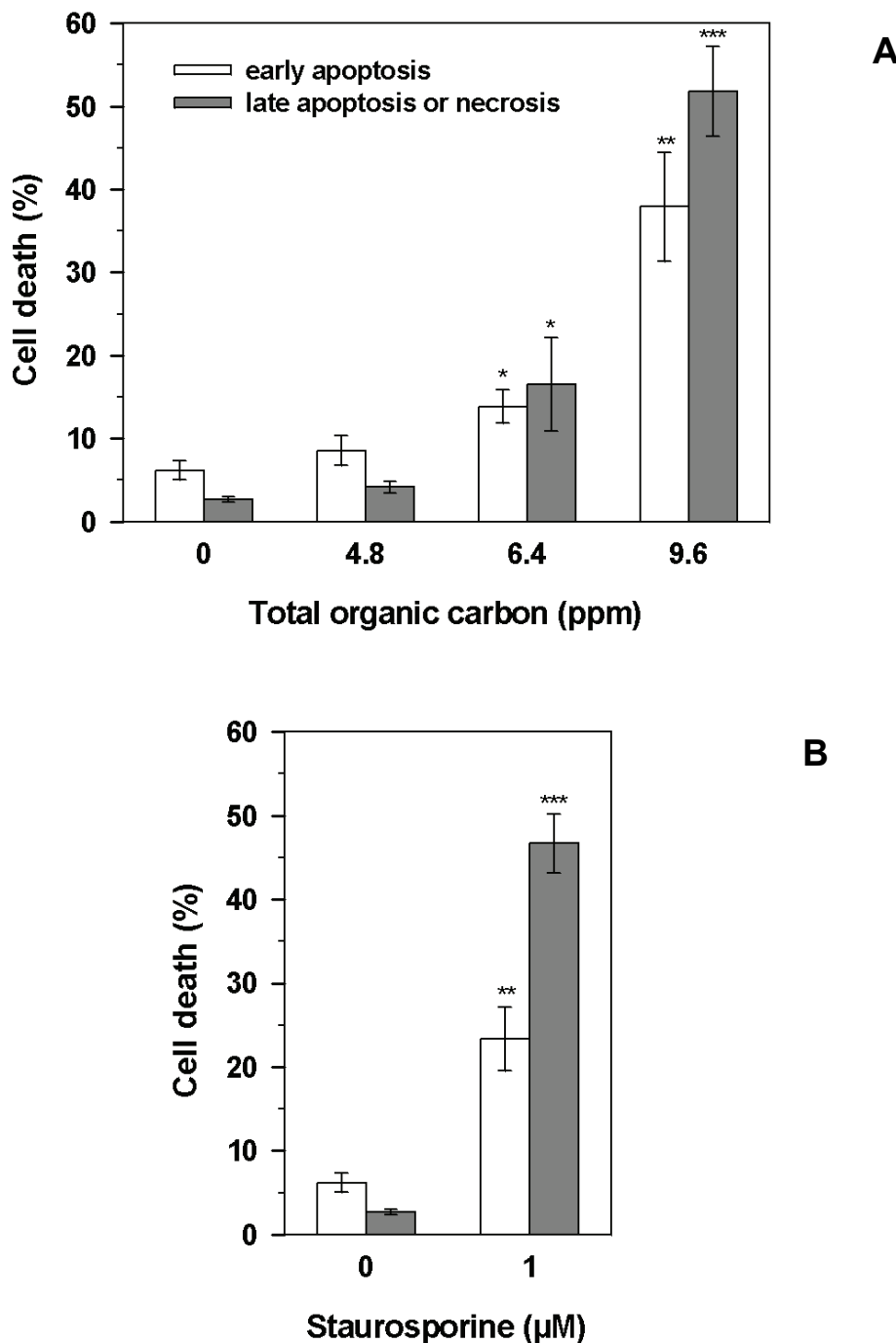


Figure 3-19: Ethylene combustion condensate induces cell death in U-937 cells

Induction of apoptosis in U-937 cells treated for 24 h with ethylene combustion condensate (A) was assessed with Annexin V-PE/ 7-AAD assay. Percentage of early apoptotic cells (Annexin V-PE+ / 7-AAD-) serves as an indicator of apoptosis induction. Fraction of Annexin V-PE+ / 7-AAD+ cells indicates percentage of late apoptotic/necrotic cells. Cells treated with staurosporine, a common apoptosis inducer, are used as a positive control (B). Significance was estimated with two-tailed Student's t-test (* p<0.05, ** p<0.01, ***p<0.001).

Effect of diesel combustion condensate on the induction of apoptosis in U-937 cells was also investigated via Annexin V-PE/7-AAD assay. The same concentration range (4.8 ppm - 9.6 ppm of total organic carbon) as for the ethylene combustion

condensate was tested (Figure 3-20). Results show a dose-dependant increase in the number of apoptotic cells. Already the low concentration of 4.8 ppm of total organic carbon significantly increases the number of apoptotic/necrotic cells. Percentage of early apoptotic as well as late apoptotic/necrotic cells is further increased at concentrations of diesel combustion condensate higher than or equal to 6.4 ppm of total organic carbon. The maximum number of early apoptotic cells (30%) is detected in cell cultures treated with diesel combustion condensate containing 9.6 ppm of total organic carbon.

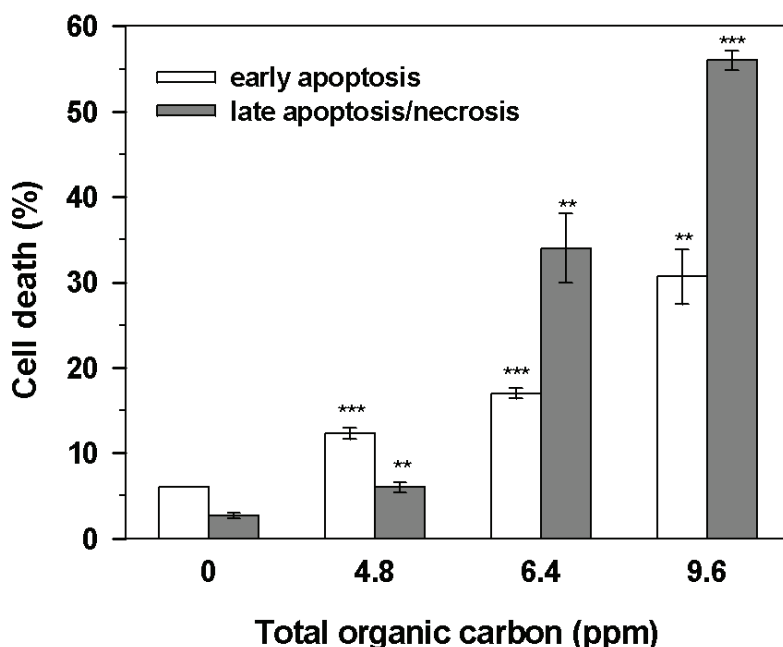


Figure 3-20: Diesel combustion condensate induces cell death in U-937 cells

U-937 cells were treated with diesel combustion condensate for 24 h and apoptosis was assessed with Annexin V-PE/ 7-AAD assay. Significance was estimated with two-tailed Student's t-test (* p<0.05, ** p<0.01, ***p<0.001).

Flow cytometric analysis of the U-937 cells treated for 24 h with ethylene combustion condensates containing \geq 6.4 ppm or diesel combustion condensates containing \geq 4.8 ppm of total organic carbon, revealed a splitting of the formerly compact U-937 cell population into two subpopulations. These two cell subpopulations were labelled as R1- and R2-gated population according to their morphological properties in FSC vs. SSC density plot (Figure 3-21 A). R2-gated cells (cells belonging to region R2) are smaller in size and have higher inner granularity compared to the R1-gated cells. Figure 3-21 illustrates this splitting into two subpopulations of U-937 cells, after treatment with the ethylene combustion condensate containing 6.4 ppm of total organic carbon. Analysis of the Annexin-PE and 7-AAD fluorescence intensities of R1-gated and R2-gated U-937 cell subpopulations (Figure 3-21 C and D,

respectively) has led to following conclusions: (i) the R1-gated cell subpopulation consists predominately (88%) of viable cells and (ii) the R2-gated cell subpopulation is predominately (78%) comprised of apoptotic/necrotic cells. This suggests that the appearance of the R2-gated cell subpopulation is due to the cytotoxic effect of the combustion condensates.

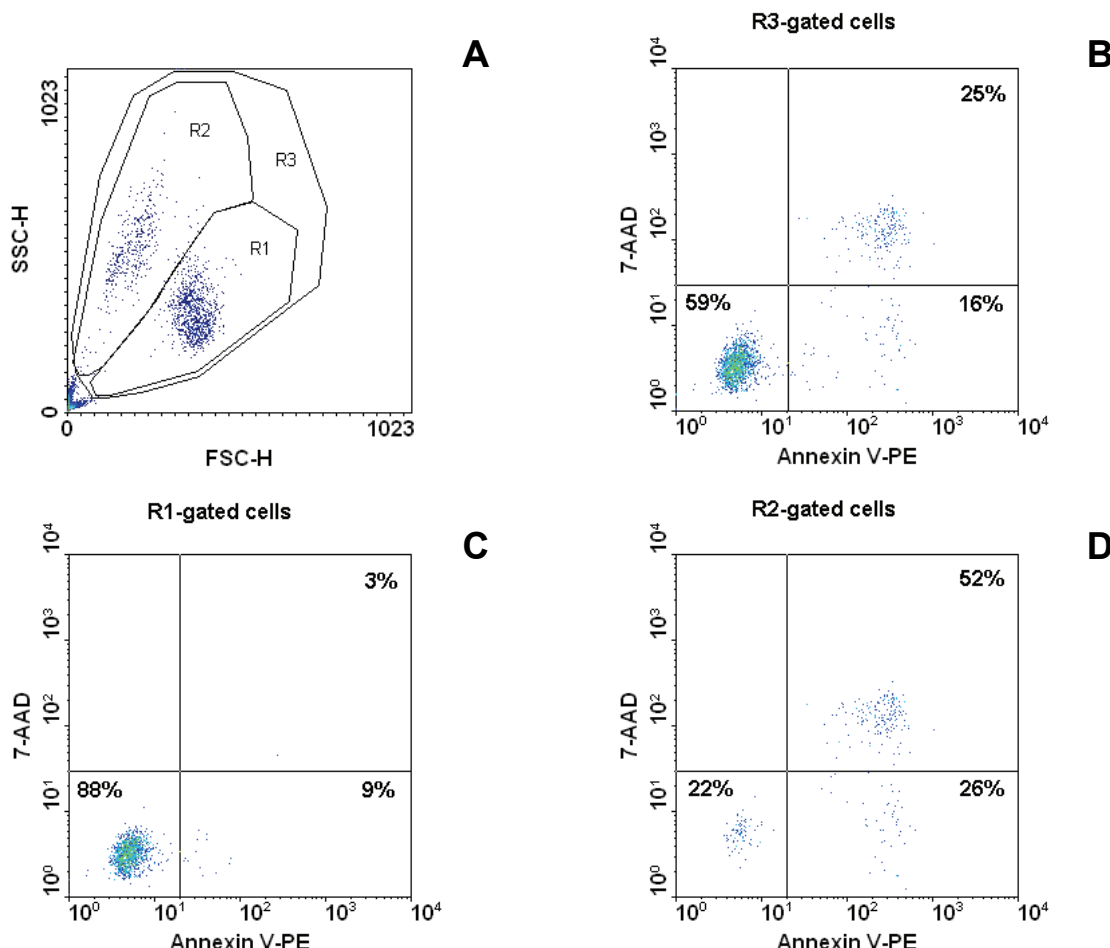


Figure 3-21: Cell viability analysis of two cell subpopulations occurring after treatment of U-937 cells with ethylene combustion condensate

After 24 h treatment of U-937 with ethylene combustion condensate (6.4 ppm of total organic carbon), cells were stained with Annexin V-PE and 7-AAD and analysed in flow cytometer. FSC vs. SSC density plot (A) revealed morphological changes in the cell population and splitting into two subpopulations (R1 and R2). Induction of apoptosis was analysed in the entire R3-gated cell population (B) and in each of the subpopulations separately: R1-gated (C) and R2-gated (D). Lower left quadrants of the Annexin V-PE vs. 7-AAD density plots show viable cells (Annexin V-PE⁻/7-AAD⁻ cells), lower right quadrants (Annexin V-PE⁺/7-AAD⁻ cells) indicate the frequency of early apoptotic cells and the upper right quadrants show the frequency of late apoptotic/necrotic cells (Annexin V-PE⁺/7-AAD⁺ cells).

3.3.3.4 Activation of caspase-3 in cells undergoing apoptosis

The active caspase-3 assay is another apoptosis assay which was used to verify the induction of apoptosis in U-937 cells after treatment with combustion condensates. This assay detects the cells undergoing apoptosis via flow cytometric analysis of the

PE-conjugated active caspase-3 antibody which is bound to the intracellular active caspase-3 (chapter 2.2.6.3). Percentage of cells displaying fluorescence intensities in the M2-region of the histogram plot was taken as a measure of apoptosis. Rate of spontaneous apoptosis in the untreated U-937 cell culture is 7% (Figure 3-22 B). Staurosporine is a well known inducer of apoptosis and it was used as a positive control in this assay. 24 h treatment with 1 μ M staurosporine induces apoptosis in 56% of U-937 cells (Figure 3-22 B).

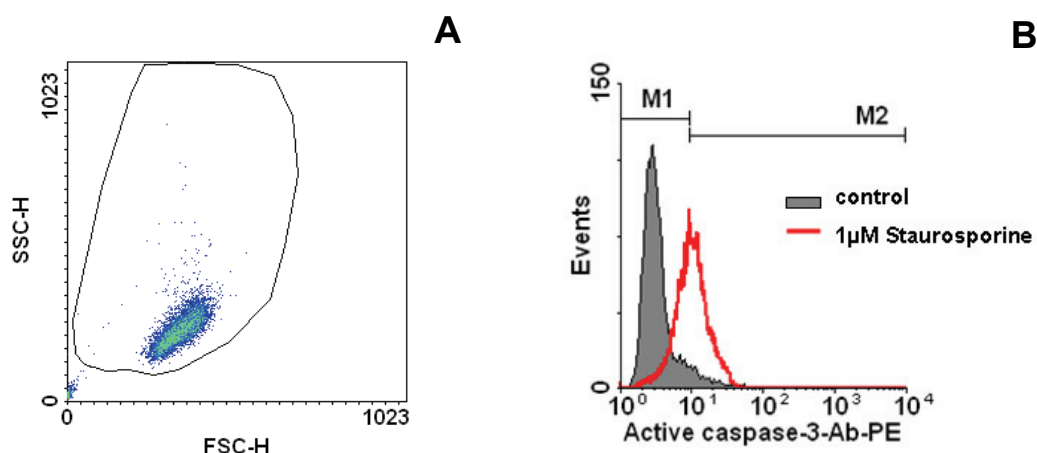


Figure 3-22: Flow cytometric analysis of apoptosis by using active caspase-3 assay: representative density-plot and histogram plot

U-937 cells were left untreated (control) or they were treated with 1 μ M staurosporine for 24 h to induce apoptosis. Representative FSC vs. SSC density plot of the untreated U-937 cells shows the cell debris exclusion method (A). PE-fluorescence profiles of the untreated cells (control) and the cells treated with 1 μ M staurosporine are shown in panel B. Cells undergoing apoptosis possess active caspase-3 and accordingly display higher fluorescence intensities (M2-marker). After treatment with staurosporine, the number of apoptotic cells increases drastically.

U-937 cells were treated with ethylene- and diesel combustion condensates containing 9.6 ppm of total organic carbon, since this concentration caused maximum observed induction of apoptosis in the previously described Annexin V-PE/7-AAD apoptosis assay (Figure 3-19 and Figure 3-20, respectively). Results of the active caspase-3 assay show that the number of apoptotic cells increases 5-fold after treatment with ethylene combustion condensate and 6-fold after treatment with diesel combustion condensate, compared to the number of apoptotic cells (7%) in the untreated culture (Figure 3-23).

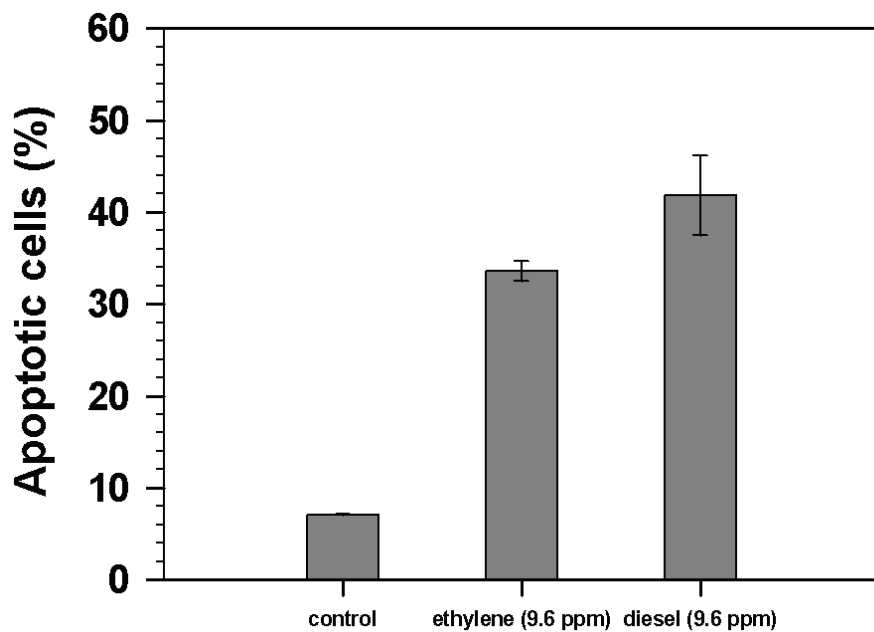


Figure 3-23: Activation of caspase-3 in U-937 cells treated with combustion condensates

After 24 h treatment with the same concentration of ethylene and diesel combustion condensate (9.6 ppm of total organic carbon), U-937 cells were fixed and permeabilised for the intracellular staining with PE-conjugated active caspase-3 antibody. The number of apoptotic cells is determined as a fraction of cell population displaying PE-fluorescence intensities in the M2-marked region of the histogram plots (not shown).

3.3.4 Effect of ethylene combustion condensate on the activation of NF- κ B signalling pathway in U-937

The NF- κ B signalling pathway has an important role in the regulation of cell stress responses. For monitoring activation of the NF- κ B pathway, U-937 cells were stably transfected with vector pNF- κ B-EGFP/Neo coding for EGFP gene under control of a promoter comprising multiple NF- κ B-binding sites.

3.3.4.1 Selection of TNF- α -inducible stably transfected U-937-pNF- κ B-EGFP/Neo clone

The plasmid pNF- κ B-EGFP/Neo (Figure 2-2) carries the *neo*^r gene which enables transfected U-937 cells to be resistant to geneticin (G418). Prior to transfection of U-937 cells with this plasmid, it was necessary to determine sensitivity of the wild-type U-937 cells towards G418. Cells were therefore treated with different doses of G418 and cytotoxicity was estimated with the MTT-test (method described in chapter

2.2.8). U-937 cells showed no survival after 7 days treatment with 1500 µg/ml G418. Therefore, this concentration was used as the selective pressure during stable transfection (Figure 3-24 A). Cells treated with 10% DMSO were used as a positive control for the MTT-test (Figure 3-24 B).

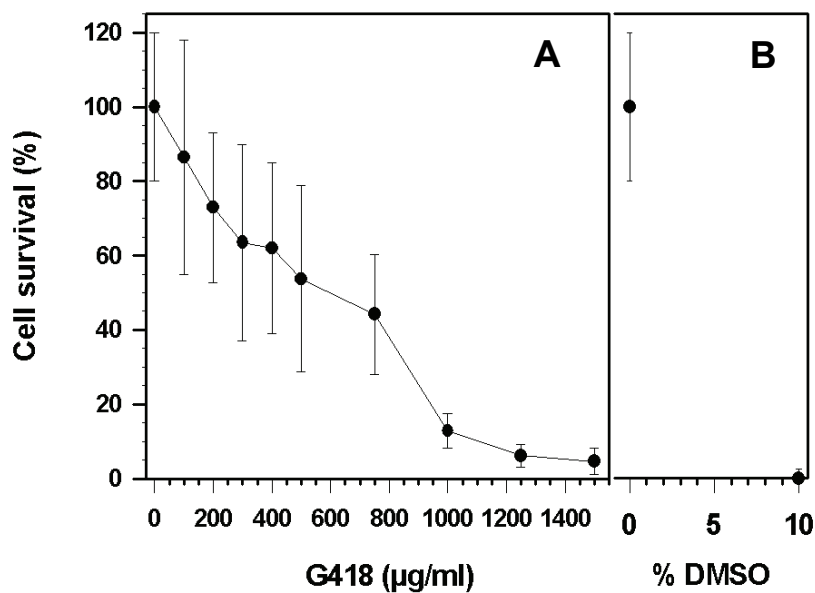


Figure 3-24: Lethal effect of 1 500 µg/ml geneticin (G418) on U-937 cells

Cells were treated with G418 antibiotic (A) or with 10% DMSO (B) for 7 days. Impairment of cell viability was analysed with MTT-test. Representative experiment shows relative survival rate for each tested concentration, estimated according to the absorbance ($\lambda = 562$ nm) of formazan complex in treated and untreated samples. Relative survival rates are given as means \pm standard deviation. There were 8 replicas for each tested concentration.

During stable transfection, an exogenous DNA integrates into the host DNA. The vector pNF-κB-EGFP/Neo, carrying the EGFP gene downstream of a synthetic promoter containing 4 copies of the κB-enhancer element, is considered to be stably integrated into the genome of U-937 cells (chapter 2.2.3.5). Activation of the NF-κB pathway leads to binding of endogenous NF-κB molecules to κB-enhancer elements, and thereby increases transcription of EGFP (Hellweg et al., 2003). Stably transfected U-937-pNF-κB-EGFP/Neo clones were screened for NF-κB-dependant EGFP expression after treatment with TNF-α (common NF-κB activator). Cells were processed and the green fluorescence output of EGFP was measured by flow cytometry as described in chapter 2.2.5.

From 50 screened clones, 41 were non-inducible (< 5% EGFP-positive cells) and 9 were inducible. The principle of this analysis is explained on the example of an

inducible U-937-pNF- κ B-EGFP/Neo clone 5a (Figure 3-25 A). This figure shows autofluorescence output of non-transfected U-937 cells (black line), which was used to set a marker M1. M2 and M3 marker were set according to the fluorescence intensities of U-937-pNF- κ B-EGFP/Neo cells. M2 marker comprises background EGFP fluorescence of the U-937-pNF- κ B-EGFP/Neo cells, in non-induced state. Cells displaying fluorescence intensities in the zone of M3 marker were considered EGFP-positive cells and they served as a measure of NF- κ B induction. Arbitrarily, M3 marker was set so that it comprises fluorescence output of approximately 2.5% of U-937-pNF- κ B-EGFP/Neo cell population in non-induced conditions (control). After 20 h treatment with 10 ng/ml TNF- α , U-937-pNF- κ B-EGFP/Neo clone 5a exhibits a strong increase in fluorescence intensities, and 44% of population are EGFP-positive (Figure 3-25 A).

Figure 3-25 (B) shows one representative non-inducible U-937-pNF- κ B-EGFP/Neo clone 3r, which has the same percentage of EGFP-positive cells (2.5%) in control conditions and after TNF- α treatment. Absence of the NF- κ B-induced EGFP-expression can be due to the fact that a promoter carrying NF- κ B-binding sites was destroyed during the linearization of the vector by cellular enzymes (Hellweg et al., 2001). Thereby, after the integration of such vector into host genome, the reporter EGFP gene came under the control of a certain cellular promoter which is not NF- κ B regulated.

U-937-pNF- κ B-EGFP/Neo clone 5a (Figure 3-25 A) displayed the strongest TNF- α -induced NF- κ B activation of all screened clones and had the lowest background of all inducible clones, which was the reason for selecting the clone 5a as a test clone for further experiments.

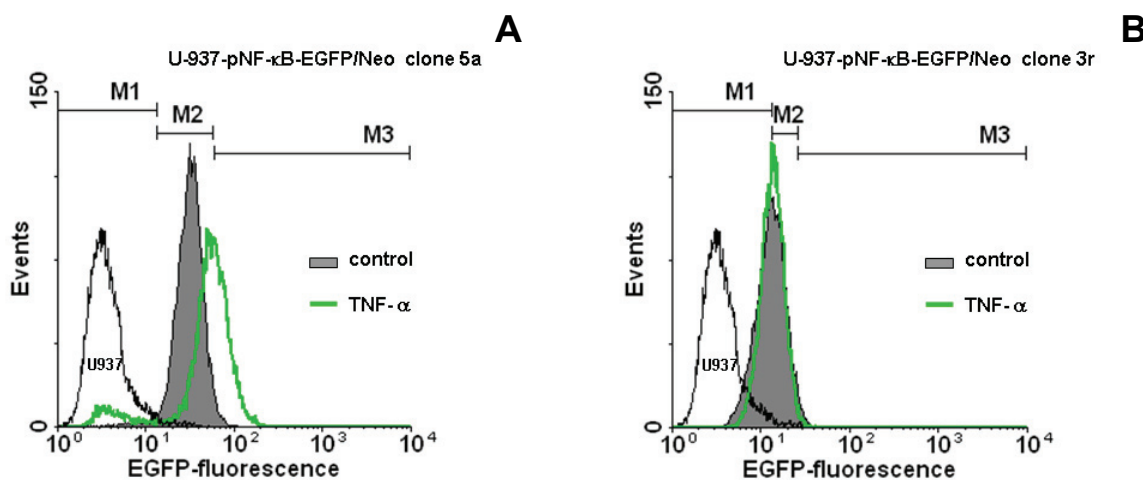


Figure 3-25: Screening of stably transfected U-937-pNF-κB-EGFP/Neo clones

EGFP-expression of representative TNF- α -inducible (A) and non-inducible (B) stably transfected U-937-pNF-κB-EGFP/Neo clones was measured via FACScan analysis. After 20 h treatment with 10 ng/ml TNF- α or 0.1% PBS (control), cells were harvested, fixed with 3.5% formaldehyde/PBS and resuspended in PBS prior to the analysis. The autofluorescence of non-transfected U-937 cells (black line) is used to set the M1 marker. M2 marker includes the fluorescence output of U-937-pNF-κB-EGFP/Neo cells treated with 0.1% PBS. Cells displaying fluorescence intensities in the area of M3 marker are EGFP-positive cells and are used as a measure of NF-κB induction.

3.3.4.2 Dose-dependant activation of the NF-κB pathway in U-937-pNF-κB-EGFP/Neo clone 5a treated with ethylene combustion condensate

Once the inducible U-937-pNF-κB-EGFP/Neo clone 5a cell line was established, it was used to assess the activation of the NF-κB signalling pathway after treatment with ethylene combustion condensate (C/O=0.93). Cells were treated with different concentrations (2.4 – 19.2 ppm of total organic carbon) for different incubation time (7 – 72 h). After incubation, cells were harvested and analysed by flow cytometry (chapter 2.2.5).

After 24 h incubation with 6.4 ppm of ethylene combustion condensate, forward scatter versus side scatter (FSC vs. SSC) density plots as well as EGFP-fluorescence intensity histogram plots indicated the splitting of one compact cell population into two subpopulations (Figure 3-26, 2. column). These cell subpopulations are designated as R1-gated (bigger cells with less inner granularity) and R2-gated (smaller cells with higher inner granularity) according to their characteristics in FSC vs. SSC plots. EGFP-fluorescence signals of these two subpopulations are shown for each incubation time and for all tested concentrations of ethylene combustion condensate (Figure 3-26, 4. and 5. column). After 24 h

incubation, there was a dose-dependant activation of NF- κ B in R1-gated subpopulation as it can be observed by an increase in the number of cells with fluorescence intensities in the M3-marked region (EGFP-positive cells). For the same incubation time-point, higher concentrations of the ethylene combustion condensate (\geq 6.4 ppm of total organic carbon) caused a decrease in the number of R1-gated cells and an increase in the number of R2-gated cells. R2-gated cell population displays lower intensities of the EGFP-fluorescence than the R1-gated cell population for each tested concentration and each time-point. Longer incubation (\geq 24 h) with low amounts of TOC (4.8 ppm) enhances the NF- κ B activation, without significantly increasing the number of R2-gated cells (Figure 3-26, 1. and 4. column). On the other hand, longer incubation (\geq 24 h) with ethylene combustion condensate containing equal to or more than 6.4 ppm of TOC, causes no further increase in the NF- κ B activation. These concentrations only induce a major decrease in the number of R1-gated cells and an increase in the number of R2-gated cells (Figure 3-26, 2. and 3. column). FSC vs. SSC density plots of the cells treated with ethylene combustion condensate containing 6.4 ppm of TOC representatively show this time-dependant shift of the cells from R1 region towards R2 region (Figure 3-26, 2. column). This shift can be explained by a predominant cytotoxic effect of the ethylene combustion condensates. Loss of the cell membrane integrity in the course of cell death could lead to the leakage of small soluble EGFP molecules and consequently cause a decrease in the measured EGFP-fluorescence intensities of the cells. Cell shrinkage and formation of apoptotic bodies are characteristic morphological changes that occur during apoptosis. R2-gated cells can also be undergoing apoptotic cell death since they are smaller in size than the R1-gated cells and possess higher inner granularity. A decrease in the EGFP-fluorescence intensities of the R2-gated population can be explained by the presence of apoptotic bodies which possess lower amounts of EGFP molecules in the cytoplasm than intact cells. The Annexin V-PE / 7-AAD apoptosis test (Figure 3-21) confirmed these assumptions by showing that the R2-gated cell subpopulation consists predominately of Annexin V-PE⁺/7-AAD⁻ and Annexin V-PE⁺/7-AAD⁺ cells (apoptotic and necrotic cells).

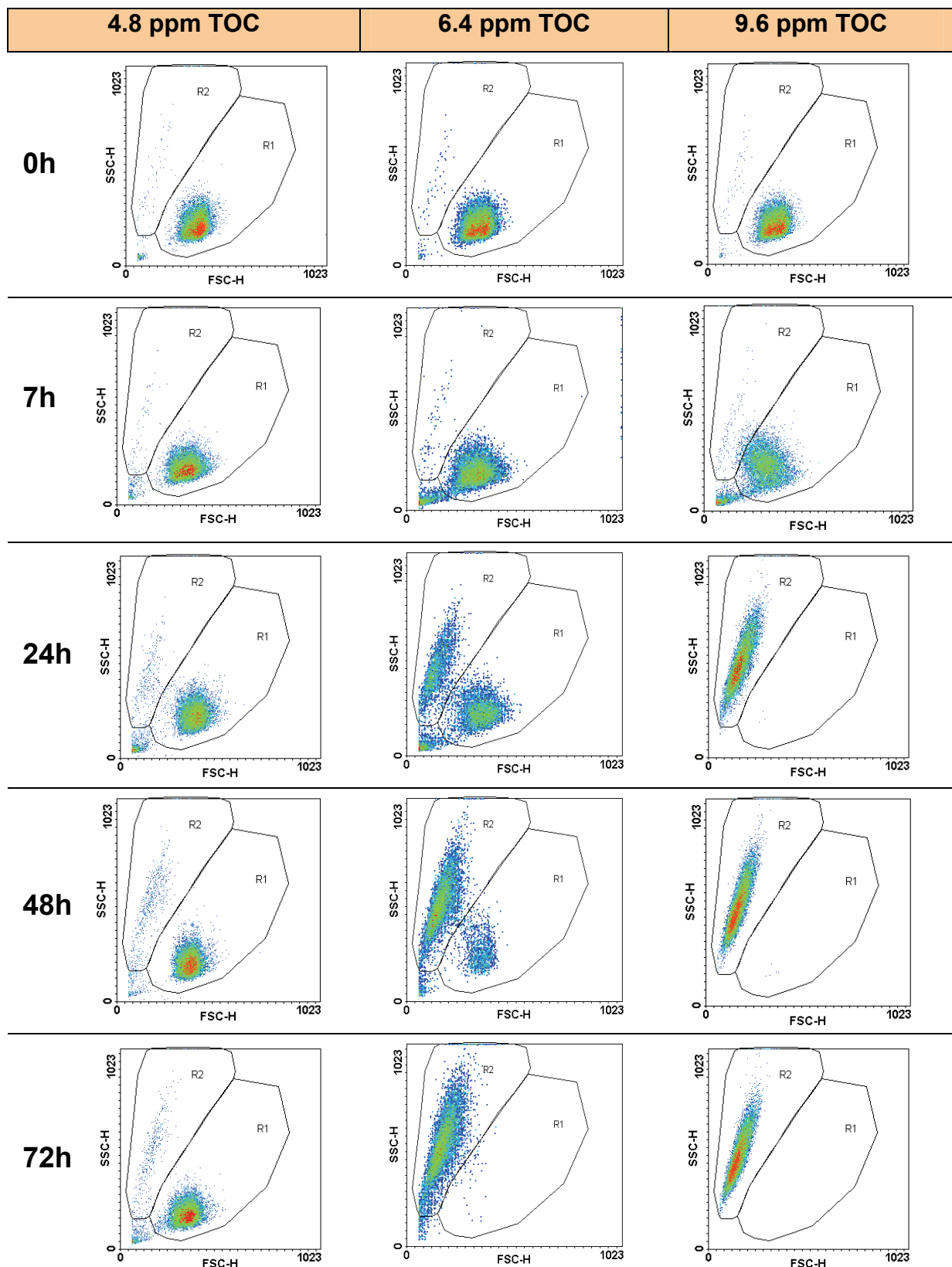
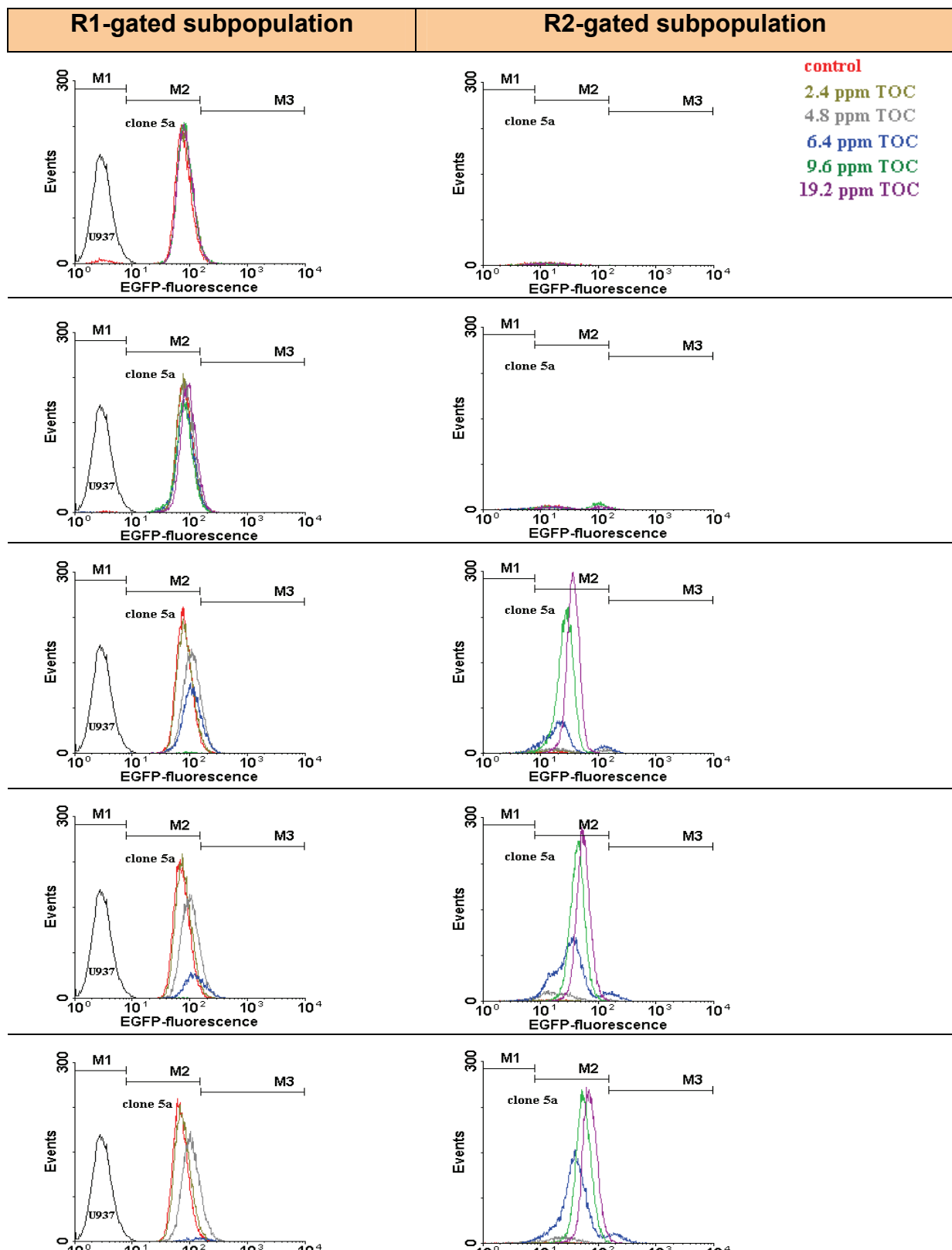


Figure 3-26: NF- κ B activation and appearance of two cell subpopulations in
 Density plots of U-937-pNF- κ B-EGFP/Neo clone 5a cells treated (0-72 h) with ethylene combustion of total organic carbon. EGFP-fluorescence intensities of R1- (4. column) and R2-gated (5. column) EGFP-fluorescence of non-transfected U-937 cells is used to set M1 marker. M2 and M3 markers

**U-937-pNF- κ B-EGFP/Neo clone 5a treated with ethylene combustion condensate**

condensate (C/O=0.93) containing 4.8 ppm (1. column), 6.4 ppm (2. column) or 9.6 ppm (3. column) cell subpopulations are shown for all tested TOC concentrations and each incubation time. depict basal and NF- κ B-induced fluorescence of U-937-pNF- κ B-EGFP/Neo cells, respectively.

According to the previously described results, 24 h was chosen as a suitable time-point to compare the activation of NF- κ B in U-937-pNF- κ B-EGFP/Neo cells. Figure 3-27 shows the dose-dependant effect of the ethylene combustion condensate ($C/O=0.93$) on NF- κ B activation in U-937-pNF- κ B-EGFP/Neo clone 5a. The fraction of the whole cell population ($R1 + R2$ -gated) which displays fluorescence intensities in the M3-zone of the EGFP-histogram plots (EGFP-positive cells) is used as a measure of NF- κ B activation. Results demonstrate a dose-dependant activation of NF- κ B in U-937-pNF- κ B-EGFP/Neo clone 5a cells treated with ethylene combustion condensates containing up to 4.8 ppm of TOC. At concentrations higher than 4.8 ppm, the number of EGFP-positive cells decreases abruptly and is not significantly different from the non-treated control group. With 9.6 ppm of TOC, the number of EGFP-positive cells is significantly lower than in the control group.

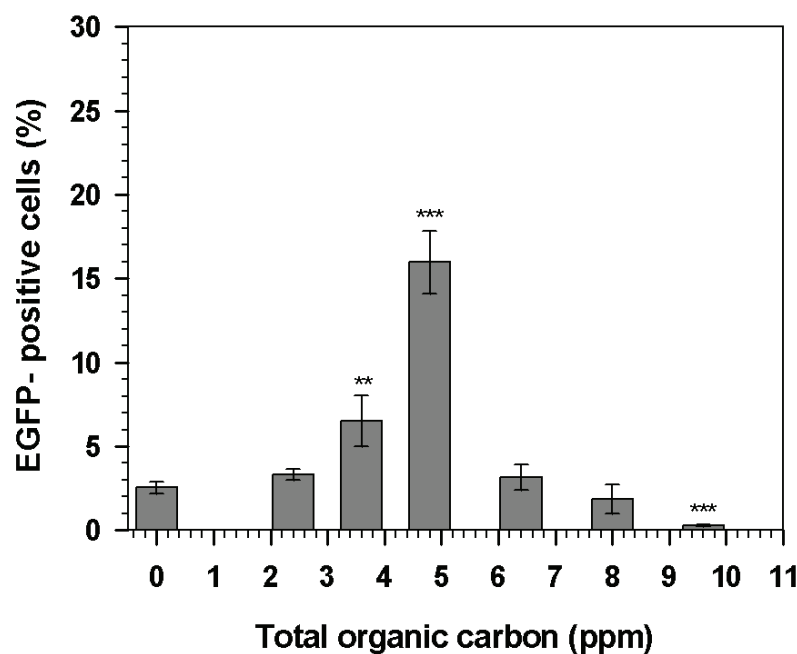


Figure 3-27: Ethylene combustion condensate induces dose-dependant NF- κ B activation in U-937-pNF- κ B-EGFP/Neo clone 5a cells

After 24 h treatment with ethylene combustion condensate ($C/O=0.93$) of different total organic carbon concentrations, cells were harvested and analysed by flow cytometry. The fraction of cells with enhanced EGFP-fluorescence intensities (EGFP-positive cells) is used as a measure of NF- κ B activation.

3.3.5 Role of NF- κ B in the ethylene combustion condensate-induced apoptosis in U-937

In order to identify the role (pro- or anti-apoptotic) of NF- κ B in the combustion condensate-induced toxicity, inhibitors of the NF- κ B pathway were used to uncover

whether the inhibition of the NF-κB signalling pathway promotes or suppresses the combustion condensate-induced apoptosis.

3.3.5.1 Selection of a suitable NF-κB inhibitor

The NF-κB signalling pathway can be inhibited at different points by various agents. MG-132 and Bay 11-7082 are two commonly used NF-κB inhibitors. MG-132 (Carbobenzoxy-L-leucyl-L-leucyl-L-leucinal) reversibly inhibits NF-κB activation by preventing proteasome-mediated degradation of IκB proteins (Gao et al., 2000). Bay 11-7082 ((E)-3-(4-Methylphenylsulfonyl)-2-propenenitrile) is a selective and irreversible NF-κB inhibitor, which inhibits IκB-α phosphorylation. By this way, IκB-α is spared from proteasome-mediated degradation and can bind to NF-κB and keep it inactivated (Pierce et al., 1997; Dai et al., 2005; Zhi et al., 2007).

The aim of the following experiments was to find a suitable NF-κB inhibitor and determine its concentration which would efficiently suppress the activation of NF-κB in U-937 cells after 24 h treatment with ethylene combustion condensate. The suitability of the inhibitors MG-132 and Bay 11-7082 and their effective concentrations were firstly estimated in the tests involving suppression of TNF-α-induced NF-κB activation. For this purpose, U-937-pNF-κB-EGFP/Neo clone 5a was co-treated with TNF-α and the NF-κB inhibitors. The NF-κB inhibition was observed as a decrease in the number of EGFP-positive cells. Results of these tests are shown for each NF-κB inhibitor separately.

NF-κB inhibition with MG-132

MG-132 inhibits TNF-α-induced NF-κB activation in U-937-pNF-κB-EGFP/Neo clone 5a, as it can be seen by a significant decrease in the percentage of EGFP-positive cells (Figure 3-28, green bars). This holds true for MG-132 concentrations in the range of 2.5 – 40 μM. In the absence of MG-132, TNF-α activates NF-κB in 13% of U-937-pNF-κB-EGFP/Neo clone 5a cells (Figure 3-28). Co-treatment with MG-132 (2.5 – 40 μM) reduces the number of EGFP-positive cells to approximately 5%.

The results show a significant NF-κB activation in cells treated only with MG-132 for 20 h (Figure 3-28, gray bars). The lowest tested MG-132 concentration (2.5 μM) causes already a 3.5-fold increase in the fraction of EGFP-positive cells, compared to

untreated cells. The NF-κB signalling pathway remains significantly activated for all other tested concentrations of MG-132. This controversial effect of MG-132 for the tested concentration range (2.5 – 40 μM) makes it an unsuitable NF-κB inhibitor for long-term incubation (20 h) experiments.

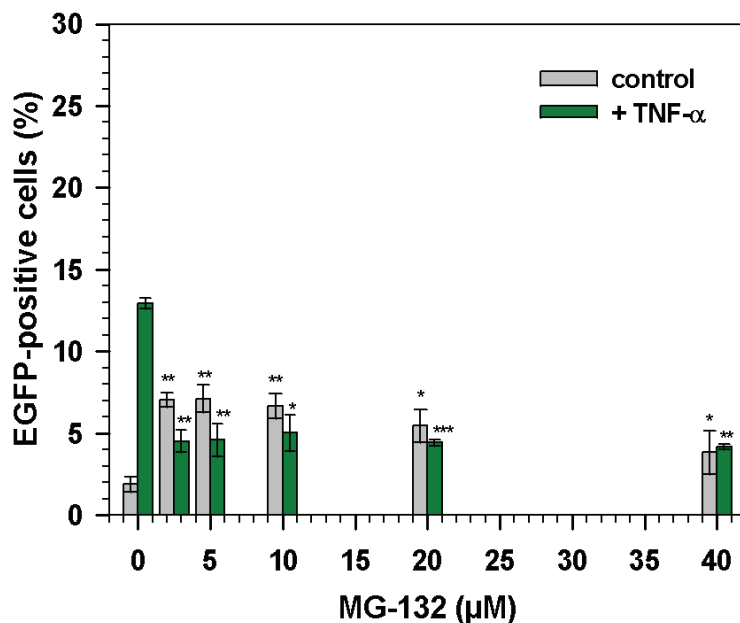


Figure 3-28: MG-132 is an unsuitable inhibitor of TNF-α-induced NF-κB activation in U-937-pNF-κB-EGFP/Neo clone 5a

U-937-pNF-κB-EGFP/Neo clone 5a cells were co-treated for 20 h with MG-132 and either 10 ng/ml TNF-α or 0.1% PBS (control). NF-κB-dependant EGFP-expression was assayed by flow cytometry. Significance was estimated with two-tailed Student's t-test (* p<0.05, ** p<0.01, ***p<0.001). For the significance test, control groups (gray bars) and TNF-α-treated groups (green bars) treated with MG-132 were compared with the corresponding groups which were not treated with MG-132.

NF-κB inhibition with Bay 11-7082

In the tested concentration range (0.5 – 8 μM) Bay 11-7082 significantly inhibits TNF-α-induced NF-κB activation in U-937-pNF-κB-EGFP/Neo clone 5a cells. This can be observed as a significant decrease in the percentage of EGFP-positive cells (Figure 3-29). At concentrations equal to or higher than 4 μM, Bay 11-7082 also significantly decreases the number of EGFP-positive cells in non-induced cell culture (Figure 3-29, gray bars). However, at concentration of 2 μM, Bay 11-7082 efficiently inhibits TNF-α-induced NF-κB activation without affecting basal NF-κB activation level in the control samples. According to these results, Bay 11-7082 is chosen at a concentration of 2 μM as a suitable NF-κB inhibitor for further investigation.

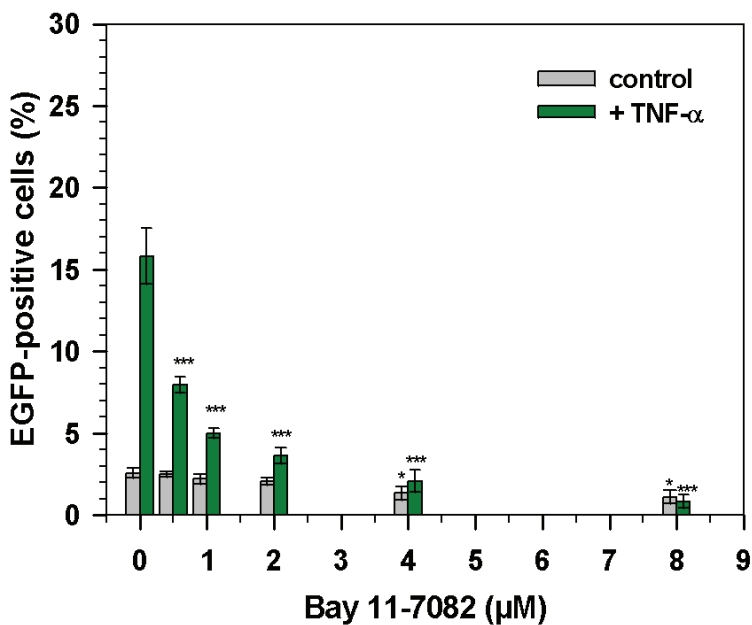


Figure 3-29: 2μM Bay 11-7082 effectively suppresses TNF-α-induced NF-κB activation in U-937-pNF-κB-EGFP/Neo clone 5a

U-937-pNF-κB-EGFP/Neo clone 5a cells were co-treated for 20 h with Bay 11-7082 and either 10 ng/ml TNF-α or 0.1% PBS (control). NF-κB-dependant EGFP-expression was assayed by flow cytometry. Significance was estimated with two-tailed Student's t-test (* p<0.05, ** p<0.01, ***p<0.001). For the significance test, control groups (gray bars) and TNF-α-treated groups (green bars) treated with Bay 11-7082 were compared with the corresponding groups which were not treated with Bay 11-7082.

Once the suitable concentration of Bay 11-7082 was determined, it was used to inhibit the ethylene combustion condensate-induced NF-κB activation in U-937-pNF-κB-EGFP/Neo clone 5a (Figure 3-30). The effect of 2 μM Bay 11-7082 was tested on cells co-treated for 24 h with ethylene combustion condensate (2.4 – 9.6 ppm of total organic carbon). Activation of the NF-κB signalling pathway is evident after 24 h treatment with only ethylene combustion condensate containing 3.6 – 4.8 ppm of TOC. Co-incubation with 2 μM Bay 11-7082 successfully reduces NF-κB activation to the level observed in control cells (dotted line in Figure 3-30). Moreover, co-treatment with 2 μM Bay 11-7082 and ethylene combustion condensate containing more than 4.8 ppm of total organic carbon, causes a decrease in NF-κB activation below this level.

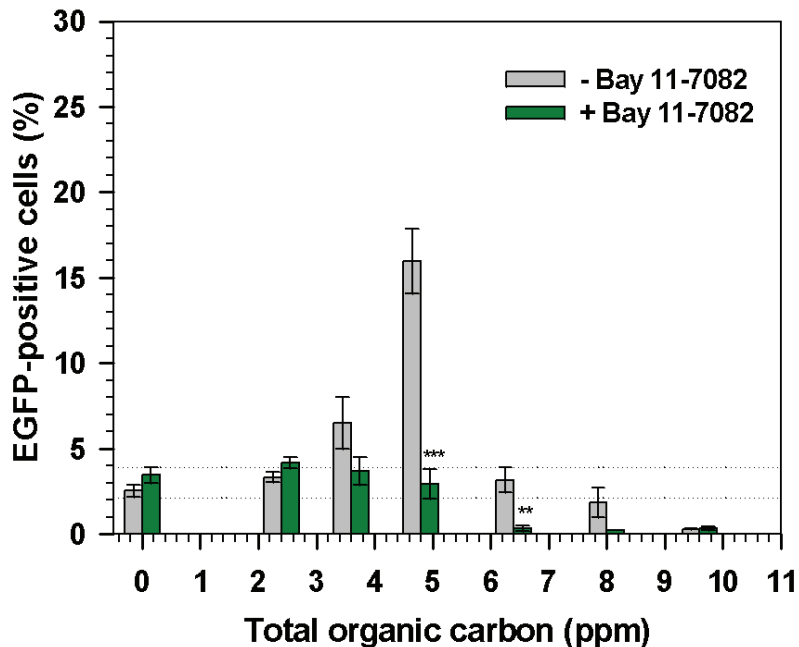


Figure 3-30: 2 μ M Bay 11-7082 efficiently inhibits ethylene combustion condensate-induced NF- κ B activation in U-937-pNF- κ B-EGFP/Neo clone 5a

Cells were co-treated for 24 h with 2 μ M Bay 11-7082 and ethylene combustion condensate. NF- κ B-dependant EGFP-expression was assayed by flow cytometry. Two-tailed Student's t-test (* $p<0.05$, ** $p<0.01$, *** $p<0.001$) was performed for each concentration of ethylene combustion condensate by comparing Bay 11-7082 treated group to the corresponding control group which was not treated with Bay 11-7082. Dotted lines indicate level of active NF- κ B in cells which were not treated with ethylene combustion condensate.

3.3.5.2 NF- κ B inhibition enhances the ethylene combustion condensate-induced apoptosis

Ethylene combustion condensate-induced NF- κ B activation in U-937 has already been shown in previously described results (Figure 3-27). Thereby, maximum activation of NF- κ B was observed after 24 h treatment with ethylene combustion condensate containing 4.8 ppm of total organic carbon. Same treatment caused very low level of apoptosis, which was comparable to the level of spontaneous apoptosis in untreated U-937 culture (Figure 3-19 A). According to these findings, it was assumed that NF- κ B has an anti-apoptotic effect in U-937 cells treated with ethylene combustion condensate. This chapter describes experiments undertaken to test this hypothesis.

U-937 cells co-treated with 2 μ M Bay 11-7082 and ethylene combustion condensate (4.8 ppm of total organic carbon) for 24 h were analysed for apoptosis (Figure 3-31). Figure 3-31 (A) shows the effect of Bay 11-7082 and ethylene combustion condensate on NF- κ B activation while Figure 3-31 (B) shows the effects on apoptosis

for the same conditions. Separate treatments with only Bay 11-7082 (2 μ M) and only ethylene combustion condensate (4.8 ppm of TOC) induced apoptotic death in 16% and 9% of the U-937 cell population, respectively (Figure 3-31 B). Co-treatment with 2 μ M Bay 11-7082 and ethylene combustion condensate containing 4.8 ppm of TOC induced apoptosis in 50% U-937 cells, which is more than the sum of the apoptotic effects after corresponding separate treatments (synergistic effect). Significant activation of NF- κ B pathway in U-937-pNF- κ B-EGFP/Neo clone 5a cells can be observed after 24 h treatment with the ethylene combustion condensate containing 4.8 ppm of TOC Figure 3-31 (A). On the other hand, co-treatment with 2 μ M Bay 11-7082 and ethylene combustion condensate (4.8 ppm of TOC) reduces the level of NF- κ B activation to the basal level of untreated culture (Figure 3-31 A). For the same treatment conditions, the level of apoptotic cells was increased (Figure 3-31 B). These results therefore show that activation of NF- κ B pathway has an anti-apoptotic effect in U-937 cells treated with ethylene combustion condensate.

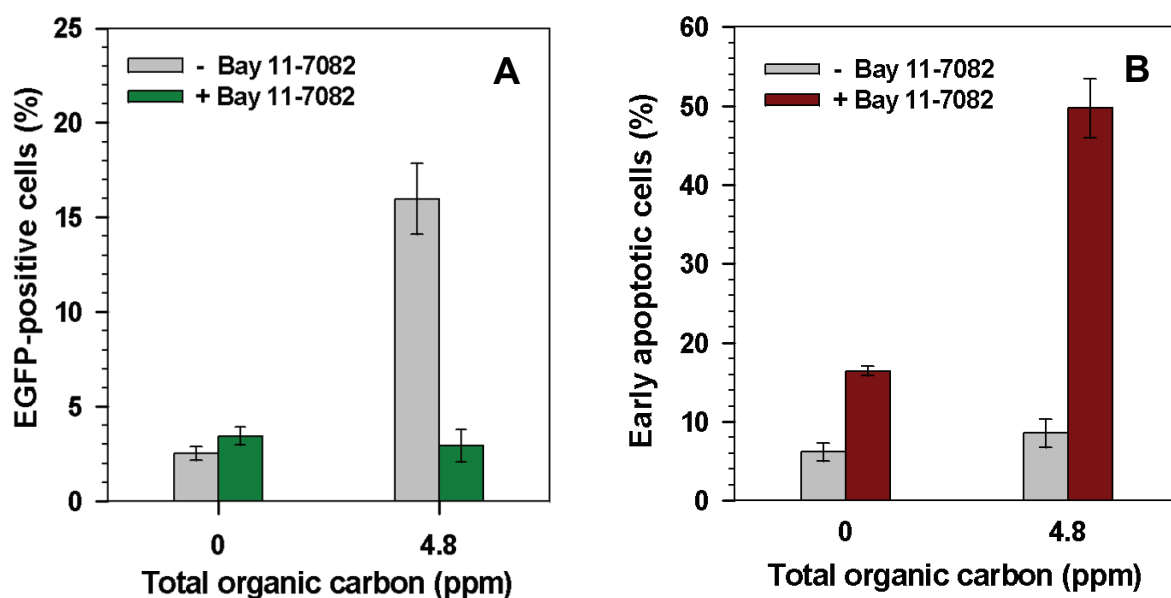


Figure 3-31: Inhibition of NF- κ B pathway increases the number of apoptotic cells in U-937 cell culture treated with ethylene combustion condensate

U-937 and U-937-pNF- κ B-EGFP/Neo clone 5a cells were co-treated with 2 μ M Bay 11-7082 and ethylene combustion condensate (C/O=0.93) containing 4.8 ppm of total organic carbon for additional 24 h. Flow cytometric measurement of EGFP-expression was used for the assessment of NF- κ B activation in U-937-pNF- κ B-EGFP/Neo clone 5a (A). Induction of apoptosis in U-937 was assessed via Annexin V-PE/ 7-AAD assay (B).

3.3.6 Effect of the ethylene combustion condensate on the expression of NF- κ B-target genes in A-549

The effect of combustion condensates on the activation of the NF- κ B signalling pathway in A-549 cells was assessed by examining the changes in expressions of NF- κ B-dependant target genes (IL-6, NF κ BIA). The expressions of NF- κ B-target genes were examined by qRT-PCR. By using the REST software (described in chapter 2.2.9.3.4), the relative gene expression ratios were calculated by normalising the expressions of target genes (genes of interest) with the expressions of selected reference genes (housekeeping genes).

A-549 cells were treated for 2 h, 6 h, or 24 h with different types of combustion samples: ethylene combustion condensate gained at non-sooting conditions (C/O=0.63), ethylene combustion condensate gained at highly sooting conditions (C/O=0.93) and diesel combustion condensate gained during no-load engine operating mode. The concentration of each of the applied samples was 10 ppm of TOC. A 48 h incubation with this concentration induced death in 50-75% of A-549 cells, depending on the type of a combustion condensate which was applied (Figure 3-15). Modulations of IL-6 and NF κ BIA gene expressions caused by treatments with combustion condensates are shown in Figure 3-32 and Figure 3-33, respectively. According to the BestKeeper analysis, GAPDH, HPRT and PBGD proved to be suitable reference genes as their expressions remained stable in all experimental treatments. Therefore, target genes' expressions were normalised with the expressions of those three housekeeping genes. The significance level of the up- or down-regulation of target genes in treated conditions compared to control conditions was examined with the Student's t-test.

Treatment with a known NF- κ B-activator TNF- α served as a positive control for the activation of the NF- κ B-dependant gene expression. For all examined time-points, treatment with 10 ng/ml TNF- α significantly up-regulated (up to ~4-fold) the expressions of IL-6 and NF κ BIA genes.

After treatment with diesel combustion condensate and ethylene combustion condensate obtained at C/O=0.63 for 2 h, 6 h or 24 h, the IL-6 expression remains nearly unchanged. A slight but significant up-regulation (~2-fold) of the IL-6 expression is observed after 24 h exposure to the ethylene combustion condensate obtained at C/O=0.93.

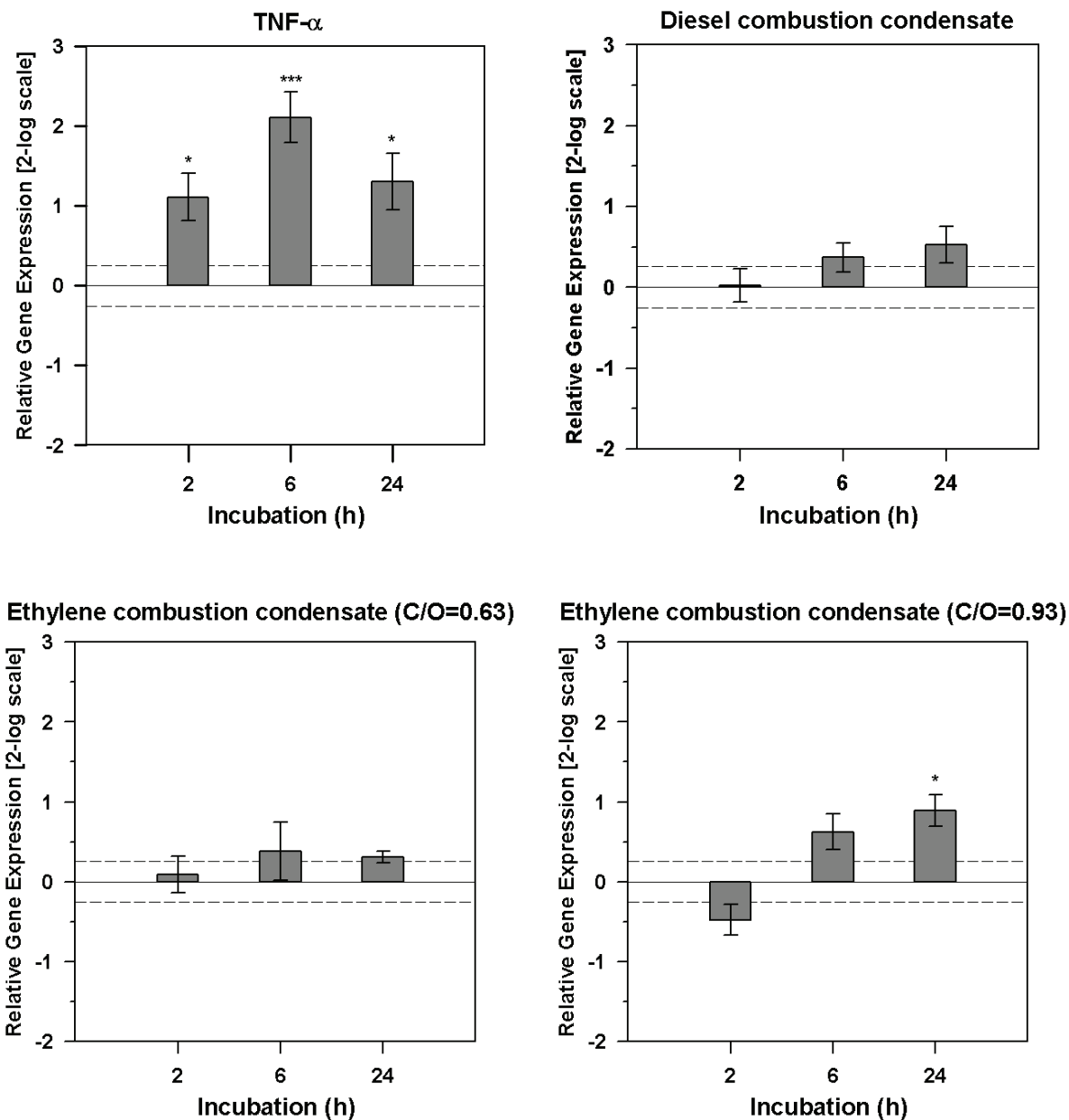


Figure 3-32: Modulation of IL-6 gene expression in A-549 after treatment with different combustion samples

Cells were treated with diesel-/ethylene combustion condensates containing 10 ppm of TOC or with 10 ng/ml TNF- α for indicated time-points. The expression of IL-6 was quantified by using real-time qRT-PCR. Relative gene expressions represent the expression of a target gene (IL-6) normalised with the expression of selected housekeeping genes (HPRT, GAPDH, and PBGD). Full line (relative gene expression= $2^0=1$) represents the mean of the negative controls (untreated cells) and slashed lines their \pm standard error. The significance level of the up- or down-regulation of target genes in treated compared to control conditions was examined with the Student's t-test.

NF κ BIA expression follows a similar pattern for all sample treatments: a down-regulation observed after 2 h and 6 h of incubation is followed by a slight up-regulation after 24 h treatment. A 2 h incubation with each of the investigated combustion condensates leads to a significant down-regulation (up to ~2-fold) of the NF κ BIA expression. Down-regulation of NF κ BIA expression is also observed after 6

h exposure to each of the examined combustion condensates except for the ethylene combustion condensate obtained at C/O=0.93. A 24 h incubation with the diesel-combustion condensate and the ethylene combustion condensate obtained at C/O=0.93 increased the level of NF κ BIA mRNA slightly but significantly (1.5-fold up-regulation), compared to the untreated control.

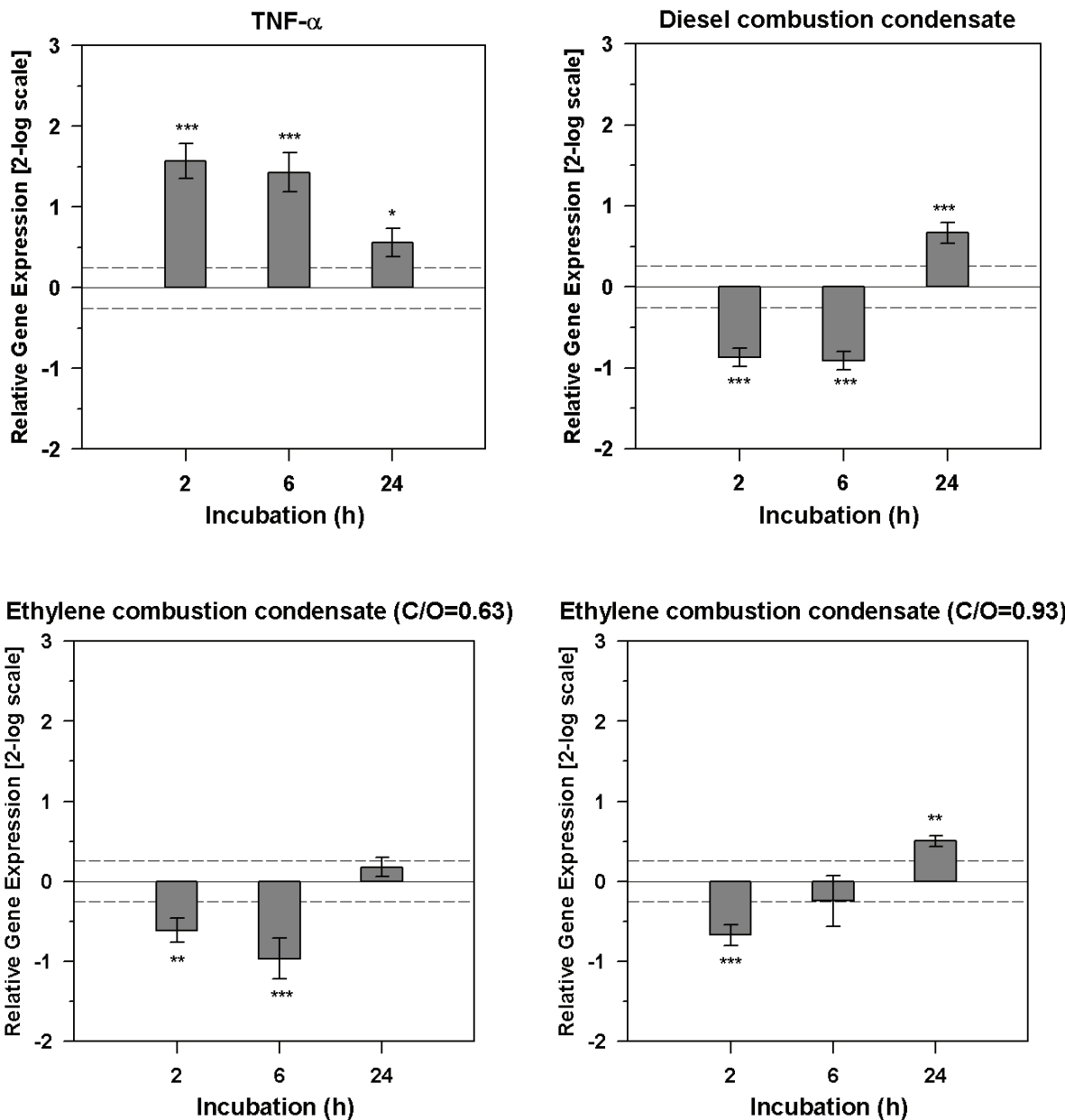


Figure 3-33: Modulation of NF κ BIA gene expression in A-549 after treatment with different combustion samples

Cells were treated with diesel/ethylene combustion condensates containing 10 ppm of TOC or with 10ng/ml TNF- α for indicated time-points. The expression of NF κ BIA was quantified by using real-time qRT-PCR. Relative gene expressions represent the expression of a target gene (NF κ BIA) normalised with the expression of selected housekeeping genes (HPRT, GAPDH, and PBGD). Full line (relative gene expression= $2^0=1$) represents the mean of the negative controls (untreated cells) and slashed lines their \pm standard error. The significance level of the up- or down-regulation of target genes in treated compared to control conditions was examined with the Student's t-test.

3.3.7 Removal of soot particles has no effect on the toxicity of ethylene combustion condensate on U-937 cells

As it was already shown with a bacterial pre-screening test (SWITCH test), the elimination of the soot particles bigger than 20 nm did not change the toxic potency of ethylene combustion condensate (Figure 3-10). Since the aim of this thesis was to test the toxic effect of the combustion condensates on human cells, formerly described results obtained with the SWITCH test had to be proven with a toxicity assay employing human cells. It was chosen to study the effect of the ethylene combustion condensate ($C/O=0.93$) and its filtrate 2 (obtained after filtration of ethylene combustion condensate through the 20 nm-pored filter) on the induction of apoptosis in U-937 cells by using Annexin V-PE / 7-AAD apoptosis assay. For this purpose, cells were treated for 24 h with the same volume concentration of the non-filtrated ethylene combustion condensate and the filtrate 2. This volume concentration corresponded to 9.6 ppm of total organic carbon in non-filtrated ethylene combustion condensate.

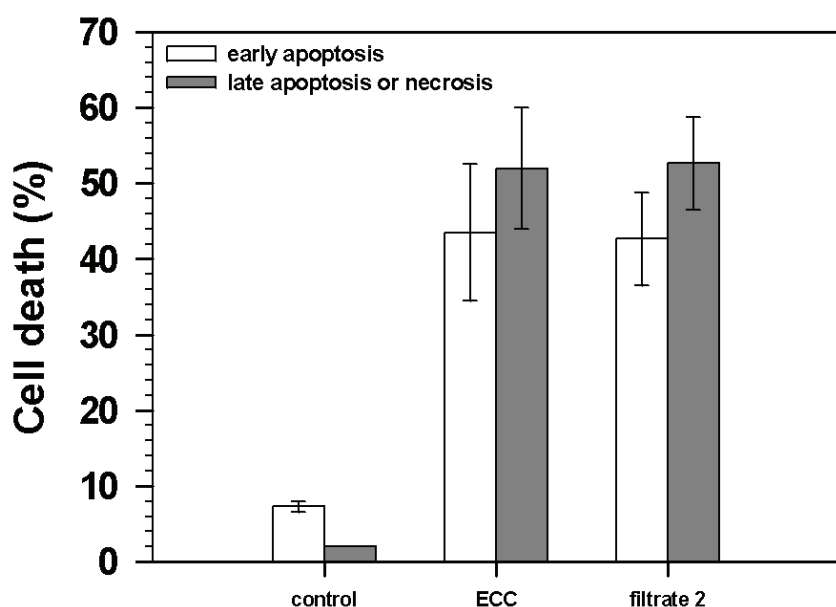


Figure 3-34: Soot particles larger than 20 nm have no significant contribution to the toxicity of ethylene combustion condensate, as estimated with apoptosis test

Induction of apoptosis in U-937 cells was assessed with Annexin V-PE / 7-AAD assay. "Filtrate 2" was obtained by filtrating the ethylene combustion condensate ($C/O=0.93$) through a 20 nm-pored filter. Cells were treated for 24 h with the same volume concentrations of the ethylene combustion condensate (ECC) and filtrate 2. Cells treated only with medium are used as a negative control.

Results show no significant difference in the toxic effects of the non-filtrated ethylene combustion condensate (ECC) and its filtrate 2 (Figure 3-34). Both treatments give

rise to the same number of early apoptotic (44%) and late apoptotic/necrotic cells (51%). This result confirms the finding obtained with the bacterial SWITCH test that soot particles larger than 20 nm in size do not significantly contribute to the toxicity of the combustion condensates.

For the elimination of soot particles ≥ 10 nm, ethylene combustion sample (C/O=0.93) was centrifuged at high speed for a long time (14 h at 116 000 $\times g$). According to the SWITCH test, the soot-free supernatant and resuspended pellet exhibited the same toxic effect as the non-centrifuged sample (Figure 3-11), indicating that toxicity of the combustion condensates is most likely not soot-mediated. For the verification of this finding, toxicity of the non-centrifuged ethylene combustion condensate, its supernatant and resuspended pellet (obtained after 14 h centrifugation at 116 000 $\times g$) was tested on U-937 cells using the Annexin V-PE / 7-AAD apoptosis assay. Cells were treated with the same volume concentrations of the formerly mentioned samples. This volume concentration corresponded to 9.6 ppm of total organic carbon in non-centrifuged sample. U-937 cells treated only with culture medium served as a negative control. After 24 h treatment, percentage of apoptotic/necrotic cells was assessed with the Annexin V-PE/ 7-AAD staining method. Results revealed 44% of early apoptotic and 52% of late apoptotic/necrotic U-937 cells after treatment with soot-free supernatant (Figure 3-35). The same effect was observed after treatment with the non-centrifuged ethylene combustion condensate, which indicates that removal of soot particles does not reduce the toxic potential of the ethylene combustion condensate. Although the concentration of soot particles in the resuspended pellet is almost twice as high as in the non-centrifuged ethylene combustion condensate, toxic effects of these two samples are the same (Figure 3-35). This confirms former findings with the SWITCH test (Figure 3-9) that an increase in concentration of soot particles in ethylene combustion condensate does not increase its toxicity. Data shown in Figure 3-35 support the conclusions drawn from the bacterial SWITCH test (Figure 3-11), that particulate matter ≥ 10 nm is not the major contributor to the toxicity of ethylene combustion condensate.

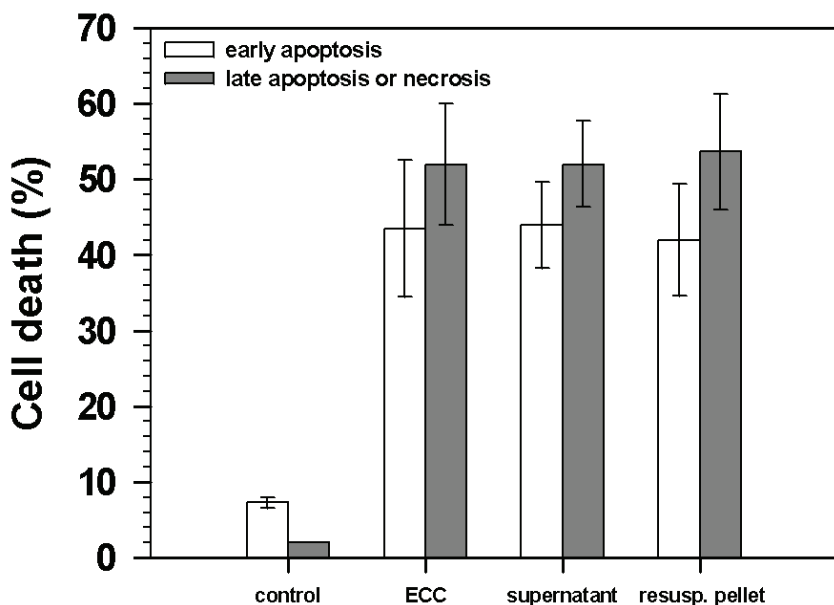


Figure 3-35: Toxic component of ethylene combustion condensate cannot be precipitated after 14 h centrifugation at 116 000 x g, as estimated with mammalian apoptosis test

Induction of apoptosis in U-937 was assessed with Annexin V-PE / 7-AAD staining method. Ethylene combustion condensate (ECC) was centrifuged at 116 000 x g for 14 h in order to obtain the soot-free supernatant and the resuspended pellet (containing almost twofold increased concentration of soot particles). Cells were treated for 24 h with the same volume concentrations of ECC, supernatant and resuspended pellet. Cells treated only with culture medium are used as a negative control.

4 Discussion

It is known that emissions from combustion sources influence human health. The main aim of this thesis was to determine the toxicity of the combustion condensates on human cells, on cellular and molecular level. For this purpose, combustion condensates were generated from a model flame (pre-mixed ethylene/oxygen flame) or from a diesel-powered engine and tested on two human cell lines A-549 and U-937. The combustion condensates obtained by the “cool trap” method consist of particulate and gaseous combustion by-products suspended in water. So far, toxicological research has focused predominately on the combustion generated particulate matter, thereby neglecting the chemical complexity of combustion exhausts. Toxicity analysis of heterogeneous environmental samples such as combustion condensates makes this *in vitro* study rare and valuable.

Characterisation of the ethylene- and diesel combustion condensates was the first step undertaken in the study of their toxic effects. In order to determine a biologically relevant dose range, combustion condensates were tested for their genotoxicity and cytotoxicity with a bacterial pre-screening assay (the SWITCH test). The contribution of soot particles to the toxicity of combustion condensates was assessed with the SWITCH test and with one human cell-based assay. Toxic effects of the combustion condensates and their mechanisms were studied in A-549 and U-937 cell lines. This included the study of effects on cellular growth, on cell cycle, on apoptosis induction, and on activation of the stress-induced NF- κ B signalling pathway. The obtained results are discussed in the following sections.

4.1 Characterisation of combustion condensates

Characterisation of ethylene- and diesel combustion condensates was the first step undertaken in this research. Physical characterisation was achieved by visual inspection, HRTEM-analysis and spectrophotometry. The chemical analysis undertaken was the measurement of the total organic carbon content.

Combustion condensates were examined for the presence of soot particles by visual inspection. Gray-coloured turbidity of stirred combustion condensates and the formation of a black sediment in non-stirred conditions indicated presence of soot particles. Turbidity of the combustion samples originating from the second and third

cool traps was less intensive than the turbidity of the respective samples from the first cool traps. This indicates a high collecting efficiency of the first cool trap. Intensity of the turbidity of ethylene combustion condensates was directly proportional to the fuel/oxygen ratio during combustion (C/O ratio), indicating higher amount of soot particles at higher C/O ratios. This is expectable, since a lack of oxygen (higher C/O ratio) leads to an incomplete combustion and, accordingly, to a higher production of soot. Sooting threshold is the lowest combustion C/O ratio at which the soot generation occurs. The sooting threshold for a premixed ethylene/oxygen flame operating at low pressures is achieved at a C/O ratio of about 0.72 (Grotheer et al., 2004). Coherent with this finding is the result of the current study showing that the ethylene combustion condensates which were generated at $C/O \leq 0.73$ are transparent, indicating no visually detectable presence of soot under these conditions. Inspection of the turbidity of diesel combustion condensates indicated less amount of suspended soot particles in the samples obtained under “4 kW-load” compared to the “no load” operating mode of a diesel generator. Berlan BSTE5000DE diesel power generator is a one-cylinder-four-stroke engine with the rated electric power output of 4.2 kW (according to manufacturer’s instructions). Efficiency of internal engine combustion is influenced by factors such as load, pressure, temperature and fuel/air ratio. According to the results of the combustion condensates’ characterisation, it seems that the diesel fuel burning conditions during no load mode (e.g. lower temperatures) were less optimal than during 4 kW-load mode, which led to a more incomplete combustion and higher soot production.

High-resolution transmission electron microscopy was used for detection and morphological characterisation of the particulate matter present in the combustion condensates. HRTEM-analysis of both ethylene- and diesel combustion samples revealed presence of large soot agglomerates containing spherical and elongated primary particles (Figure 3-1). Diameter of the smallest observed primary particles was approximately 10 nm. Higher degree of graphite-like inner structure was observed for the soot originating from the ethylene combustion, compared to the soot generated during incomplete diesel combustion (Figure 3-1). This difference in the soot structure is not surprising, since the impact of the type of fuel and burning conditions on the soot nanostructure has been already documented (Vander Wal et al., 2004; Su et al., 2004). Differences in soot nanostructures are probably due to a different soot-formation mechanism (Su et al., 2004). Although having slightly

different nanostructures, ethylene and diesel soot have shown similarities in the morphology of their outer surfaces. Both ethylene and diesel soot possess rough outer surfaces, covered with small, strongly curved fullerene-like structures (Figure 3-1 B, D). Surface irregularities and the presence of fullerene-like structures were also evidenced on the surface of Euro IV heavy-duty (HD) diesel soot (Müller et al., 2005; Su et al., 2008). The fullerenes are non-planar carbon clusters, which contain hexagonal and pentagonal aromatic carbon rings (Choho et al., 1995). The presence of pentagonal carbon rings in soot surface structure contributes to higher curvature of the soot surface and, accordingly, to higher C-C bond strain and higher reactivity of soot (Su et al., 2004). High soot reactivity towards oxidation can be an advantageous feature for the catalytic oxidation after-treatment of soot in vehicle engines (Müller et al., 2005). On the other hand, soot surface reactivity can be a cause of undesirable interactions with the cell structures. Increased surface reactivity may lead to membrane damage, protein denaturation, and DNA cleavage (Xia et al., 2006). Higher cytotoxic and inflammatory potential was observed for the soot originating from contemporary low-emission diesel engines (Euro IV) compared to the soot from an old diesel engine operating under black smoke conditions (Su et al., 2008). This effect is attributed to the higher reactivity of the Euro IV diesel soot due to its “defective” surface structure. Roughness of the soot also increases its outer surface area which serves as an adsorbent for other, potentially toxic combustion by-products.

Spectrophotometry is one of the commonly used tools for detection and analysis of combustion generated particles (Sgro et al., 2001; D’Anna et al., 2005; Commodo et al., 2007). Soot particles absorb similar intensity of light in the UV and visible light range (D’Anna et al., 2005), whereas nanoparticles only absorb in the UV range. UV-spectrophotometry of the ethylene-/diesel combustion condensates revealed broad band absorption in the UV region (200 - 300 nm) (Figure 3-2 A). This indicates presence of nanoparticles (size of 2-4 nm) in the combustion condensates (Sgro et al., 2001; Sgro et al., 2003; Commodo et al., 2007). Considering these findings, the absorbance measured at 250 nm (Abs_{250}) was chosen here as an indicator for the presence of nanoparticles in the examined combustion condensates. As shown in Figure 3-2 (A), ethylene combustion condensates generated at higher C/O ratios exhibit higher absorbance intensities at 250 nm. This indicates that the concentration of nanoparticles in the combustion exhaust increases with increasing carbon/oxygen

ratio during combustion. Nanoparticles are also considered to be soot-precursors (Grotheer et al., 2004), and their elevated concentrations under conditions favouring the production of soot (high C/O ratio) is therefore understandable and expected. Ethylene combustion condensate generated at non-sooting conditions (C/O=0.68) displays absorption at $\lambda < 300$ nm and no absorption at $\lambda > 300$ nm, which indicates the absence of soot particles in this sample (Figure 3-2 A). This is in accordance with the results of other research groups that also detected nanoparticles under non-sooting conditions (Minutolo et al., 1999; Sgro et al., 2003). For the ethylene combustion condensate generated at highly sooting conditions (C/O=0.93), there was a measurable absorption at $\lambda > 300$ nm (e.g. $\text{Abs}_{400}=0.5$) which can be attributed to the presence of soot particles. Considering the fact that soot absorbs almost consistently in both UV and visible region of the light (Sgro et al., 2003), it can be assumed that soot also contributes to Abs_{250} values. However, the intensity of absorption of the formerly mentioned combustion condensate at 250 nm is significantly higher ($\text{Abs}_{250}=4$) than the absorption related to the soot contribution ($\text{Abs}_{>300} \sim 0.5$). Accordingly, the soot contribution to Abs_{250} can be neglected. Even if the corresponding soot absorbance contributions at $\lambda=250$ nm would be subtracted from the total absorbance measured at 250 nm for each of the tested ethylene combustion condensates, there would still be a substantial excess absorbance which can be attributed solely to nanoparticles. Accordingly, Abs_{250} parameter predominately describes the concentration of nanoparticles and its use as an indicator for nanoparticles is thereby justified.

Chemical characterisation of the combustion condensates comprised the analysis of their total content of organic carbon (TOC). The term organic carbon refers to a variety of organic compounds which are emitted in the atmosphere during combustion processes (Merola et al., 2001). Total organic carbon analysis is extensively used in environmental research as a screening tool for the determination of carbon content in the quality control of water samples. According to the results presented in this work, TOC content of the combustion samples depends on the combustion conditions such as C/O ratio and engine operating mode (load/no-load). Combustion of diesel in the generator operating at no-load regime gives rise to higher TOC content of diesel combustion condensates compared to the “load” regime (Table 3-2). The higher the C/O ratio was during the ethylene combustion, the higher was the TOC content of the produced combustion samples (Table 3-1). As already

mentioned, high C/O ratios lead to incomplete combustion and, accordingly, higher amounts of organic combustion by-products (e.g. soot, nanoparticles, PAHs, aldehydes, and others) which are all comprised in the TOC measurements. Ethylene- and diesel combustion samples originating from the first cool traps were used for the biological assays because of their higher TOC content compared to the samples collected in the second and in the third cool trap. Results of the bacterial pre-screening assay have shown that the same amount of TOC in ethylene combustion samples exerts the same toxicity, regardless of the cool trap they originate from (Figure 3-8) or of the C/O ratio applied for the samples' generation (Figure 3-4; Figure 3-5). Accordingly, less amount of the samples collected in the first cool traps can be used in order to produce the same toxic effect as if the samples from the other two cool traps would have been used. This enabled more economic utilisation of the available amount of combustion samples. For the same reason, TOC-rich ethylene combustion condensates generated at C/O=0.93 and the diesel combustion condensates generated at no-load engine operating mode were applied in diverse biological tests with human cell lines. Although ethylene combustion at C/O>0.93 conditions would have produced combustion samples that are even richer in TOC content than the samples obtained at C/O=0.93, clogging of the sampling nozzle at such highly sooting conditions disabled the generation of combustion condensates at these burning conditions.

4.2 SWITCH test as a pre-screening tool for the combustion condensates' toxicity assessment

The aim of this thesis was to assess toxic effects of ethylene- and diesel combustion condensates on human cells. Prior to this, toxic potential of combustion condensates was firstly monitored by using the bacterial SWITCH test. This test served as a pre-screening assay for the assessment of genotoxic and cytotoxic potency of the examined combustion samples. It was also used to estimate the biologically relevant dose range for the experiments with human cell lines.

Rapidity, reliability, reproducibility and sensitivity are some of the characteristics of the SWITCH test which make it a suitable tool for biomonitoring toxic effects of a certain agent. The SWITCH test has already been successfully applied for the toxicity assessment of X-rays / UV radiation (Stojicic et al., 2005), diverse chemicals

(Baumstark-Khan et al., 2001) and polluted environmental samples (Baumstark-Khan et al., 2005). Thereby, the results of the genotoxicity assessment of a given substance with the SWITCH test were comparable with the results obtained with other well-established genotoxicity assays (Baumstark-Khan et al., 2001) such as the Ames test. However, it is important to note that the performance of the SWITCH test and the interpretation of its results is much less time- and labour consuming compared to the Ames test. The SWITCH test delivers results in approximately 8 h, whereas the results of the Ames test can be obtain earliest after 48 h. The SWITCH test utilises the bacterial strain *S. typhimurium* TA1535, which is one of the tester strains in the Ames test (Ames et al., 1973). This strain carries a mutation (*rfa*⁻) that results in a deficient lipopolysaccharide layer which coats the surface of bacteria. As a consequence, the strain is more sensitive to chemical mutagens. An additional mutation (*uvrB*⁻) eliminates the excision DNA damage repair system (Ames et al., 1973) and consequently triggers faster the SOS response in the presence of mutagens. This makes the SWITCH test a very sensitive bioassay, since it assesses the genotoxicity of a given agent by measuring the SOS-dependant bioluminescence. One of the advantages of the SWITCH test over other SOS-dependant assays for the genotoxicity assessment (e.g. umu test) is that it is independent of external substrate supply (Stojicic et al., 2005). This is due to the fact that the pSWITCH plasmid carries the genes for the luciferase (*luxAB*) and the fatty acid reductase (*luxCDFE*) enzymes, whose expression is under control of a strong SOS-dependant promoter (Ptitsyn et al., 1997). The fatty acid reductase regenerates the substrate for the luciferase by converting fatty acids into aldehydes. Regeneration of the luciferase substrate ensures that the SOS-Lux reporter system is activated as long as DNA damage is present. However, the conversion of fatty acids into aldehydes also requires ATP, so that bioluminescence production only occurs in living cells. This is important, since only mutated viable cells have a carcinogenic potential. Furthermore, the simplicity of the SWITCH test is reflected in the use of GFP as a reporter element for cytotoxicity assessment, since GFP-fluorescence is also independent of a substrate or a cofactor (Chalfie et al., 1994).

According to the results of the SWITCH test, ethylene and diesel combustion condensates displayed cytotoxic and genotoxic effect for concentrations > 10 ppm of total organic carbon. Ethylene combustion condensates generated at different combustion conditions (C/O ratios ranging from 0.63 to 0.93) induced 50% cell death

(LC₅₀) and maximum genotoxic effect in the concentration range between 21 and 46 ppm of TOC. Similarly, diesel combustion condensates (generated during 4kW-load or no-load engine operating modes) induced maximum genotoxic effect and 50% cell death in the concentration range of 19 - 24 ppm of TOC. In the SWITCH test, the intensity of the bioluminescence signal is directly proportional to the concentration of a genotoxin and thereby to the extent of induced DNA damage. Maximum luminescence output (mean lux peak value) induced by ethylene or diesel combustion condensates was 4- to 7-fold higher than the luminescence output measured in untreated cells. According to their lux peak values, both ethylene and diesel combustion condensates can be classified as slightly genotoxic. This is evident after comparison of their genotoxicity with the effects of a powerful chemical genotoxin such as mitomycin C. According to the SWITCH test, maximum relative light output induced by this DNA intrastrand cross-linking agent was nearly 60 (Baumstark-Khan et al., 2001).

Taken together, the SWITCH data have shown that diesel and ethylene combustion condensates exhibit both genotoxic and cytotoxic effects. The SWITCH test proved to be a useful tool for rapid screening of the toxic potential of combustion condensates.

4.2.1 TOC content is a proper dose metric for the evaluation of combustion condensates' toxicity

TOC content was used in this work for the characterisation of the combustion condensates. One of the tasks was to evaluate whether there is a correlation between TOC and the toxicity of combustion condensates.

In this study, a direct-proportional correlation between total organic carbon content of ethylene-/diesel combustion condensates and their toxic potential was shown by using different bioassays and different cell models. As demonstrated with the SWITCH test, same amount of TOC in ethylene combustion samples exerts the same toxicity, irrespective of the combustion C/O ratios during sample generation (Figure 3-4, Figure 3-5). Also, diesel combustion condensates of same TOC content have the same toxic effect, regardless of the type of engine operating mode which was applied for sample generation (Figure 3-6). Cytotoxicity assays employing human cells have also demonstrated that cellular responses are directly proportional

to the TOC content of tested samples. Combustion condensates reduce the viability of A-549 (Figure 3-15) and U-937 (Figure 3-14) cells dose-dependently. Different apoptotic assays (Annexin V-PE/7-AAD assay, Active caspase-3 assay and DNA content analysis) demonstrated a dose-dependant induction of apoptosis in U-937 cells after treatment with ethylene- or diesel combustion condensates (chapter 3.3.3). All aforementioned findings, which show that combustion condensates' toxicity is TOC-dependant, indicate that the organic fraction of combustion exhausts plays a pivotal role in their toxicity. Direct comparison of this finding with published studies is not possible, since they focused mainly on particulate matter, thereby neglecting gaseous combustion by-products. Nevertheless, several studies have shown a strong link between the organic fraction extracted from airborne particulate matter and detrimental health effects. Induction of oxidative stress was related to organics which are adsorbed on the outer surface of airborne particles (Li et al., 2003). Exposure to the organic carbon fraction of PM_{2.5} was associated with reduction of heart rate variability in patients with or at risk for cardiovascular diseases (Chuang et al., 2007).

In summary, total organic carbon content is a suitable dose metric for the assessment of toxicity induced by combustion derived samples.

4.2.2 Toxicity of combustion condensates is not soot-mediated

One of the goals in the current work was to study the contribution of soot to the toxicity of analysed combustion condensates. The toxic potential of soot particles was presumed according to existing literature data (Su et al., 2008). Also, the HRTEM-analysis of soot originating from ethylene or diesel combustion (chapter 3.1.2) suggests that soot particles from the investigated samples possess potentially high reactivity due to the irregularities of their outer surfaces (Su et al., 2004).

Although the link between the exposure to diesel exhaust and lung cancer mortality has been shown in epidemiological studies (Garshick et al., 2004), the specific components of diesel exhaust responsible for its carcinogenicity have not yet been identified (Davis et al., 2007). So far, adverse health effects of diesel exhaust were mostly attributed to soot particles and specifically to the organics/metals which are adsorbed to their surface (Donaldson et al., 2005). Results presented in this thesis clearly show that soot particles ($d \geq 10$ nm) are not major contributors to the

genotoxic/cytotoxic potency of the ethylene combustion condensates. First indications that soot is not responsible for the observed toxic effects of combustion condensates came from the SWITCH test results shown in Figure 3-5. There was no statistically significant difference in the LC₅₀ values of ethylene combustion condensates generated at different C/O ratios (ranging from 0.63 to 0.93). The sooting threshold is considered to be the lowest combustion C/O ratio at which soot is generated. It is an empiric value and according to Grotheer et al. (2004) it is achieved at C/O=0.72 for premixed ethylene/oxygen flames operating at low pressures. At comparable TOC-levels, the toxic potency of ethylene combustion samples obtained at non-sooting (C/O=0.63, C/O=0.68) or only slightly sooting conditions (C/O=0.73) was not statistically different from the toxicity of the samples obtained at medium- (C/O=0.78) and highly sooting conditions (C/O=0.83, C/O=0.88 and C/O=0.93) (Figure 3-5). This indicated that soot might not play a significant role in the toxicity of ethylene combustion exhausts.

More plausible evidence that toxicity of investigated combustion condensates is not soot-mediated came from the filtration and centrifugation experiments. Soot aggregates are comprised of primary soot particles, each sized in the range of 10-30 nm (Sgro et al., 2003; Grotheer et al., 2004; Grotheer et al., 2007). Ethylene combustion condensate originating from the highly sooting flame (C/O=0.93) was filtrated through 100 nm- and 20 nm-pored filters in order to eliminate soot from the samples. Filtrate 1 and filtrate 2, obtained after filtration of ethylene combustion condensate through 100 nm-pored and 20 nm-pored filters, respectively, displayed no measurable absorbance at 600 nm, indicating absence of soot (Table 3-3). Results of the cytotoxicity assays with bacterial (Figure 3-10) and human cell models (Figure 3-34) showed no difference in the toxicity of combustion condensate prior to and after filtration. These results suggest that non-soluble soot particles larger than 20 nm are not responsible for the observed toxicity of combustion condensates. Ultracentrifugation (14 h at 116 000 x g) was performed in order to exclude even the smallest primary soot particles (d~10 nm) from the ethylene combustion samples. Absence of soot particles in the supernatant was confirmed by absorbance measurements at 600 nm (Table 3-3). The results show that toxicity induced by non-centrifuged combustion condensate does not significantly differ from the toxic potential of soot-free supernatant (Figure 3-11, Figure 3-35). Accordingly, non-soluble combustion generated particles ≥ 10 nm are not responsible for the observed

detrimental effects. The centrifugation method ($20\ 817\ \times g$ for 90 min) was used to increase the concentration of soot in ethylene combustion condensates by 2-4-fold. These increased concentrations of soot particles do not change the toxicity of the samples (Figure 3-9). This is another evidence that soot is not the major contributor to the toxicity of ethylene combustion condensates.

The findings that soot does not play an essential role in the toxicity of combustion exhausts are somewhat surprising and unexpected, considering the already existing *in vitro* (Matsuo et al., 2003; Su et al., 2008) and *in vivo* (Dybdahl et al., 2004) studies which show toxic effects of soot particles. However, in order to observe significant responses, many studies have applied very high doses of soot particles, which can be 10- to 100-fold higher than the ambient levels measured in polluted areas (Andre et al., 2006). Su and his co-workers (2008) have noticed toxic and pro-inflammatory effects after 24 h treatment of macrophages with 30 µg/ml diesel soot particles. In the presented work, toxic effect on U-937 cells was observed after 24 h incubation with ethylene- or diesel combustion condensates containing ≥ 6.4 ppm of total organic carbon (Figure 3-19, Figure 3-20). In order to estimate the concentration of soot particles in combustion condensates, a standard calibration curve was recorded by measuring the absorbance at 600 nm (Abs_{600}) of the soot model particles (carbon black) suspended in water (data not shown). Derived from these measurements, diesel combustion condensate (6.4 ppm of total organic carbon) contains 0.1 µg/ml of soot particles, while the ethylene combustion condensate of the same TOC-concentration contains 0.4 µg/ml of soot. These concentrations of soot particles are lower than the soot concentration (30 µg/ml) applied in the study by Su et al. (2008) by 75- to 300-fold, which can explain why soot was not contributing to the toxicity of ethylene combustion condensates.

In conclusion, the results shown here have demonstrated that soot particles ($d \geq 10$ nm) in environmentally relevant concentrations are not major contributors to the observed detrimental effects of combustion condensates. This finding further implies that the reduction of soot emissions from vehicles by implementing filters, does not eliminate the toxic potency of exhaust. Results presented here should be taken into account for future research and development strategies in car industry.

4.3 Effects of combustion condensates on human cells

Two human cell lines (A-549 and U-937) served as *in vitro* models to study toxic effects of the combustion condensates and their mechanisms. This comprised the investigation of effects on cellular growth, on cell cycle, on apoptosis induction, and on activation of the NF- κ B signalling pathway.

4.3.1 Combustion condensates have a cytotoxic effect on A-549 and U-937

Cytotoxic effects of ethylene combustion condensate ($C/O=0.93$) were observed on both A-549 and U-937 cell lines. A 50% reduction in U-937 cell growth (LC_{50}) is achieved after 48 h treatment with ethylene combustion condensate containing 5 ppm of total organic carbon (Figure 3-14). Similar toxicity ($LC_{50}=7$ ppm of TOC) was observed in A-549 (Figure 3-15) after same treatment conditions. This indicates that these two cell lines have comparable sensitivities towards ethylene combustion condensate. Ethylene combustion condensate generated at $C/O=0.63$ and at $C/O=0.93$, as well as diesel combustion condensate (obtained at no-load engine operating regime) are toxic towards A-549 cells in the concentration range below 10 ppm ($LC_{50}\leq 10$ ppm of TOC). Slight differences between the toxic effects of ethylene and diesel combustion derived samples can be based on the differences in the nature of fuels and combustion by-products. Diesel fuel is a mixture of diverse hydrocarbons, whose combustion gives rise to a high variety of by-products (Shauer et al., 1999), among which a lot of them are considered potentially toxic. On the other hand, combustion of defined gases, such as ethylene, results in more homogenous combustion reactions and thus less complex by-products.

The respiratory system is the main portal of entry for potentially toxic combustion generated by-products. Due to their phagocytic activity, alveolar macrophages and alveolar epithelial type II cells (Mason et al., 1977) play a significant role in the host defence against inhaled pathogens. Besides this role, the main functions of alveolar epithelial type II cells are the synthesis, secretion and recycling of all surfactant components. Surfactant regulates the alveolar surface tension (Mason et al., 1977), which is important for efficient ventilation and alveolar stability. The loss of type II cells has, therefore, a detrimental effect for the alveolus and for normal respiratory function. A-549 cells have properties of type II lung epithelial cells (Lieber et al.,

1976). The results presented here raise serious health concerns since they show that prolonged exposure of A-549 cells to combustion exhausts induces cell death.

Monocytes are macrophage precursors which reside in blood. Under normal physiological conditions, monocytes migrate from blood towards various target organs (e.g. the lungs) where they differentiate into macrophages (e.g. alveolar macrophages). This migration is markedly enhanced in response to inflammation (Li et al., 1998). Toxic effect of combustion exhausts on monocytes, as it was documented in this work by using the human U-937 monocyte-like cell model, can contribute to the reduction of macrophage-precursor pool which consequently leads to an attenuation of the first-line host defence against combustion exhausts.

After verifying that combustion condensates have a cytotoxic effect on U-937 and A-549 cells, further experiments were undertaken to investigate the mode of cell death. Apoptosis seems to be a predominant type of cell death in U-937 cells treated with combustion condensates. In cell cycle analysis, appearance of cells in the sub-G1 region (Figure 3-16) indicates apoptosis induction in U-937 cells treated for 24 h with ethylene combustion condensate containing ≥ 6.4 ppm of total organic carbon. Microscopic investigation of DAPI-stained cells clearly shows condensation and fragmentation of DNA (characteristic for apoptotic cells) in U-937 cells after same treatment (Figure 3-18 B, C). The Annexin V-PE / 7-AAD assay (Figure 3-19 A, Figure 3-20) and the Active caspase-3 assay (Figure 3-23) verified the induction of apoptosis in U-937 cells that were treated either with ethylene- or with diesel combustion condensates. The Annexin V-PE / 7-AAD assay allows detection of cells at early stages of apoptosis (early apoptotic cells) and distinguishes them from late apoptotic/necrotic cells whose cell membrane is damaged. After 24 h treatment with ethylene- or diesel combustion condensates (containing ≥ 6.4 ppm of TOC) the number of early apoptotic cells was lower than the number of late apoptotic and necrotic cells. This suggests that apoptosis might not be the only cell death mode induced by the combustion condensates and that the U-937 cells might also be dying via necrosis. This could be due to a cytotoxin-mediated depletion of intracellular ATP which causes apoptotic cells to undergo secondary necrosis (Troyano et al., 2003). According to Nicotera et al. (1998), two classical types of cell death (apoptosis and necrosis) can occur simultaneously in cell cultures exposed to the same stimulus and usually the intensity of that stimulus decides the prevalence of either apoptosis or necrosis. Indeed, higher concentrations (≥ 6.4 ppm of TOC) of ethylene combustion

condensate and especially diesel combustion condensate increased the number of late apoptotic/necrotic cells to a higher degree than the number of early apoptotic cells.

In A-549 cells treated with ethylene combustion condensates ($C/O=0.93$) containing 2.4 - 9.6 ppm of TOC, cell cycle analysis (Figure 3-17) and microscopic evaluation of DNA morphological changes (Figure 3-18) have shown no sign of apoptosis induction. The cytotoxic effect (impairment of cell growth) on A-549 cells was observed within the same concentration range (Figure 3-15). It can be therefore attributed to a non-apoptotic cell death mode such as necrosis.

Overall, combustion condensates induce cell death in A-549 and U-937 cells in a TOC content-dependant manner. Although the sensitivity of these two cell lines towards the same combustion condensate was quite comparable, the predominant mode of cell death differed for both lines. While apoptosis is characteristic for U-937 cells, A-549 cells die predominately by a non-apoptotic cell death.

4.3.2 Combustion condensates activate NF- κ B signalling pathway

One of the aims in this thesis was to study the effect of combustion condensates on the activation of NF- κ B signalling pathway. As described earlier (chapter 1.4), NF- κ B plays one of the key roles in the regulation of cell stress responses and NF- κ B activation is associated with many diseases.

In order to study the activation of NF- κ B pathway, U-937 cells were stably transfected with the pNF- κ B-EGFP/Neo plasmid. In such recombinant cells the expression of EGFP reporter gene is controlled by a synthetic promoter containing NF- κ B binding sequences as enhancer elements. Thereby, it is possible to monitor and quantify the activation of the NF- κ B signalling pathway in transfected cells simply by measuring the yields of green fluorescence of the reporter protein. U-937-pNF- κ B-EGFP/Neo clone 5a was selected as a model for the experiments due to its high inducibility compared to all the other screened clones. The results presented in this thesis show a dose-dependant increase in NF- κ B activation after 24 h treatment of U-937-pNF- κ B-EGFP/Neo clone 5a cells with ethylene combustion condensate ($C/O=0.93$). NF- κ B activation was clearly observed for concentrations ≤ 4.8 ppm of TOC. At concentrations > 4.8 ppm of TOC, the level of NF- κ B activation is comparable to or lower than the basal level of the NF- κ B activation in untreated cells. A decrease in

the NF- κ B activation at concentrations > 4.8 ppm of TOC could be due to a cytotoxic effect of ethylene combustion condensate in this dose range. Indeed, significantly higher levels of apoptotic and necrotic cells were observed in U-937 cells treated with ethylene combustion condensates containing > 4.8 ppm of TOC, compared to the untreated cells (Figure 3-19). One of the possible explanations is that direct cytotoxic effects of ethylene combustion condensates cause ruptures in the cell membrane and a subsequent leakage of the small soluble EGFP reporter molecules (Baumstark-Khan et al., 1999). This in turn contributes to a decrease of the measured EGFP-fluorescence signal, which served as a measure of NF- κ B activation.

Dose-dependant activation of NF- κ B signalling pathway was also reported in U-937 cells treated with cigarette smoke condensate (Anto et al., 2002). In that study, NF- κ B activation was achieved already after 15 min incubation with 1-10 μ g/ml of cigarette smoke condensate. This early detection of NF- κ B activation was possible by utilising electrophoretic mobility shift assay which measures the amount of NF- κ B translocated into the nucleus and/or bound to the DNA. The translocation of NF- κ B to the nucleus and binding to its target genes' promoters are the events that precede the EGFP transcription, translation, protein folding and maturation. Accordingly, the NF- κ B-activation reporter assay, which was applied in this study, detects NF- κ B activation at later time-points. On the other hand, by measuring the EGFP fluorescence in living cells, this assay allows the kinetic measurements with identical cell populations.

The NF- κ B activation in A-549 was investigated via the expression of two NF- κ B target genes: IL-6 and NF κ BIA. Interleukin-6 is one of the pro-inflammatory cytokines whose transcription is regulated by NF- κ B (Table 1-3). IL-6 is produced by a variety of cells (e.g. monocytes, epithelial cells) in response to stimuli such as cytokines, viruses, bacteria and cigarette smoke (Ahn and Aggarwal, 2005). In A-549 cells, no significant change in the IL-6 gene expression was observed after short-term incubation (2 h and 6 h) with ethylene- or diesel combustion condensates (Figure 3-32). Longer incubation (24 h) with ethylene combustion condensate (generated at C/O=0.93) significantly increased the level of IL-6 mRNA. This ~2-fold up-regulation of IL-6 suggests a mild pro-inflammatory effect of 24 h exposure to ethylene combustion condensate. Airway inflammation seems to be a central response to combustion exhausts (Lee et al., 2005; Swiston et al., 2008). Increased levels of pro-

inflammatory cytokines (IL-1, IL-6, TNF- α) and chemokines (IL-8) have been observed in response to the acute exposure to forest fire smoke (Swiston et al., 2008). NF- κ B-induced increase in IL-8 production in A-549 cells exposed to motorcycle exhaust particles has also been reported (Lee et al., 2005). Vogel et al. (2005) have shown that organic components of diesel exhaust and urban dust particles mediate an increase in TNF- α and IL-8 gene expressions in U937 cell line. A 2-fold up-regulation of a pro-inflammatory cytokine IL-1 β was observed in mice lungs after exposure to the ultrafine carbonaceous particles (soot-analogues) for 24 h (Andre et al., 2006).

TNF- α , a common NF- κ B activator (Chan and Aggarwal, 1994), was used in this thesis as a positive control for the NF- κ B-regulated gene expression. As expected, TNF- α significantly up-regulated (up to ~4-fold) the expressions of IL-6 and NF κ BIA genes for all examined time-points (Figure 3-32, Figure 3-33). It has been documented by our group that a sustained up-regulation (~8-fold) of IL-6 and NF κ BIA genes in A-549 cells occurs after treatment with 10 ng/ml TNF- α for 30 min onward (Arenz et al., 2006).

NF κ BIA codes for one of the NF κ B inhibitory proteins, I κ B α . Diesel- and ethylene combustion condensates induced a down-regulation (1.5-2-fold) of NF κ BIA after 2 h and/or 6 h incubation, which was followed by a slight (~1.5-fold) but significant up-regulation after 24 h treatment (Figure 3-33). Similar pattern of NF κ BIA gene expression in response to propane combustion condensate was reported by Arenz et al. (2006). In that study, a down-regulation (~2-fold) of NF κ BIA gene for the incubation time \leq 4 h followed by a slight up-regulation (~1.5-fold) for later exposure times (24 h) was observed in A-549 cells treated with a propane combustion condensate (C/O=0.85), at concentrations that allowed 60% cell survival.

As already mentioned, a 24 h treatment with ethylene combustion condensate obtained at C/O=0.93 induced an up-regulation of both IL-6 and NF κ BIA genes (Figure 3-32, Figure 3-33). When NF κ BIA is up-regulated, the “negative feedback loop” is activated, which should terminate the NF- κ B response by an increased cytoplasmic binding of NF- κ B by I κ B α (Han et al., 1999). However, continuous presence of a certain NF- κ B inducing agent can lead to an “auto-activating loop” as the NF- κ B-induced up-regulation of pro-inflammatory cytokines acts itself as a positive feedback on NF- κ B activation (Ali and Mann, 2004). Therefore, for future

research in this field it would be interesting to analyse the NF- κ B-dependant gene expressions for later time-points (> 24 h) and to investigate whether the activation of NF κ BIA-mediated negative feedback loop attenuates the NF- κ B-induced inflammatory response in A-549 or not. Thereby, gene expression profiles of other inflammatory markers could also be taken into account.

4.3.3 Anti-apoptotic role of NF- κ B in the U-937 cell line treated with ethylene combustion condensate

One of the aims in this research was to analyse the interactions between the activation of NF- κ B pathway and apoptosis induction in cells treated with combustion condensates. Thereby, the goal was to elucidate whether the activation of NF- κ B signalling pathway is related to pro- or anti-apoptotic effects.

Co-treatment with ethylene combustion condensate (4.8 ppm of TOC) and the NF- κ B inhibitor Bay 11-7082 drastically increases the number of apoptotic cells in U-937 culture, compared to the cell culture treated only with combustion condensate (Figure 3-31). The result reveals the anti-apoptotic role of NF- κ B in U-937 cells treated with ethylene combustion condensate. This finding is in line with other published reports. Inhibition of NF- κ B binding activity has been reported to result in diesel exhaust particle-induced apoptotic response in alveolar macrophages (Kafoury and Madden, 2005).

Besides a positive, pro-survival effect, the observed NF- κ B-mediated suppression of apoptosis could also indicate a tumour-promoting effect of combustion condensates. Survival of cells with genetic abnormalities (e.g. increased level of mutations) can lead to cancerogenesis (Ames, 1973). Activation of NF- κ B has been implicated in chemical carcinogenesis and tumourigenesis (Kim et al., 2000). Also, the link between combustion-related air pollution and increased lung cancer mortality has already been documented (Pope et al., 2002; Garshick et al., 2004).

According to the results concerning NF- κ B activation and induction of apoptosis in U-937 cells, the following mechanism of the toxicity of ethylene combustion condensates can be hypothesised: lower doses of ethylene combustion condensate (≤ 4.8 ppm of TOC) activate NF- κ B signalling pathway which suppresses the induction of apoptosis; higher doses (> 4.8 ppm of TOC) induce apoptosis either via direct cytotoxic effects on the cells, or by inhibiting a pro-survival NF- κ B pathway.

4.4 Outlook

Results shown here have demonstrated that soot particles (≥ 10 nm) have no significant role in the observed detrimental effects of combustion condensates. Also, it was shown that the toxic component(s) of combustion condensates can pass through 20 nm-pored filter. This implies that combustion by-products such as nanoparticles (< 10 nm) and/or water soluble gases (e.g. formaldehyde) might have a decisive role in toxicity of combustion condensates. Still, in order to be able to elucidate which constituent(s) of the combustion condensates could be responsible for the observed toxic effects, a thorough quantitative chemical analysis (high performance liquid chromatography, gas chromatography combined with mass spectrometry) of the combustion condensates would be necessary. Size exclusion chromatography (SEC) is a method which is applied for the separation and characterisation (determination of molecular weight) of different carbonaceous combustion products, such as PAHs, nanoparticles and soot (Apicella et al., 2006). Fractionation of combustion condensates via SEC would allow testing of the toxic potency of these combustion products separately. Unfortunately, the commonly applied eluent (N-methyl-2-pyrrolidinone) for SEC proved to be very toxic in the SWITCH test already at low concentrations such as 2% v/v (data not shown). Accordingly, this method as such cannot be used in biological applications without further improvements.

Gene-expression analysis, performed on lung epithelial A-549 cell line treated for 24 h with ethylene combustion condensate (generated at C/O=0.93), revealed a slight but significant up-regulation of IL-6 cytokine, indicating a mild pro-inflammatory effect. Such finding should be verified in animal studies by analysing bronchoalveolar lavage fluids for the presence of polymorphonuclear leukocytes (marker of inflammation) and for the level of pro-inflammatory cytokines.

5 Summary

Combustion exhausts emitted from traffic and industry sources represent the main contributors to air pollution in urban areas, and as such they have been associated with increased mortality and cardiorespiratory morbidity. Despite intense research, the mechanism of these correlations is still not fully understood. Most of the studies published so far have focused their research on only soot particles or their surrogates (e.g. carbon black), thereby neglecting other combustion by-products present in exhausts. The “cool trap” method, applied in this work, collects particulate and gaseous components of the combustion exhaust. Utilisation of such heterogeneous mixtures can give a better insight in the toxicity of combustion exhausts.

The main aim of this work was to study the toxicity of combustion condensates on human alveolar (A-549) and human monocyte-like (U-937) cell lines. The combustion condensates originated from premixed ethylene/oxygen laboratory flames or from diesel fuel combustion. Pre-screening of toxicity was performed by using bacterial SWITCH test which utilises the recombinant *S. typhimurium* TA1535 pSWITCH strain.

Physical characterisation of the combustion condensates, performed via HRTEM and spectrophotometry, has verified the presence of combustion generated particles: soot and nanoparticles. Total organic carbon (TOC) analysis revealed that TOC content of combustion condensates depends on combustion conditions (C/O ratio, engine operating mode) during sample generation. TOC content proved to be a suitable dose measure for the toxicity assessment of combustion condensates.

Combustion condensates’ toxic effects (genotoxic and cytotoxic) were observed with the SWITCH test. Thereby, ethylene combustion condensates generated at different combustion conditions (C/O ratios ranging from 0.63 to 0.93) and diesel combustion condensates (generated during 4kW-load or no-load engine operating modes) induced 50% cell death (LC_{50}) and maximum genotoxic effect in the concentration range between 19 to 46 ppm of TOC.

TOC content-dependant toxicity of combustion condensates was demonstrated on both human cell lines by using various assays (crystal violet staining, Annexin V-PE/7-AAD, Active caspase-3). Ethylene combustion condensate (generated at C/O=0.93) had a comparable detrimental effect on A-549 and U-937 cell growth

(LC₅₀=5-7). While U-937 cells died predominately via apoptosis, no apoptosis induction was observed in A-549 cells.

The NF-κB activation in U-937 was clearly observed after 24 h incubation with ethylene combustion condensates containing up to 4.8 ppm of TOC. At concentrations higher than 4.8 ppm of TOC, the level of NF-κB activation decreased rapidly down to or below the basal level of the NF-κB activation in untreated cells. Although the anti-apoptotic activity of NF-κB was clearly evidenced in this work, it can only be speculated whether the observed decrease in NF-κB activity is a cause or a consequence of the apoptosis induction in this dose range.

The NF-κB activation in A-549 was investigated via expressions of two NF-κB target genes: IL-6 and NFκBIA. Short-term exposure (2 h and 6 h) to ethylene- or diesel combustion condensates had no impact on the IL-6 gene expression. Longer incubation (24 h) with ethylene combustion condensate (generated at C/O=0.93) increased the level of IL-6 and NFκBIA mRNA slightly but significantly, indicating NF-κB activation and a mild pro-inflammatory effect.

Data presented here clearly show that the toxicity of combustion condensates is directly proportional to their TOC content and that it is not soot-mediated. Moreover, they show that toxicologically relevant constituent(s) of combustion condensates can neither be retained with a 20 nm pore-sized filter nor precipitated by 14 h centrifugation at 116 000 x g.

6 Appendix

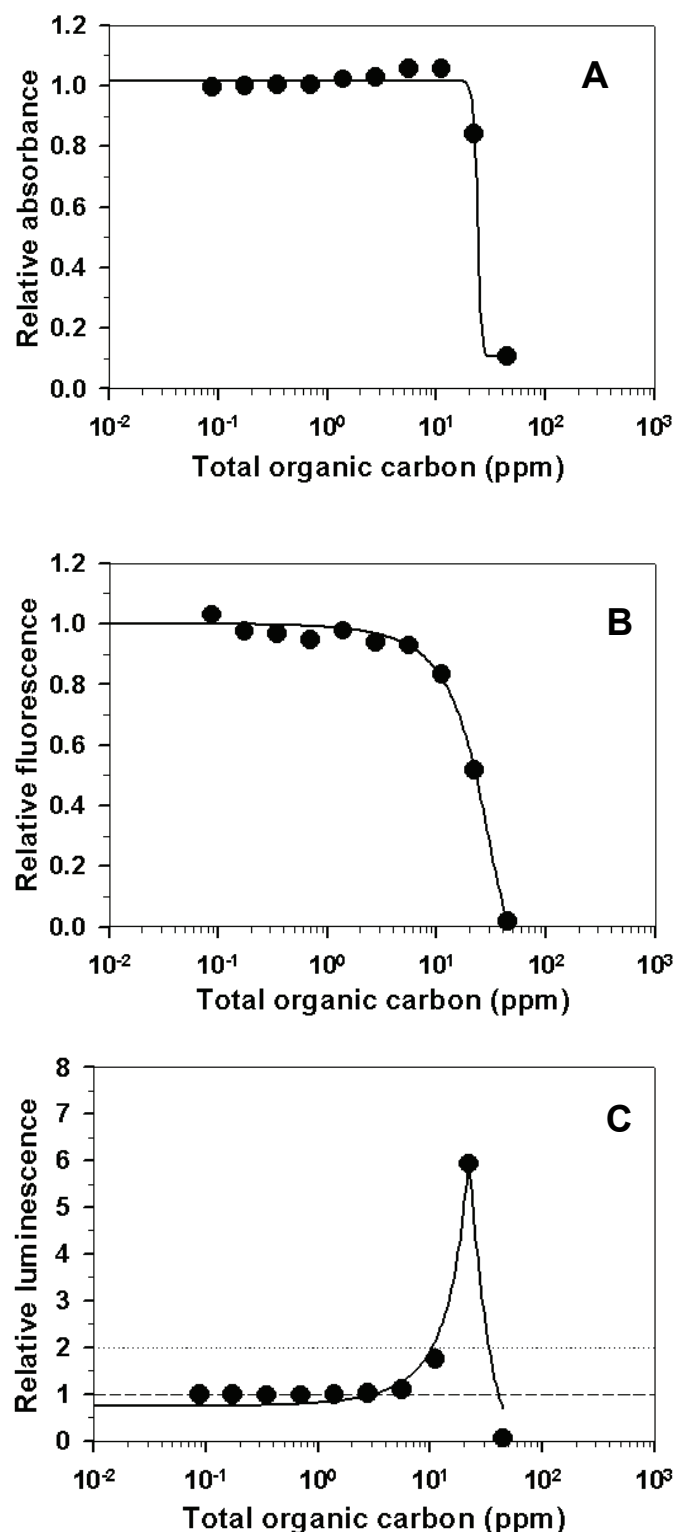


Figure 6-1: Toxicity of ethylene combustion condensate generated at C/O=0.63

Toxicity of ethylene combustion condensates was assessed with SWITCH test. Dashed line (relative luminescence = 1) reflects the relative luminescence of the untreated culture. Dotted line (relative luminescence = 2) represents the threshold for defining genotoxicity.

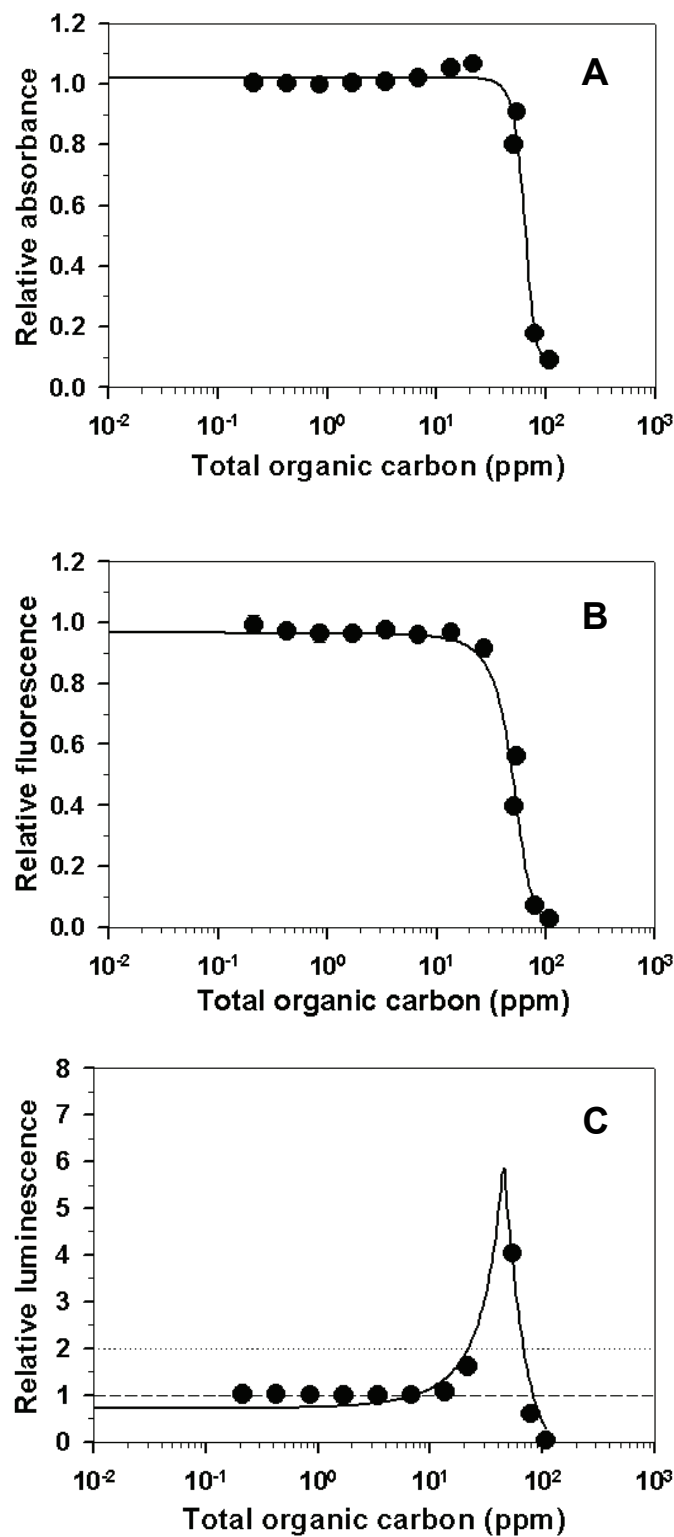


Figure 6-2: Toxicity of ethylene combustion condensate generated at C/O=0.68

Toxicity of ethylene combustion condensates was assessed with SWITCH test. Dashed line (relative luminescence = 1) reflects the relative luminescence of the untreated culture. Dotted line (relative luminescence = 2) represents the threshold for defining genotoxicity.

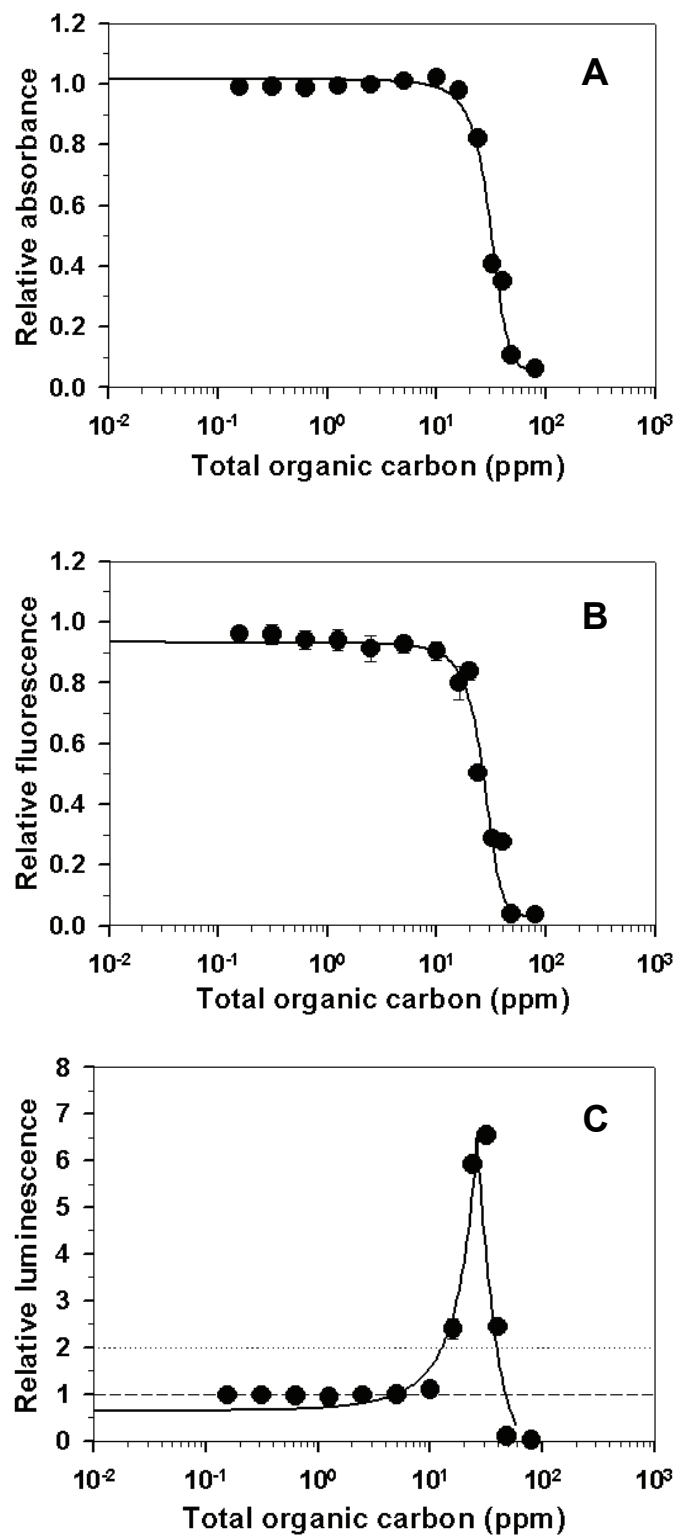


Figure 6-3: Toxicity of ethylene combustion condensate generated at C/O=0.73

Toxicity of ethylene combustion condensates was assessed with SWITCH test. Dashed line (relative luminescence = 1) reflects the relative luminescence of the untreated culture. Dotted line (relative luminescence = 2) represents the threshold for defining genotoxicity.

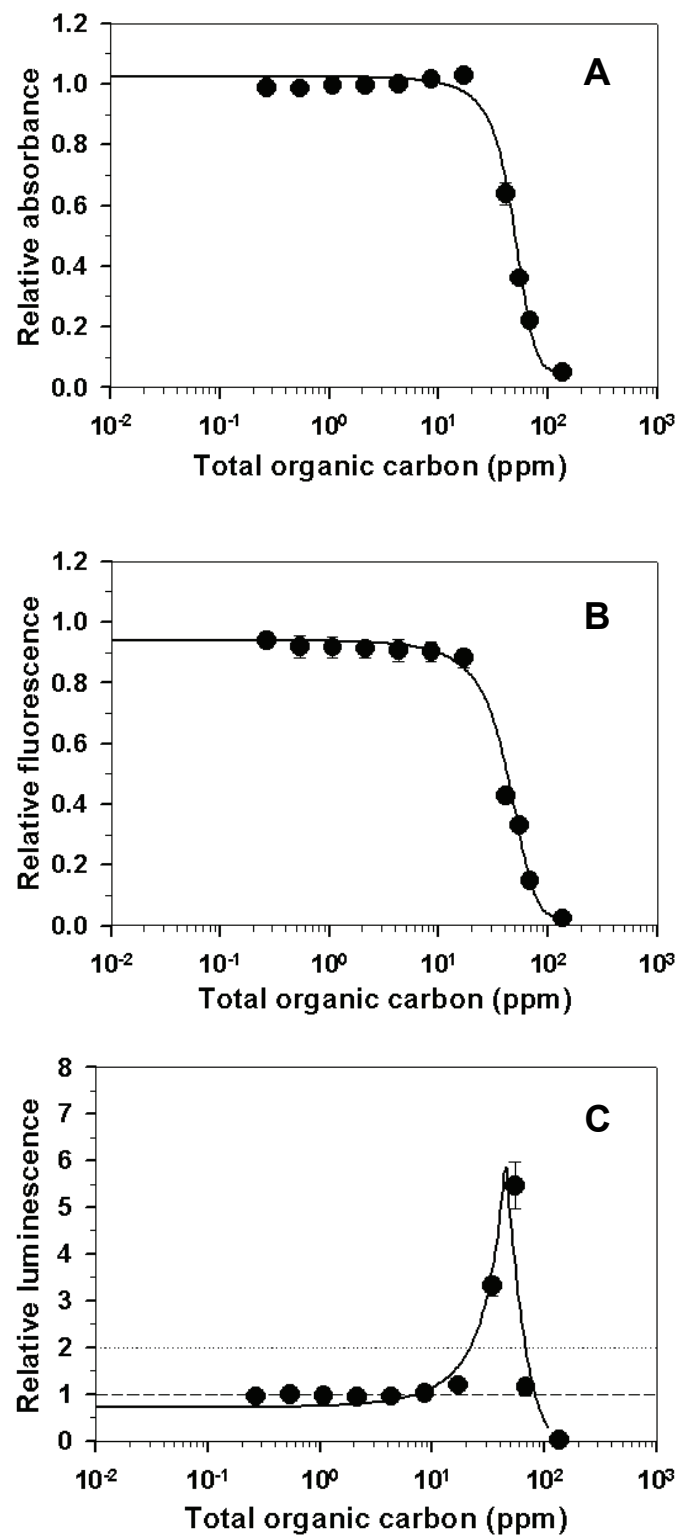


Figure 6-4: Toxicity of ethylene combustion condensate generated at C/O=0.78

Toxicity of ethylene combustion condensates was assessed with SWITCH test. Dashed line (relative luminescence = 1) reflects the relative luminescence of the untreated culture. Dotted line (relative luminescence = 2) represents the threshold for defining genotoxicity.

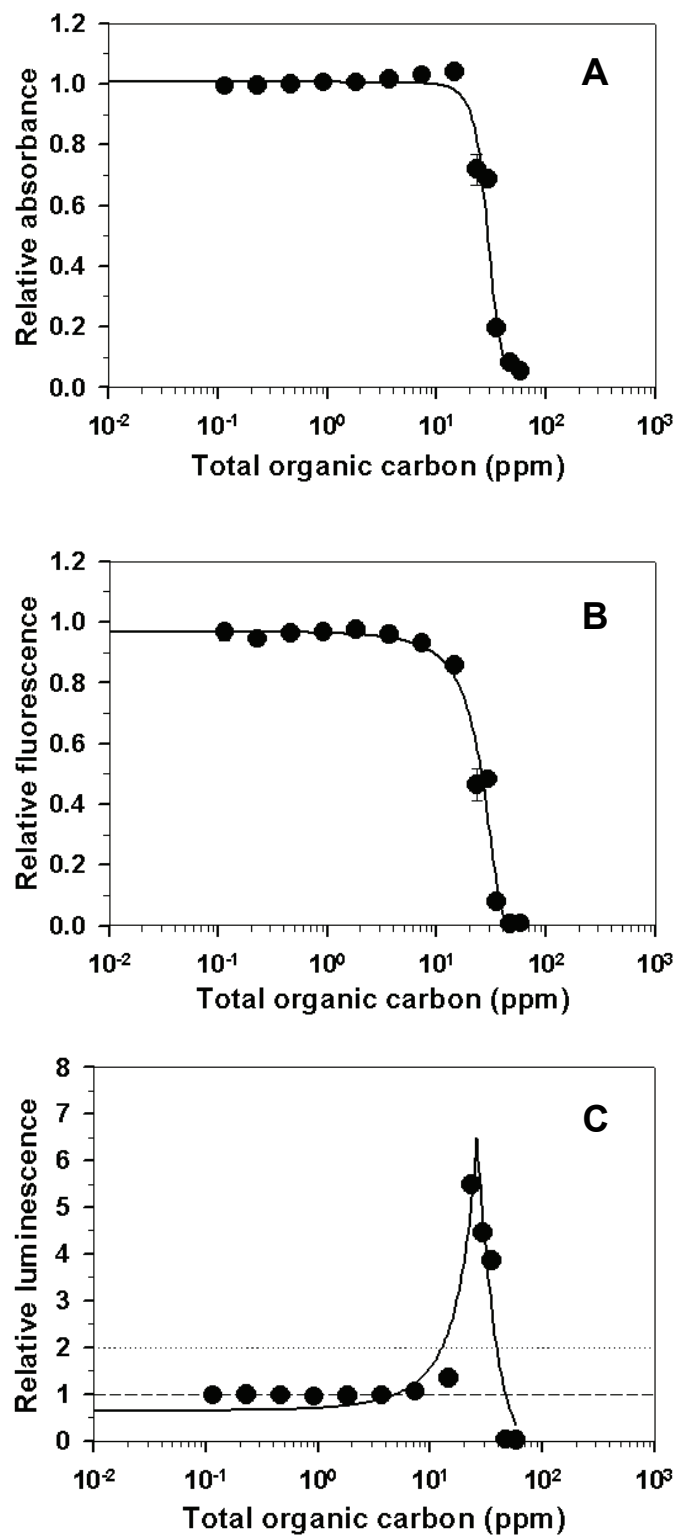


Figure 6-5: Toxicity of ethylene combustion condensate generated at C/O=0.83

Toxicity of ethylene combustion condensates was assessed with SWITCH test. Dashed line (relative luminescence = 1) reflects the relative luminescence of the untreated culture. Dotted line (relative luminescence = 2) represents the threshold for defining genotoxicity.

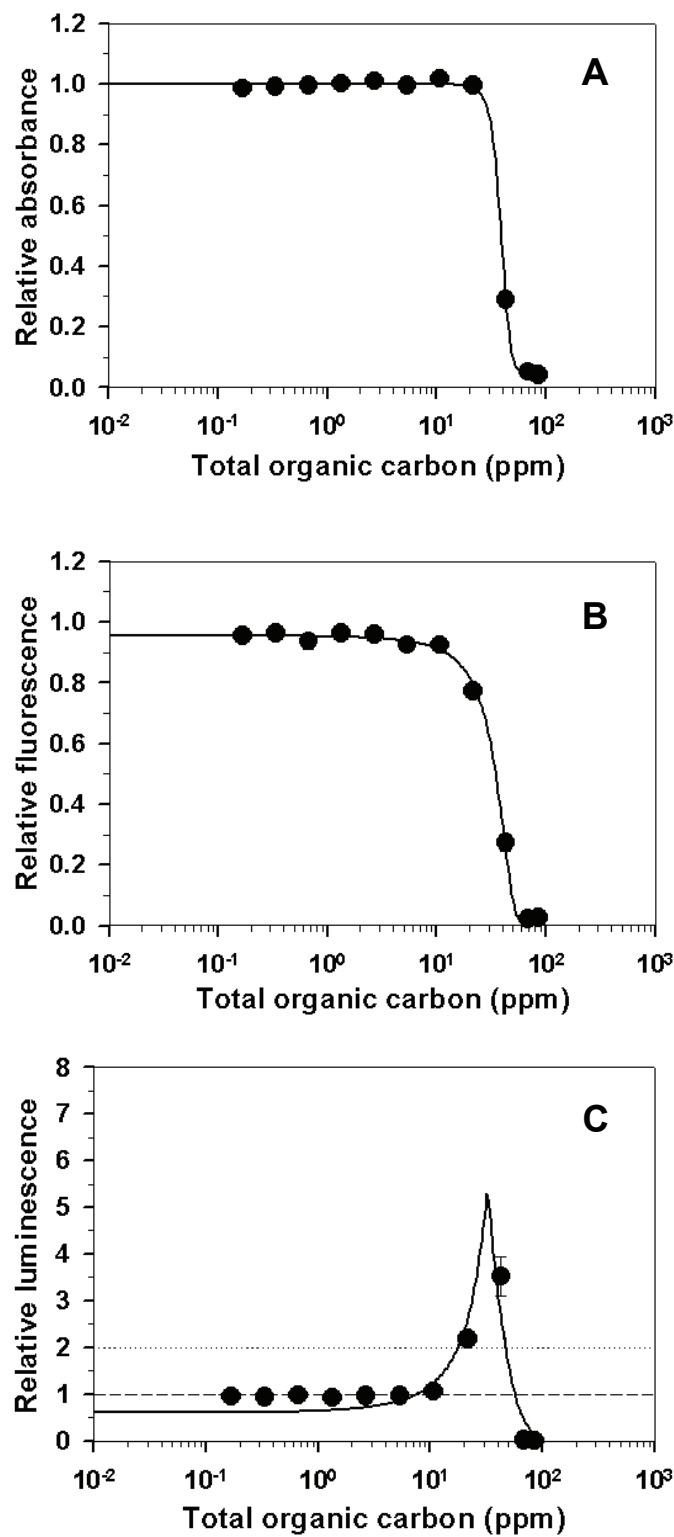


Figure 6-6: Toxicity of ethylene combustion condensate generated at C/O=0.88

Toxicity of ethylene combustion condensates was assessed with SWITCH test. Dashed line (relative luminescence = 1) reflects the relative luminescence of the untreated culture. Dotted line (relative luminescence = 2) represents the threshold for defining genotoxicity.

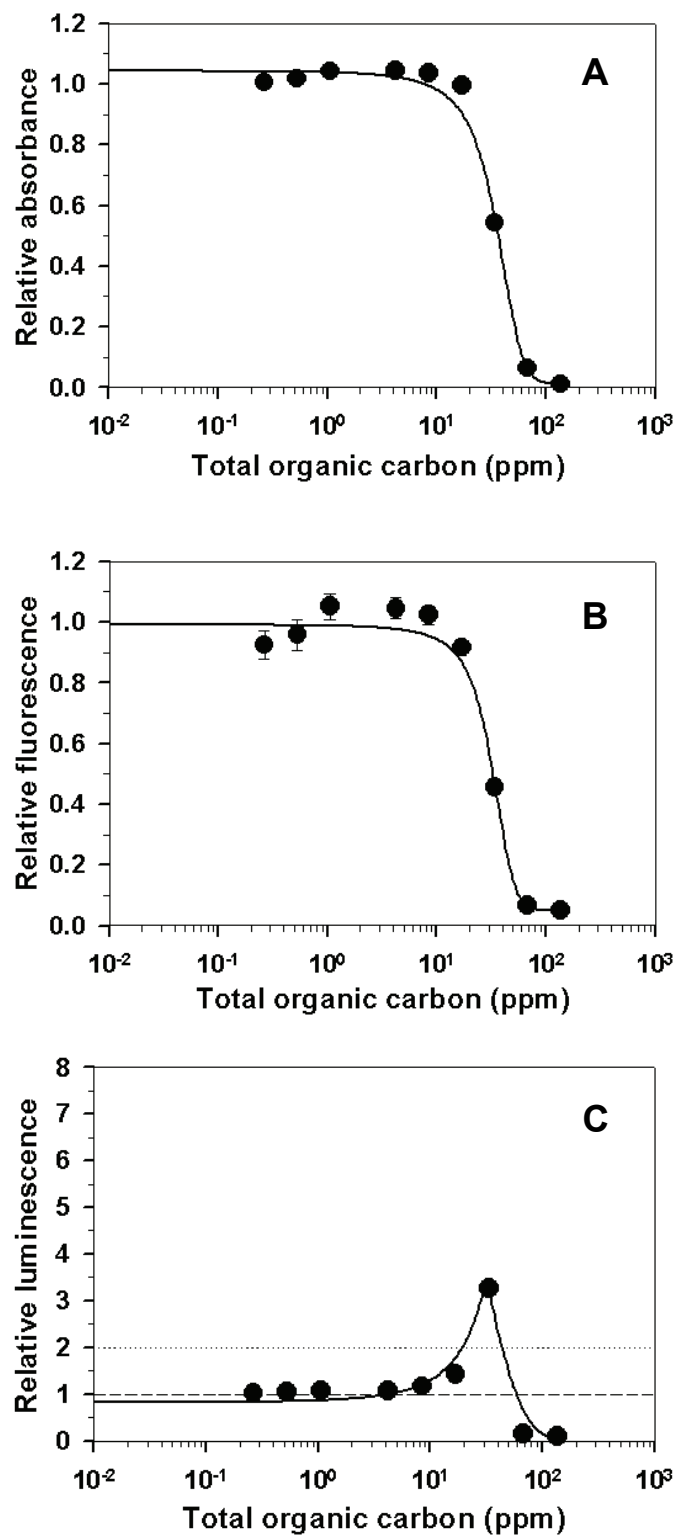


Figure 6-7: Toxicity of ethylene combustion condensate generated at C/O=0.93

Toxicity of ethylene combustion condensates was assessed with SWITCH test. Dashed line (relative luminescence = 1) reflects the relative luminescence of the untreated culture. Dotted line (relative luminescence = 2) represents the threshold for defining genotoxicity.

7 References

- Ahn, K. S., and Aggarwal, B. B.** (2005). Transcription factor NF- κ B: a sensor for smoke and stress signals. *Ann N Y Acad Sci* 1056: 218–233.
- Ali, S., and Mann D. A.** (2004). Signal transduction via the NF- κ B pathway: a targeted treatment modality for infection, inflammation and repair. *Cell Biochem Funct* 22: 67-79.
- Ames, B. N.** (1973). Carcinogens are mutagens: their detection and classification. *Environ Health Perspect* 6: 115-118.
- Ames, B. N., Lee, F. D., and Durston, W. E.** (1973). An improved bacterial test system for the detection and classification of mutagens and carcinogens. *Proc Natl Acad Sci USA* 70: 782–786.
- Andre, E., Stoeger, T., Takenaka, S., Bahnweg, M., Ritter, B., Karg, E., Lentner, B., Reinhard, C., Schulz, H., and Wjst, M.** (2006). Inhalation of ultrafine carbon particles triggers biphasic pro-inflammatory response in the mouse lung. *Eur Respir J* 28: 275-285.
- Anto, R. J., Mukhopadhyay, A., Shishodia, S., Gairola, C. G., and Aggarwal, B. B.** (2002). Cigarette smoke condensate activates nuclear transcription factor- κ B through phosphorylation and degradation of I κ B α : correlation with induction of cyclooxygenase-2. *Carcinogenesis* 23 (9): 1511-1518.
- Apicella, B., Millan, M., Herod, A. A., Carpentieri, A., Pucci, P., and Ciajolo, A.** (2006). Separation and measurement of flame-formed high molecular weight polycyclic aromatic hydrocarbons by size-exclusion chromatography and laser desorption/ionization time-of-flight mass spectrometry. *Rapid Commun Mass Spectrom* 20: 1104–1108.
- Arenz, A., Hellweg, C. E., Stojicic, N., Baumstark-Khan, C., and Grotheer, H.-H.** (2006). Gene expression modulation in A549 human lung cells in response to combustion-generated nano-sized particles. *Ann N Y Acad Sci* 1091: 170-183.
- Arenz, A., Stojicic, N., Lau, P., Hellweg, C. E., and Baumstark-Khan, C.** (2007). Suitability of commonly used housekeeping genes in gene expression studies for space radiation research. *Adv Space Res* 39: 1050-1055.
- Baeza-Squiban, A., Bonvallot, V., Boland, S., and Marano F.** (1999). Diesel exhaust particles increase NF- κ B DNA binding activity and c-fos proto-oncogene expression in human bronchial epithelial cells. *Toxicol In Vitro* 13: 817-822.
- Barnes, P. J., and Adcock, I. M.** (1998). Transcription factors and asthma. *Eur Respir J* 12: 221-234.
- Baumstark-Khan, C., Cioara, K., Rettberg, P., and Horneck, G.** (2005). Determination of geno- and cytotoxicity of groundwater and sediments using the recombinant SWITCH test. *J Environ Sci Health A* 40: 245-263.

- Baumstark-Khan, C., Palm, M., Wehner, J., Okabe, M., Ikawa, M., and Horneck, G.** (1999). Green fluorescent protein (GFP) as a marker for cell viability after UV irradiation. *J Fluoresc* 9 (1): 37-43.
- Baumstark-Khan, C., Rode, A., Rettberg, P., and Horneck, G.** (2001). Application of the Lux-Fluoro test as bioassay for combined genotoxicity and cytotoxicity measurements by means of recombinant *Salmonella typhimurium* TA1535 cells. *Anal Chim Acta* 437: 23-30.
- Bell, M. L., Dominici, F., Ebisu, K., Zeger, S. L., and Samet, J. M.** (2007). Spatial and temporal variation in PM_{2.5} chemical composition in the United States for health effects studies. *Environ Health Perspect* 115 (7): 989-995.
- Borm, P. J. A., Robbins, D., Haubold, S., Kuhlbusch, T., Fissan, H., Donaldson, K., Schins, R., Stone, V., Kreyling, W., Lademann, J., Krutmann, J., Warheit, D., and Oberdörster, E.** (2006). The potential risks of nanomaterials: a review carried out for ECETOC. *Part Fibre Toxicol* 3: 11-45.
- Brown, D. M., Donaldson, K., Borm, P. J., Schins, R. P., Dehnhardt, M., Gilmour, P., Jimenez, L. A., and Stone, V.** (2004). Calcium and ROS-mediated activation of transcription factors and TNF- α cytokine gene expression in macrophages exposed to ultrafine particles. *Am J Physiol Lung Cell Mol Physiol* 286: 344-353.
- Bünger, J., Krahl, J., Weigel, A., Schröder, O., Brüning, T., Müller, M., Hallier, E., and Westphal, G.** (2006). Influence of fuel properties, nitrogen oxides, and exhaust treatment by an oxidation catalytic converter on the mutagenicity of diesel engine emissions. *Arch Toxicol* 80: 540-546.
- Bustin, S. A.** (2000). Absolute quantification of mRNA using real-time reverse transcription polymerase chain reaction assays. *J Mol Endocrinol* 25: 169-193.
- Casillas, A. M., Hiura, T., Li, N., and Nel, A. E.** (1999). Enhancement of allergic inflammation by diesel exhaust particles: permissive role of reactive oxygen species. *Ann Allergy Asthma Immunol* 83: 624-629.
- Cass, G. R.** (1998). Organic molecular tracers for particulate air pollution sources. *Trends Anal Chem* 17 (6): 356-365.
- Chalfie, M., Tu, T., Euskirchen, G., Ward, W. W., and Prasher, D. C.** (1994). Green fluorescent protein as a marker for gene expression. *Science* 263 (5148): 802-805.
- Chan, H., and Aggarwal B. B.** (1994). Role of tumour necrosis factor receptors in the activation of nuclear factor κ B in human histiocytic lymphoma U-937 cells. *J Biol Chem* 269 (50): 31424-31429.
- Choho, K., Langenaeker, W., van de Woude, G., and Geerlings, P.** (1995). Reactivity of fullerenes. Quantum-chemical descriptors versus curvature. *J Mol Struct* 338: 293-301.
- Christman, J. W., Sadikot, R. T., and Blackwell, T. S.** (2000). The role of nuclear factor- κ B in pulmonary diseases. *Chest* 117: 1482-1487.

- Chuang, K. J., Chan, C. C., Su, T. C., Lin, L. Y., and Lee, C. T.** (2007). Associations between particulate sulphate and organic carbon exposures and heart rate variability in patients with or at risk for cardiovascular diseases. *J Occup Environ Med* 49 (6): 610-617.
- Commodo, M., Violi, S., D'Anna, A., D'Alessio, A., Allouis, C., Beretta, F., and Minutolo, P.** (2007). Soot and nanoparticle formation in laminar and turbulent flames. *Combust Sci Technol* 179: 387-400.
- Cormier, S. A., Lomnicki, S., Backes, W., and Dellinger, B.** (2006). Origin and health impacts of emissions of toxic by-products and fine particles from combustion and thermal treatment of hazardous wastes and materials. *Environ Health Perspect* 114 (6): 810-817.
- Cyrys, J., Stölzel, M., Heinrich, J., Kreyling, W. G., Menzel, N., Wittmaack, K., Tuch, T., and Wichmann H.-E.** (2003). Elemental composition and sources of fine and ultrafine ambient particles in Erfurt, Germany. *Sci Total Environ* 305: 143-156.
- D'Alessio, A., D'Anna, A., Gambi, G., and Minutolo, P.** (1998). The spectroscopic characterisation of UV absorbing nanoparticles in fuel rich soot forming flames. *J Aerosol Sci* 29: 397-409.
- D'Anna, A., Rolando, A., Allouis, C., Minutolo, P., and D'Alessio, A.** (2005). Nano-organic carbon and soot particle measurements in a laminar ethylene diffusion flame. *P Combust Inst* 30: 1449-1456.
- Dai, Y., Rahmani, M., Dent, P., and Grant, S.** (2005). Blockade of histone deacetylase inhibitor-induced RelA/p65 acetylation and NF- κ B activation potentiates apoptosis in leukemia cells through a process mediated by oxidative damage, XIAP downregulation, and c-Jun N-terminal kinase 1 activation. *Mol Cell Biol* 25 (13): 5429-5444.
- Davis, M. E., Blicharz, A. P., Hart, J. E., Laden, F., Garshick, E., and Smith, T. J.** (2007). Occupational exposure to volatile organic compounds and aldehydes in the U.S. trucking industry. *Environ Sci Technol* 41 (20): 7152-7158.
- Dockery, D. W., Pope, C. A. 3rd, Xu, X., Spengler, J. D., Ware, J. H., Fay, M. E., Ferris, B. G., and Speizer, F. E.** (1993). An association between air pollution and mortality in six U. S. cities. *N Engl J Med* 329 (24): 1753-1759.
- Donaldson, K., and Stone, V.** (2003). Current hypothesis on the mechanisms of toxicity of ultrafine particles. *Ann Ist Super Sanita* 39 (3): 405-410.
- Donaldson, K., Tran, L., Jimenez, L. A., Duffin, R., Newby, D. E., Mills, N., MacNee, W., and Stone, V.** (2005). Combustion-derived nanoparticles: a review of their toxicology following inhalation exposure. *Part Fibre Toxicol* 2: 10-23.
- Dybdahl, M., Risom, L., Bornholdt, J., Autrup, H., Loft, S., and Wallin, H.** (2004). Inflammatory and genotoxic effects of diesel particles in vitro and in vivo. *Mutat Res* 562: 119-131.

- Foxwell, B., Browne, K., Bondeson, J., Clarke, C., de Martin, R., Brennan, F., and Feldmann, M.** (1998). Efficient adenoviral infection with I κ B- α reveals that macrophage tumor necrosis factor α production in rheumatoid arthritis is NF- κ B dependent. Proc Natl Acad Sci USA 95: 8211-8215.
- Gao, Y., Lecker, S., Post, M. J., Hietaranta, A. J., Li, J., Volk, R., Li, M., Sato, K., Saluja, A. K., Steer, M. L., Goldberg, A. L., and Simons, M.** (2000). Inhibition of ubiquitin-proteasome pathway-mediated I κ B α degradation by a naturally occurring antibacterial peptide. J Clin Invest 106 (3): 439-448.
- Garshick, E., Laden, F., Hart, J. E., Rosner, B., Smith, T. J., Dockery, D. W., and Speizer, F. E.** (2004). Lung cancer in railroad workers exposed to diesel exhaust. Environ Health Perspect 112 (15): 1539-1543.
- Geiser, M., Rothen-Rutishauser, B., Kapp, N., Schürch, S., Kreyling, W., Schulz, H., Semmler, M., Im Hof, V., Heyder, J., and Gehr, P.** (2005). Ultrafine particles cross cellular membranes by nonphagocytic mechanisms in lungs and in cultured cells. Environ Health Perspect 113 (11): 1555-1560.
- Gillies, R. J., Didier, N., and Denton, M.** (1986). Determination of cell number in monolayer cultures. Anal Biochem 159: 109-113.
- Grotheer, H.-H., Pokorny, H., Barth, K.-L., Thierley, M. and Aigner, M.** (2004). Mass spectrometry up to 1 million mass units for the simultaneous detection of primary soot and of soot precursors (nanoparticles) in flames. Chemosphere 57: 1335-1342.
- Grotheer, H.-H., Pokorny, H., Happold, J., Gonzalez Baquet, T., Thierley, M., Aigner, M., Baumstark-Khan, C., Hellweg, C. E., and Arenz, A.** (2007). On combustion generated particles and their biological effects. Part I: Measurement of nanoparticles and their detection in and behind flames. Curr Nanosci 3: 199-205.
- Han, Y., Meng, T., Murray, N. R., Fields, A. P., and Brasier, A. R.** (1999). Interleukin-1-induced nuclear factor- κ B-I κ B α autoregulatory feedback loop in hepatocytes. A role for protein kinase C α in post-transcriptional regulation of I κ B α resynthesis. J Biol Chem 274 (2): 939-947.
- Harrison, R. M.** (2004). Key pollutants-airborne particles. Sci Total Environ 334-335: 3-8.
- Hellweg, C. E., Baumstark-Khan, C., and Horneck, G.** (2001). Enhanced green fluorescent protein as a reporter protein for biomonitoring of cytotoxic effects in mammalian cells. Anal Chim Acta 427: 191-199.
- Hellweg, C. E., Baumstark-Khan, C., and Horneck, G.** (2003). Generation of stably transfected mammalian cell lines as fluorescent screening assay for NF- κ B activation-dependent gene expression. J Biomol Screen 8 (5): 511-521.
- Higuchi, R., Fockler, C., Dollinger, G., and Watson, R.** (1993). Kinetic PCR analysis: real-time monitoring of DNA amplification reactions. Biotechnology 11: 1026-1030.

- Janssens, S., and Tschopp, J.** (2006). Signals from within: the DNA-damage-induced NF- κ B response. *Cell Death Differ* 13 (5): 773-784.
- Kafoury, R. M., and Madden, M. C.** (2005). Diesel exhaust particles induce the over expression of tumor necrosis factor-alpha (TNF-alpha) gene in alveolar macrophages and failed to induce apoptosis through activation of nuclear factor-kappaB (NF- κ B). *Int J Environ Res Public Health* 2 (1): 107-113.
- Karin, M., and Ben-Neriah, Y.** (2000). Phosphorylation meets ubiquitination: the control of NF- κ B activity. *Annu Rev Immunol* 18: 621-663.
- Kerr, J. F. R., Wyllie, A. H., and Currie, A. R.** (1972). Apoptosis: a basic biological phenomenon with wide-ranging implications in tissue kinetics. *Br J Cancer* 26: 239-257.
- Kim, D. W., Sovak, M. A., Zanieski, G., Nonet, G., Romieu-Mourez, R., Lau, A. W., Hafer, L. J., Yaswen, P., Stampfer, M., Rogers, A. E., Russo, J., and Sonenshein, G. E.** (2000). Activation of NF- κ B/Rel occurs early during neoplastic transformation of mammary cells. *Carcinogenesis* 21 (5): 871-879.
- Kreyling, W. G., Semmler, M., Erbe, F., Mayer, P., Takenaka, S., Schulz, H., Oberdörster, G., and Ziesenis, A.** (2002). Translocation of ultrafine insoluble iridium particles from lung epithelium to extrapulmonary organs is size dependent but very low. *J Toxicol Environ Health A* 65 (20): 1513-1530.
- Kuhlbusch, T. A. J., John, A. C., Fissan, H., Schmidt, K.-G., Schmidt, F., Pfeffer, H.-U., and Gladtke, D.** (1999). PM10 and PM2.5 mass concentration, chemical composition, and size distribution measurements at three different sites in the Ruhr-area, Germany. *J Aerosol Sci* 30: 45-46.
- Lanki, T., de Hartog, J. J., Heinrich, J., Hoek, G., Janssen, N. A. H., Peters, A., Stölzel, M., Timonen, K. L., Vallius, M., Vanninen, E., and Pekkanen, J.** (2006). Can we identify sources of fine particles responsible for exercise-induced ischemia on days with elevated air pollution? The ULTRA study. *Environ Health Perspect* 114 (5): 655-660.
- Lee, C. C., Cheng, Y. W., and Kang, J. J.** (2005). Motorcycle exhaust particles induce IL-8 production through NF- κ B activation in human airway epithelial cells. *J Toxicol Environ Health A* 68 (17-18): 1537-1555.
- Leeuwen, C. J., and Vermeire, T. G.** (2007). Risk assessment of chemicals-an introduction. 2nd edition. Springer. Berlin, Germany.
- Leist, M., and Jäättelä, M.** (2001). Four deaths and a funeral: from caspases to alternative mechanisms. *Nat Rev Mol Cell Biol* 2: 589-598.
- Li, N., Sioutas, C., Cho, A., Schmitz, D., Misra, C., Sempf, J., Wang, M., Oberley, T., Froines, J., and Nel, A.** (2003). Ultrafine particulate pollutants induce oxidative stress and mitochondrial damage. *Environ Health Perspect* 111 (4): 455-460.

- Li, N., Venkatesan, M. I., Miguel, A., Kaplan, R., Gujuluva, C., Alam, J., and Nel., A.** (2000). Induction of heme oxygenase-1 expression in macrophages by diesel exhaust particle chemicals and quinones via the antioxidant-responsive element. *J Immunol* 165: 3393-3401.
- Li, X. C., Miyasaka, M., and Issekutz, T. B.** (1998). Blood monocyte migration to acute lung inflammation involves both CD11/CD18 and Very Late Activation Antigen-4-dependent and independent pathways. *J Immunol* 161: 6258-6264.
- Lieber, M., Smith, B., Szakal, A., Nelson-Rees, W., and Todaro, G.** (1976). A continuous tumour-cell line from a human lung carcinoma with properties of type II alveolar epithelial cells. *Int J Cancer* 17 (1): 62-70.
- Lippmann, M., Frampton, M., Schwarz, J., Dockery, D., Schlesinger, R., Koutrakis, P., Froines, J., Nel, A., Finkelstein, J., Godleski, J., Kaufman, J., Koenig, J., Larson, T., Luchtel, D., Liu, L.-J. S., Oberdörster, G., Peters, A., Sarnat, J., Sioutas, C., Suh, H., Sullivan, J., Utell, M., Wichmann, E., and Zelikoff, J.** (2003). The U. S. Environmental Protection Agency particulate matter health effects research centers program: a midcourse report of status, progress and plans. *Environ Health Perspect* 111: 1074-1092.
- Liu, Z. G., Hsu, H., Goeddel, D. V., and Karin, M.** (1996). Dissection of TNF receptor 1 effector functions: JNK activation is not linked to apoptosis while NF-kappaB activation prevents cell death. *Cell* 87 (3): 565–576.
- Martin, S. J., O'Brien, G. A., Nishioka, W. K., McGahon, A. J., Mahboubi, A., Saido, T. C., and Green, D. R.** (1995). Proteolysis of fodrin (non-erythroid spectrin) during apoptosis. *J Biol Chem* 270 (12): 6425-6428.
- Mason, R. J., Dobbs, L. G., Greenleaf, R. D., and Williams, M. C.** (1977). Alveolar type II cells. *Fed Proc* 36 (13): 2697-2702.
- Matsuo, M., Shimada, T., Uenishi, R., Sasaki, N., and Sagai, M.** (2003). Diesel exhaust particle-induced cell death of cultured normal human bronchial epithelial cells. *Biol Pharm Bull* 26 (4): 438-447.
- Merola, S. S., Gambi, G., Allouis, C., Beretta, F., Borghese, A., and D'Alessio, A.** (2001). Analysis of exhausts emitted by i.c. engines and stationary burners, by means of u.v. extinction and fluorescence spectroscopy. *Chemosphere* 42: 827-834.
- Minutolo, P., Gambi, G., D'Alessio, A., and Carlucci, S.** (1999). Spectroscopic characterisation of carbonaceous nanoparticles in premixed flames. *Atmos Environ* 33: 2725-2732.
- Mossmann, T.** (1983). Rapid colorimetric assay for cellular growth and survival: application to proliferation and cytotoxicity assays. *J Immunol Methods* 65: 55-63.
- Müller, J.-O., Su, D. S., Jentoft, R. E., Kröhnert, J., Jentoft, F. C., and Schlögl, R.** (2005). Morphology-controlled reactivity of carbonaceous materials towards oxidation. *Catal Today* 102-103: 259–265.

- Nemmar, A., Hoet, P. H. M., Vanquickenborne, B., Dinsdale, D., Thomeer, M., Hoylaerts, M. F., Vanbilloen, H., Mortelmans, L., and Nemery, B.** (2002). Passage of inhaled particles into the blood circulation in humans. *Circulation* 105: 411-414.
- Nemmar, A., Vanbilloen, H., Hoylaerts, M. F., Hoet, P. H. M., Verbruggen, A., and Nemery, B.** (2001). Passage of intratracheally instilled ultrafine particles from the lung into the systemic circulation in hamster. *Am J Respir Crit Care Med* 164: 1665-1668.
- Nicotera, P., Leist, M., and Ferrando-May, E.** (1998). Intracellular ATP, a switch in the decision between apoptosis and necrosis. *Toxicol Lett* 102-103: 139-142.
- Oberdörster, G.** (2000). Toxicology of ultrafine particles: in vivo studies. *Phil Trans R Soc A* 358 (1775): 2719-2740.
- Oberdörster, G.** (2001). Pulmonary effects of inhaled ultrafine particles. *Int Arch Occup Environ Health* 74 (1):1-8.
- Oberdörster, G., Oberdörster, E., and Oberdörster J.** (2005). Nanotoxicology: an emerging discipline evolving from studies of ultrafine particles. *Environ Health Perspect* 113 (7): 823-839.
- Oberdörster, G., Sharp, Z., Atudorei, V., Elder, A., Gelein, R., Kreyling, W., and Cox, C.** (2004). Translocation of inhaled ultrafine particles to the brain. *Inhal Toxicol* 16 (6-7): 437-445.
- Oberdörster, G., Sharp, Z., Atudorei, V., Elder, A., Gelein, R., Lunts, A., Kreyling, W., and Cox, C.** (2002). Extrapulmonary translocation of ultrafine carbon particles following whole-body inhalation exposure of rats. *J Toxicol Environ Health A* 65 (20): 1531-1543.
- Oda, Y., Nakamura, S., Oki, I., Kato T., and Shinagawa, H.** (1985). Evaluation of the new system (umu-test) for the detection of environmental mutagens and carcinogens. *Mutat Res* 147: 219-229.
- Ormerod, M. G., Payne, A. W., and Watson, J. V.** (1987). Improved programme for the analysis of DNA histograms. *Cytometry* 8 (6): 637-641.
- Pagan, I., Costa, D. L., McGee, J. K., Richards, J. H., and Dye, J. A.** (2003). Metals mimic airway epithelial injury induced by in vitro exposure to Utah Valley ambient particulate matter extracts. *J Toxicol Environ Health A* 66 (12): 1087-1112.
- Pahl, H. L.** (1999). Activators and target genes of Rel/NF-κB transcription factors. *Oncogene* 18: 6853-6866.
- Peters, A., Wichmann, H. E., Tuch, T., Heinrich, J., and Heyder, J.** (1997). Respiratory effects are associated with the number of ultrafine particles. *Am J Respir Crit Care Med* 155 (4): 1376-1383.
- Pfaffl, M. W.** (2001). A new mathematical model for relative quantification in real-time RT-PCR. *Nucleic Acids Res* 29 (9): 2002-2007.

- Pfaffl, M. W., Horgan, G. W., and Dempfle, L.** (2002). Relative expression software tool (REST) for group-wise comparison and statistical analysis of relative expression results in real-time PCR. *Nucleic Acids Res* 30 (9): 2-10.
- Pfaffl, M. W., Tichopad, A., Prgomet, C., and Neuvians, T. P.** (2004). Determination of stable housekeeping genes, differentially regulated target genes and sample integrity: BestKeeper-Excel-based tool using pair-wise correlations. *Biotechnol Lett* 26: 509-515.
- Pierce, J. W., Schoenleber, R., Jesmok, G., Best, J., Moore, S. A., Collins, T., and Gerritsen, M. E.** (1997). Novel inhibitors of cytokine-induced I κ B α phosphorylation and endothelial cell adhesion molecule expression show anti-inflammatory effects in vivo. *J Biol Chem* 272 (34): 21096–21103.
- Pope, C. A. 3rd, Burnett, R. T., Thun, M. J., Calle, E. E., Krewski, D., Ito, K., and Thurston, G. D.** (2002). Lung cancer, cardiopulmonary mortality, and long-term exposure to fine particulate air pollution. *JAMA* 287 (9): 1132-1141.
- Pope, C. A. 3rd, and Dockery, D. W.** (2006). Health effects of fine particulate air pollution: lines that connect. *J Air Waste Manag Assoc* 56 (6): 709-742.
- Pope, C. A. 3rd, Thun, M. J., Namboodiri, M. M., Dockery, D. W., Evans, J. S., Speizer, F. E., and Heath, C. W. Jr.** (1995). Particulate air pollution as a predictor of mortality in a prospective study of U. S. adults. *Am J Respir Crit Care Med* 151: 669-674.
- Ptitsyn, L. R., Horneck, G., Komova, O., Kozubek, S., Krasavin, E. A., Bonev, M., and Rettberg, P.** (1997). A biosensor for environmental genotoxin screening based on an SOS lux assay in recombinant *Escherichia coli* cells. *Appl Environ Microbiol* 63 (11): 4377-4384.
- Quay, J. L., Reed, W., Samet, J., and Devlin, R. B.** (1998). Air pollution particles induce IL-6 gene expression in human airway epithelial cells via NF- κ B activation. *Am J Respir Cell Mol Biol* 19: 98-106.
- Quillardet, P., Huisman, O., Ari, R. D., and Hofnung, M.** (1982). SOS chromotest, a direct assay of induction of an SOS function in *Escherichia coli* K-12 to measure genotoxicity. *Proc Natl Acad Sci* 79: 5971-5975.
- Rabbow, E., Stojicic, N., Walrafen, D., Baumstark-Khan, C., Rettberg, P., Schulze-Varnholt, D., Franz, M., and Reitz, G.** (2006). The SOS-LUX-TOXICITY-Test on the International Space Station. *Res Microbiol* 157: 30-36.
- Rasmussen, R.** (2001). Quantification on the LightCycler. In Meuer, S., Wittwer, C., and Nakagawara, K. (eds). *Rapid cycle real-time PCR, methods and application*. Springer Press. Heidelberg. p. 21-34.
- Ryan, K. M., Ernst, M. K., Rice, N. R., and Vousden, K. H.** (2000). Role of NF- κ B in p53-mediated programmed cell death. *Nature* 404: 892–897.

- Sanders, E. J., and Wride, M. A.** (1995). Programmed cell death in development. *Int Rev Cytol* 163: 105-173.
- Saxena, R. K., Gilmour, M. I., and Hays, M. D.** (2008). Isolation and quantitative estimation of diesel exhaust and carbon black particles ingested by lung epithelial cells and alveolar macrophages in vitro. *Biotechniques* 44: 799-805.
- Schauer, J. J., Kleeman, M. J., Cass, G. R., and Simoneit, B. R. T.** (1999). Measurement of emissions from air pollution sources. 2. C₁ through C₃₀ organic compounds from medium duty diesel trucks. *Environ Sci Technol* 33: 1578-1587.
- Schauer, J. J., Kleeman, M. J., Cass, G. R., and Simoneit, B. R. T.** (2002). Measurement of emissions from air pollution sources. 5. C₁ - C₃₂ organic compounds from gasoline-powered motor vehicles. *Environ Sci Technol* 36: 1169-1180.
- Sgro, L. A., Basile, G., Barone, A. C., D'Anna, A., Minutolo, P., Borghese, A., and D'Alessio, A.** (2003). Detection of combustion formed nanoparticles. *Chemosphere* 51: 1079-1090.
- Sgro, L. A., Minutolo, P., Basile, G., and D'Alessio, A.** (2001). UV-visible spectroscopy of organic carbon particulate sampled from ethylene/air flames. *Chemosphere* 42: 671-680.
- Sillanpää, M., Hillamo, R., Saarikoski, S., Frey, A., Pennanen, A., Makkonen, U., Spolnik, Z., van Grieken, R., Branis, M., Brunekreef, B., Chalbot, M.-C., Kuhlbusch, T., Sunyer, J., Kerminen, V.-M., Kulmala, M., and Salonen, R. O.** (2006). Chemical composition and mass closure of particulate matter at six urban sites in Europe. *Atmos Environ* 40: 212-223.
- Simeonova, P. P., Toriumi, W., Kommineni, C., Erkan, M., Munson, A. E., Rom, W. N., and Luster, M. I.** (1997). Molecular regulation of IL-6 activation by asbestos in lung epithelial cells: role of reactive oxygen species. *J Immunol* 159 (8): 3921-3928.
- Stoeger, T., Reinhard, C., Takenaka, S., Schroepel, A., Karg, E., Ritter, B., Heyder, J., and Schulz, H.** (2006). Instillation of six different ultrafine carbon particles indicates a surface area threshold dose for acute lung inflammation in mice. *Environ Health Perspect* 114 (3): 328-333.
- Stojicic, N., Walrafen, D., Baumstark-Khan, C., Rabbow, E., Rettberg, P., Weisshaar, M.-P., and Horneck, G.** (2005). Genotoxicity testing on the International Space Station: preparatory work on the SOS-LUX test as part of the space experiment TRIPLE-LUX. *Adv Space Res* 36: 1710-1717.
- Stone, V., Tuinman, M., Vamvakopoulos, J. E., Shaw, J., Brown, D., Petterson, S., Faux, S. P., Borm, P., MacNee, W., Michaelangeli, F., and Donaldson, K.** (2000). Increased calcium influx in a monocytic cell line on exposure to ultrafine carbon black. *Eur Respir J* 15: 297-303.

- Su, D. S., Jentoft, R. E., Müller, J.-O., Rothe, D., Jacob, E., Simpson, C. D., Tomovic, Z., Müllen, K., Messerer, A., Pöschl, U., Niessner, R., and Schlögl, R.** (2004). Microstructure and oxidation behaviour of Euro IV diesel engine soot: a comparative study with synthetic model soot substances. *Catal Today* 90: 127–132.
- Su, D. S., Serafino, A., Müller J.-O., Jentoft, R. E., Schlögel, R., and Fiorito, S.** (2008). Cytotoxicity and inflammatory potential of soot particles of low-emission diesel engines. *Environ Sci Technol* 42: 1761-1765.
- Sundström, C., and Nilsson, K.** (1976). Establishment and characterization of a human histiocytic lymphoma cell line (U-937). *Int J Cancer* 17 (5): 565-577.
- Swiston, J. R., Davidson, W., Attridge, S., Li, G. T., Brauer, M., and van Eeden, S. F.** (2008). Wood smoke exposure induces a pulmonary and systemic inflammatory response in firefighters. *Eur Respir J* 32 (1): 129-138.
- Tai, D.-I., Tsai, S.-L., Chang, Y.-H., Huang, S.-N., Chen, T.-C., Chang, K. S. S., and Liaw, Y.-F.** (2000). Constitutive activation of nuclear factor κB in hepatocellular carcinoma. *Cancer* 89: 2274-2281.
- Tang, P. S., Mura, M., Seth, R., and Liu, M.** (2008). Acute lung injury and cell death: how many ways can cells die? *Am J Physiol Lung Cell Mol Physiol* 294: 632-641.
- Thellin, O., Zorzi, W., Lakaye, B., de Borman, B., Coumans, B., Hennen, G., Grisar, T., Igout, A., and Heinen, E.** (1999). Housekeeping genes as internal standards: use and limits. *J Biotechnol* 75: 291-295.
- Troyano, A., Sancho, P., Fernandez, C., de Blas, E., Bernardi, P., and Aller, P.** (2003). The selection between apoptosis and necrosis is differentially regulated in hydrogen peroxide-treated and glutathione-depleted human promonocytic cells. *Cell Death Differ* 10: 889-898.
- Unfried, K., Albrecht, C., Klotz, L.-O., von Mikecz, A., Grether-Beck, S., and Schins, R. P. F.** (2007). Cellular responses to nanoparticles: target structures and mechanisms. *Nanotoxicology* 1: 1-20.
- US Environmental Protection Agency (EPA).** (2002) Health assessment document for diesel engine exhaust. Prepared by the National Center for Environmental Assessment, Washington, DC, for the Office of Transportation and Air Quality; EPA/600/8-90/057F. Available from: National Technical Information Service, Springfield, VA; PB2002-107661, and <http://www.epa.gov/ncea>
- Vander Wal, R. L., and Tomasek, A. J.** (2004). Soot nanostructure: dependence upon synthesis conditions. *Combust Flame* 136: 129-140.
- Vaux, D. L., and Korsmeyer, S. J.** (1999). Cell death in development. *Cell* 96: 245-254.

- Vogel, C. F. A., Sciullo, E., Wong, P., Kuzmicky, P., Kado, N., and Matsumura, F.** (2005). Induction of proinflammatory cytokines and C-reactive protein in human macrophage cell line U937 exposed to air pollution particulates. *Environ Health Perspect* 113 (11): 1536-1541.
- von Klot, S., Wölke, G., Tuch, T., Heinrich, J., Dockery, D. W., Schwartz, J., Kreyling, W. G., Wichmann, H. E., and Peters, A.** (2002). Increased asthma medication use in association with ambient fine and ultrafine particles. *Eur Respir J* 20: 691-702.
- Wang, C. Y., Mayo, M. W., and Baldwin, A. S. Jr.** (1996). TNF- and cancer therapy-induced apoptosis: potentiation by inhibition of NF- κ B. *Science* 274: 784– 787.
- Wang, T., Zhang, X., and Li, J. J.** (2002). The role of NF- κ B in the regulation of cell stress responses. *Int Immunopharmacol* 2: 1509-1520.
- Wittmaack, K.** (2007). In search of the most relevant parameter for quantifying lung inflammatory response to nanoparticle exposure: particle number, surface area or what? *Environ Health Perspect* 115 (2): 187-194.
- Xia, T., Kovochich, M., Brant, J., Hotze, M., Sempf, J., Oberley, T., Sioutas, C., Yeh, J. I., Wiesner, M. R., and Nel, A. E.** (2006). Comparison of the abilities of ambient and manufactured nanoparticles to induce cellular toxicity according to an oxidative stress paradigm. *Nano Lett* 6 (8): 1794-1807.
- Zhang, A., Wu, Y., Lai, H. W. L., and Yew, D. T.** (2004). Apoptosis - a brief review. *Neuroembryology* 3: 47-59.
- Zhi, L., Ang, A. D., Zhang, H., Moore, P. K., and Bhatia, M.** (2007). Hydrogen sulfide induces the synthesis of proinflammatory cytokines in human monocyte cell line U937 via the ERK-NF- κ B pathway. *J Leukoc Biol* 81: 1322-1332.

8 Abbreviations

°C	degree Celzius
µg	microgram
µl	microlitre
µM	micromole
µm	micrometer
AAD (7-AAD)	7-aminoactinomycin-D
Abs	absorbance (optical density)
ACGIH	American Conference of Government Industrial Hygienists
ANOVA	analysis of variance
ATCC	American Type Culture Collection
ATP	adenosine triphosphate
B2M	beta-2-microglobulin
Bcl-2	B-cell leukemia/lymphoma 2 gene
bp	base pair
C/O ratio	carbon/oxygen ratio
caspase	cystein-dependant aspartat-specific protease
CCD	charge-coupled device
cDNA	complementary deoxyribonucleic acid
CEN	Comité Européen de Normalisation
cm	centimetre
conc.	concentration
COX-2	cyclooxygenase-2
CP	crossing point
C _t	threshold cycle
D	diameter
DAPI	4',6-diamidino-2-phenylindole
deion.	deionised
DLR	Deutsches Zentrum für Luft- und Raumfahrt
DMSO	dimethyl sulfoxide
DNA	deoxyribonucleic acid
DT	doubling time
e.g.	exempli gratia (lat.)- for example
ECC	ethylene combustion condensate
EDTA	ethylenediaminetetraacetic acid
EGFP	enhanced green fluorescent protein
EPA	Environmental Protection Agency
et al.	et altera (lat.)- and others
etc.	et cetera (lat.)- and so on
EU	European Union
FACS	fluorescence-activated cell sorting
FACScan	fluorescence-activated cell scanner
FBS	foetal bovine serum
Flu	fluorescence
FSC	forward scatter
fwd	forward
G	Gauge- a measure for needle diameter
G	gram; acceleration due to gravity (9.81 m/s ²)
GAPDH	glyceraldehyde-3-phosphate dehydrogenase

GFP	green fluorescent protein
gr.	greek
H	hour
HPLC	high pressure liquid chromatography
HPRT	hypoxanthine-guanine phosphoribosyltransferase
HRTEM	high resolution transmission electron microscopy
i.e.	id est (lat.) - that is
IC	inorganic carbon
ICAM-1	intercellular adhesion molecule-1
IKK	I κ B-kinase
IL	interleukin
iNOS	inducible nitric oxide synthase
ISO	International Organisation for Standardisation
I κ B	inhibitory protein of nuclear factor κ B
kDa	kilodalton
kV	kilovolt
kW	kilowatt
L	litre
lac	lactose
LB	Luria Bertani
LC ₅₀	lethal concentration - concentration of a toxicant that is lethal to 50% of the exposed population
LD ₅₀	lethal dose – a dose of a toxicant that is lethal to 50% of the exposed population
Lux	luminescence
MCP-1	monocyte chemoattractant protein-1
MEM	minimal essential medium
mg	milligram
MHC	major histocompatibility complex
min	minute
ml	millilitre
mm	millimeter
mRNA	messenger RNA
MTT	3-(4,5-dimethylthiazole-2-yl)-2,5-diphenyltetrazolium bromide
Neo	neomycin
NF- κ B	nuclear factor kappa B
NF- κ BIA	inhibitor of NF- κ B
ng	nanogram
nitro-PAHs	nitrated polycyclic aromatic hydrocarbons
nm	nanometer
NMP	N-methyl-2-pyrrolidinone
NP	nanoparticles
Pa	pascal
PAHs	polycyclic aromatic hydrocarbons
PBGD	porphobilinogen deaminase
PBS	phosphate buffered saline
PCR	polymerase chain reaction
PE	phycoerythrin
PI	propidium iodide
PM	particulate matter

PM _x	particulate matter ("x" stands for the maximum size of a particle given in µm; e.g. PM ₁₀ symbolizes particulate matter smaller than 10 µm)
ppm	parts per million
PS	phosphatidylserine
qRT-PCR	quantitative real-time reverse transcription PCR
rel	relative
REST	Relative Expression Software Tool
rev	reverse
RIN	RNA integrity number
RNA	ribonucleic acid
RNase	ribonuclease
ROS	reactive oxygen species
rpm	rotations (rounds) per minute
S	Svedberg unit
SDS	sodium dodecyl sulphate
SEC	size exclusion chromatography
SEM	standard error of mean
SSC	side scatter
SWITCH	Salmonella weighting of induced toxicity (genotoxicity) and cytotoxicity for human health
TBE	tris base/ boric acid /EDTA
TC	total carbon
TEM	transmission electron microscopy
TK	thymidine kinase
TNF-α	tumour necrosis factor alpha
TOC	total organic carbon
U	unit
U	unified atomic mass unit
US/USA	United States of America
UV	ultraviolet
v/v	volume per volume
VCAM-1	vascular cell adhesion molecule-1
w/v	weight per volume
WinMDI	Windows multiple document interface
XIAP	X-linked inhibitor of apoptosis protein